DEVELOPMENT OF NANOFLUIDS BASED HORIZONTAL HEAT STORAGE UNIT

SAMAN PARIA

FACULTY OF ENGINEERING
UNIVERSITY OF MALAYA
KUALA LUMPUR

2016

DEVELOPMENT OF NANOFLUID BASED HORIZONTAL HEAT STORAGE UNIT

SAMAN PARIA

THESIS SUBMITTED IN FULFILMENT OF THE REQUIREMENTS FOR THE DEGREE OF DOCTOR OF PHILOSOPHY

FACULTY OF ENGINEERING
UNIVERSITY OF MALAYA
KUALA LUMPUR

2016

ABSTRACT

Nanofluids are well suited to heat transfer and there are prospective applications in solar energy recovery. A number of studies on the performance of nanofluids in heat transfer have been conducted including their effect on the rearrangement of flow passage configurations.

Use of Phase Change Material (PCM) as thermal energy storage (TES) unit is critical to solve the mismatch between energy supply and demand as well as to improve the efficient application of solar energy. The significant limitation in the tube-in-shell PCM storage is the volumetric expansion/shrinkage of PCM during charging and discharging process. Therefore, the PCM is not completely filled to the brim of the cavities.

The principal objectives of the present study are to deal with the energy storage (melting or charging) and energy removal (solidification or discharging) processes by using Paraffin wax as a PCM in an unique horizontal shell and tube heat exchanger with 0, 24 and 48 radial fins in the laminar flow regime. The main source of irreversibility was through entropy generation from the phase change heat transfer, although the viscous dissipation was incorporated.

The previous researchers have reported that the container must be filled up to 75% to 80% of its capacity. It is well known that the heat transfer equations for the heat exchangers is defined by the symmetric model. Thus, the PCM behavior is not controllable around the finned tube and it cannot follow the symmetric pattern. The motivation of this study was to design and construct a novel unit storage system with a hollow container around the horizontal cylindrical tube containing the PCM as the storage material. The effects of nanoparticle concentration were examined for various nano fluids, inlet temperature of heat transfer fluid (HTF), different HTF flow rates and the external fin surface areas to improve the heat transfer between the paraffin and HTF. The results

indicate that the HTF flow rate has more influence on the paraffin charging process than at the discharging process.

The charging time was reduced by varying the HTF flow rate and the fin density, 58% and 76% respectively. For design A, it can be found that the impact of increasing the fins in melting is 20% more than the solidification. In case of different designs (A and B) the effect of enhancement of the flow rate on melting is approximately 1.5 times more than that of the solidification. It has been observed that the impact of 10°C change at the inlet temperature on the melting process reduces the processing time around 50% than at the same temperature variation in the solidification process. Nano fluids have the minimum impact on the solidification process compared to that on the melting process. Use of nanofluids has reduced the melting time 3 to 5 times more compared to the reduction in solidification time. Incorporation of more fins could meltmore mass and shorten the melting completion time. In melting process, the fin effect is about 30% stronger than the alteration effect of Reynolds number.

ABSTRAK

Nanofluids adalah amat sesuai untuk pemindahan haba dan terdapat bakal aplikasi dalam pemulihan tenaga solar. Beberapa kajian mengenai prestasi nanofluids dalam pemindahan haba telah dijalankan termasuk kesannya pada penyusunan semula konfigurasi saluran aliran.

Penggunaan Fasa Tukar bahan (PCM) sebagai penyimpanan tenaga haba (TES) unit adalah penting untuk menyelesaikan ketidaksepadanan antara penawaran tenaga dan permintaan serta untuk meningkatkan permohonan cekap tenaga solar. Had ketara dalam simpanan PCM tiub di shell adalah pengembangan / pengecutan isipadu PCM semasa pengecasan dan proses melaksanakan. Oleh itu, PCM itu tidak benar-benar dipenuhi dengan sesak rongga.

Objektif utama kajian ini adalah untuk berurusan dengan penyimpanan tenaga (lebur atau mengecas) dan penyingkiran tenaga (pemejalan atau melaksanakan) proses dengan menggunakan dihadiri oleh penyelidik bagi lilin sebagai PCM dalam shell dan tiub mendatar penukar haba yang unik dengan 0, 24 dan 48 sirip radial dalam rejim aliran lamina. Sumber utama ketakbolehbalikan adalah melalui generasi entropi daripada pemindahan haba perubahan fasa, walaupun pelesapan likat telah ditubuhkan.

Para penyelidik sebelum ini melaporkan bahawa bekas mesti diisi sehingga 75% kepada 80% daripada kapasitinya. Adalah diketahui umum bahawa persamaan pemindahan haba bagi penukar haba ditakrifkan oleh model simetri. Oleh itu, tingkah laku PCM tidak dikawal sekitar tiub bersirip dan ia tidak boleh mengikuti corak yang simetri. Motivasi kajian ini adalah untuk mereka bentuk dan membina sistem penyimpanan unit novel dengan bekas kosong sekitar tiub silinder mendatar mengandungi PCM sebagai bahan simpanan. Kesan kepekatan nanoparticle telah

diperiksa untuk pelbagai cecair nano, suhu masuk pemindahan haba cecair (HTF), kadar aliran HTF yang berbeza dan kawasan permukaan sirip luar untuk meningkatkan pemindahan haba antara parafin dan HTF. Keputusan menunjukkan bahawa kadar aliran HTF mempunyai pengaruh yang lebih kepada proses pengecasan parafin daripada di dalam proses penyahcasan.

Masa pengecasan telah dikurangkan dengan mengubah kadar HTF aliran dan ketumpatan sirip, masing-masing 58% dan 76%. Untuk reka bentuk A, ia boleh didapati bahawa kesan meningkatkan sirip di lebur adalah 20% lebih daripada pemejalan. Dalam kes reka bentuk yang berbeza (A dan B) kesan peningkatan kadar aliran pada lebur adalah kira-kira 1.5 kali lebih tinggi daripada pemejalan. Ia telah diperhatikan bahawa kesan perubahan 10 ° C pada suhu masuk pada proses lebur mengurangkan masa pemprosesan sekitar 50% berbanding pada perubahan suhu yang sama dalam proses pemejalan. cecair nano mempunyai kesan minimum pada proses pemejalan berbanding dengan yang di proses lebur. Penggunaan nanofluids telah mengurangkan masa lebur 3 hingga 5 kali lebih berbanding dengan pengurangan dalam masa pemejalan. Penubuhan lebih sirip boleh meltmore massa dan memendekkan masa siap lebur. Dalam proses lebur, kesan sirip adalah kira-kira 30% lebih kuat daripada kesan perubahan itu nombor Reynolds.

ACKNOWLEDGEMENTS

I would like to acknowledge Associate Professor Dr. Ahmed Aly Diaa Mohammed Sarhan, and Dr. Kazi Md. Salim Newaz for their invaluable guidance and support throughout my graduate study. I would like to thank Professor Wan Jeffrey Bassirun for allowing me to use his lab facilities. I do also deeply appreciate Dr. Saeid Baradaran and Dr. Mohammad Reza Safaie for their valuable help on my research. I would like to thank all of my lab mates in my group. Without their suggestion and assistance during my graduate study period, I may not be able to finish my PhD degree. Finally, I would like to thank my family for their unending support and encouragement throughout my career. I would like to thank University of Malaya for the financial support offered by the IPPP,UMRG and HIR grants.

TABLE OF CONTENTS

LIST OF FIGURES

LIST OF TABLES

LIST OF SYMBOLS AND ABBREVIATIONS

AL_2O_3	Aluminium oxide
ANOVA	Analysis of variance
AR	Aspect ratio
x, y	Cartesian coordinates (m)
Cu	Copper
D	Diameter (m)
FTHX	Finned-tube heat exchanger
HDR	Heat discharge rate
Q	Heat flux (W m^{-2})
H	Heat transfer coefficient (W m^{-2} K^{-1})
HTF	Heat transfer fluid
LHESS	Latent heat energy storage system
LHSU	Latent heat storage unit
G	Internal energy distribution function
$\overline{u}$	Mean velocity (m s^{-1})
MWCNT	Multi-walled carbon nanotube
HNO_3	Nitric acide
NF	Number of fins
N	Number of phases
Nu	Nusselt number
Pr	Prandtl number
m_p	Particle mass (kg)
PCM	Phase change material
P	Pressure (N m^{-2})

RANS	Reynolds averaged navier stokes
Re	Reynolds number
STHX	Shell and tube heat exchanger
SNR (S/N)	Signal noise ratio
SDS	Sodium dodecyl sulfate
SDHW	Solar domestic hot water
H_2SO_4	Sulfuric acid
C_p	Specific heat capacity (J kg^{-1} K^{-1})
S	Surface area
T	Temperature (K)
K	Thermal conductivity (W m^{-1} K^{-1})
TES	Thermal energy storage
T	Time (s)
TiO_2	Titanium(IV) oxide
E	Total energy (J kg^{-1})
K	Turbulent kinetic energy (m^{-2} s^{-2})
u=(u,v)	Velocities vector and its components in x and y directions (m s^{-1})
W	Width of the copper tube (m)

Greek Symbols

ρ	Density (kg m^{-3})
μ	Dynamic viscosity (Pa s)
N	Kinematics viscosity (m^2 s^{-1})
φ	Volume fraction of nanoparticles

Subscripts

ave	Average
F	Base fluid
b	Bulk
C	Cold wall
eff	Effective
F	Fin
H	Hot wall
i, j,	Indices
I	Inlet
L	Liquid
M	Mean
nf	Nanofluid
np	Nanoparticles
o	Outside
W	Point W
p	Secondary phase
s	Solid
T	Thermal
t	Thickness
W	Wall

List of Appendices

CHAPTER 1: INTRODUCTION

1.1 Background of Study

Nowadays, energy storage is of great importance. It plays a vital role in almost all areas of technology and knowledge such as, electrical, heat, potential or chemical form. In spite of the various motivations for the current technological development in different areas of energy storage, the same total stimulus is applied: it must be considered that earth energy resource or the solar one is not permanently available. Every form of energy from the solar to the oil fields, and the geothermal heat, all will die out.For this reason, energy storage is highly required in order to extract the energy in case of being not promptly accessible that is apparently observed in solar panel in which the solar radiations are changed into electrical potential energy for future application. The thermal energy storage has been observed by the dawn of civilization insofar as through the earliest stage of written history, ice has been made by people to preserve things in cold condition from the warm weather environment.

The motive to store various forms of energy from different sources based on ecological and economic aims has yield such thinking. Since the last few decades, the global energy supply has been continued with a high rate of demand. It should be mentioned that a rising consumption level of electricity, coal and crude oil in the developing countries are attributed to the industrial changes. This level of demand results in raising the total energy prices to an uncommon level. Consequently, the energy storage is highly needed and the use of other fresh sources to provide the peoples requirement is investigated. In addition, seeking the ways with higher level of efficiency that are environmentally-friendly and more affordable to extract and store energy for future application is on the rise. The introductory part of this research tries to shed the light on different forms of energy storage and their usages. Lastly, thermal energy storage which is introduced as the main area of this research applying paraffin wax as PCM and nanofluids as the heat exchanging

liquids in a novel shell and tube PCM set-up with or without fins on tubes have been investigated briefly before the detailed study has presented in the literature review.

As previously mentioned, there are plenty of reasons encouraging us to promote energy storage. Aside from environmental and economic advantages, reliability and portability are considered as the other reasons to be given emphasis. Electrochemical batteries which provide a remarkable portable electricity source are the best example. A conventional gas generator that applies the conserved heat of combustion is observed as reliable and easily transported. When the power is failed, the gasoline is combusted and then applied to propel the generator's rotor. Later, the electricity is generated. The mentioned energy storage forms are the examples of various types of recent technology. Initially, it seems highly interesting to see the variety of energy storage in practice in the daily life. Only the key forms of energy storage has been presented in this research which are depicted in Figure 1.1.

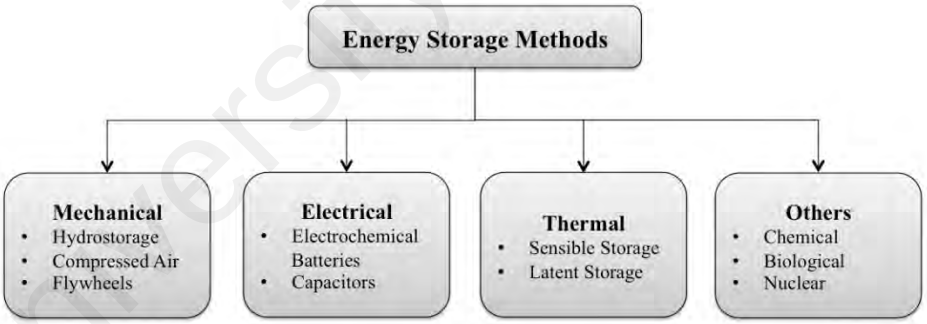

Figure 1.1: Some of the more common modes of energy storage.

Various forms of thermal, mechanical and electrical energy storage have been argued along with a summarized outline of each of them, though the focus of this study is on the thermal energy storage and due to that this is explained more and in details.

1.1.1 Mechanical Energy Storage

Mechanical energy storage can be presented usually in the form of kinetic energy or momentum which is able to be restored in various forms for future use. Flywheel is a typical example of mechanical energy storage which is able to provide or receive rotational energy when needed. In simple words, flywheel is a wheel fixed with an axle called moment of inertia or angular mass. While angular momentum from the axle is moved to the flywheel, it causes a rotation and storing the angular momentum as angular velocity. Initially, although this system may not look like a highly remarkable form of energy storage, some of the public transit vehicles apply flywheels in order to raise the energy efficiency. As an example, it can be mentioned that big city buses with regular stops on their way may meet fuel efficiencies and they can use flywheels to lower their usage of fuel up to 50% (Dincer & Rosen, 2002).

The assumption of this technology justifies it as in every bus stop, the kinetic energy which is also called momentum is moved to the flywheel through the bus axles, instead of dissipated via the brake pads. The whole process goes to the opposite direction when the bus should accelerate after the stop and in this case, the flywheel's rotational energy is moved back to the axle in order to give a forward acceleration. Trains and subways that need a high level of energy for accelerating and decelerating are other vehicles that employ flywheels for the same aims. Except for the flywheel, other forms of mechanical energy can be observed in daily life. The example is a wind-up watch which stores this type of energy in the springs implanted inside the watch. It should be mentioned that two other types of energy storage called compressed air storage and hydro storage hugely become trendier with increasing the energy demand. As previously mentioned, the energy supply is not perpetual and consequently the energy price differs. On the other hand, most of the generating stations of electricity power are operated at an optimum and steady level and they can make sufficient level of energy to provide for the whole population. Though,

in case of electricity being in low demand, for example at the night time, the production still carries on due to high cost of start-up. Therefore, it can be said that the energy storage is a feasible alternative for those who desire to save money and energy. As already told, another type of energy storage is hydro storage which is in gravitational potential form of energy. The mechanism is explained so that at the night time, the rate of electricity is cheaper; pumping water is done by a lower to higher elevation. But during the raising rates, the hydro storage is employed to operate turbines as well as producing electricity at the initial cost fraction. The same process happens while working with compressed air storage. In time of low demand for electricity, a storage container receives the compressed air and the air is employed to operate the turbines when the demand for electricity is high. However, despite the fact that mechanical energy storage is highly adoptable and advantageous, a huge interest is drawn towards chemical energy storage which will be presented later.

1.1.2 Electrical Energy Storage

Since the electric cell was introduced by Alessandro Volta in 1800, the electrical energy storage has been drawing a huge attention. However, the early batteries were not well-developed (they were composed of a copper and zinc electrode dipped in sulfuric acid); it was observed that the battery industry providing the power for laptops and cell phones has increasingly become flourished. Despite the fact that the battery is part of a specific division of electrical energy storage named as electrochemical storage, several usages of electrical storage forms that possess a high significance which could be found as capacitors or tools that is able to store energy in the electric field between two charged plates. They are mostly employed as electronic tools in order to maintain a more fixed power supply, though the batteries are charged or replaced. Researches are presently being done in order to improve the super capacitors which are capacitors with two layers. A certain amount of electrical energy kept by the mentioned tools is the same as the

rechargeable batteries, though retaining a shelf life thousands of times more than the available rechargeable batteries in market nowadays. The majority of other kinds of systems which store electrical energy are based on changing the surplus of the energy to chemical or mechanical or the thermal form which is the focus of this research. It is necessary to address other ways of storing energy prior to start the discussion about the thermal energy storage.

1.1.3 Other Energy Storage Methods

Nuclear, chemical and biological energy storage is another way of storing energy that plays the key role in meeting the global demand. The people's life would tremendously rely on chemical energy storage; the hydrogen economy that has been improving in the near paste since a few years ago scientists had contributed in making a secure and environmentally friendly way to store electrical energy in hydrogen mode. The justification is as follows: energy is employed in order to transfer the hydrogen atoms from a lower energy level like water to a higher one like hydrogen gas. In order to conduct this, electricity can be employed in the reverse of a voltaic cell for separating hydrogen from water to generate oxygen and hydrogen. The hydrogen gas is meant to electrochemically be employed in fuel cells or burned in operating generators which are highly safe to the nature since water is their mere byproduct when reacting.

On the other hand, another form of energy storage system called biological energy storage has been observed since the beginning of life. It is observed that all the living organisms are nearly bale to store energy in various ways, needs to get it out when the energy level is low. Plants can be mentioned as examples that are able to store surplus energy as starches or other forms of carbon compounds. These forms are easily split into glucose and employed for respiration. Moreover, animals would be able to store the surplus energy as fats, glycogen or even other compounds that have the capacity to be

broken into glucose for the final aim of getting energy out of it. Therefore, despite the fact that energy storage notions are not always easy to explain, the major metabolic functions that are highly relied on the biological and biochemical energy storage help us to stay alive. In spite of this fact that technology is not well-improved yet to store energy efficiently in nuclear materials, deriving nuclear energy from radioactive materials has been being done for decades. Nuclear fission reactors have drawn a huge attention, because of the fact that the influence of ecological and global warming is decreasingly aroused as compared to fossil fuel burning. In 1900s, Albert Einstein discovered the mass-energy equivalence, as can be seen as the foundation of nuclear reactions.

There is still a long way to develop the conversion between energy and mass in the attainable ways promptly and it is expected to be a more applicable and feasible in future. It should be highlighted that in spite of the fact that nuclear, chemical and biological energy storage are the main types of energy storage, thermal storage is another form of energy storage which is addressed in this thesis. Thermal energy storage (TES) has attracted a huge attention in the last few decades but there is almost no research work discussing it before 1980s. TES is considered as the least complicated energy storage. The mechanism is that energy in the form of heat or cold is kept in a medium and thermal energy is further used for several heating or cooling aims. The next part explains a more complete and comprehensive study of different forms of TES and their usages.

1.1.4 Heat Transfer

A common situation encountered by the chemical engineer is heat transfer to fluid flowing through a tube. This can occur in heat exchangers, boilers, condensers, evaporators, and a host of other process equipment. Therefore, it is useful to know how to estimate heat transfer coefficients in this situation. The flow of a fluid can be classified in a straight circular tube into either laminar or turbulent flow. Fully developed

incompressible, Newtonian, steady flow conditions are assumed from here on. Fully developed flow implies that the tube is long compared with the entrance length in which the velocity distribution at the inlet adjusts itself to the geometry and no longer changes with distance along the tube. In discussing heat transfer to or from a fluid flowing through a straight circular tube, it is useful to distinguish between the axial or main flow direction, and the directions that lie in a plane perpendicular to the tube axis. In that plane, transverse heat flow can be broken into radial and azimuthal components.

The principal difference between laminar and turbulent flow, as far as heat transfer is concerned, is that an additional mechanism of heat transfer in the radial and azimuthal directions becomes available in turbulent flow. This is commonly termed "eddy transport" and is intense, providing much better transfer of energy across the flow at a given axial position than in laminar flow, wherein conduction is typically the only mechanism that operates in the transverse directions (an exception occurs when there are secondary flows in the transverse direction, such as in coiled tubes). Another difference worthwhile noting is the extent of the "thermal entrance region" in which the transverse temperature distribution becomes "fully developed." This region is relatively short in turbulent flow (precisely because of the intense turbulent transverse transport of energy), whereas it tends to be long in laminar flow. Heat transfer correlations, based on experimental results, are typically divided into those applicable in the thermal entrance region, and those that apply in the "fully developed" region. In the case of laminar flow, it is important to be aware of this distinction, and normally a laminar flow heat exchanger is designed to be short, to take advantage of relatively high heat transfer rates that are achievable in the thermal entrance region.

1.1.5 Nano Fluids

By wide spread application of heat transfer in industry, the demand for efficiency has significantly risen, which resulted in development of recent inventive methods. Improving the efficiency of heat treatment devices has enhanced the energy consumption on one hand and has reduced the size of such devices on the other, result the material and production costs to be reduced. Such enhancements were possible through increasing the surface area in contact per unit volume which causes devastating pressure drops and requires more powerful pumps. In addition to that, the price of heat transfer equipment shall increase. Nanotechnology advancements in general along with application of nanofluids as heat transfer liquids are breakthrough in the past two decades.

Choi, in 1995 was the first to present the concept of nanofluids (S. U. S. Choi & Eastman, 1995). Nanofluids are basically heat conducting fluids which consist of a base fluid incorporating suspended particles in the range of 1~100 nm. Meanwhile solid particles obtain better thermal conductivity compared to conventional base fluid, as a result the addition of solid nanoparticles is expected to increase thermal conductivity of the nanofluid (Abouali & Ahmadi, 2012; Afshar, Shams, Nainian, & Ahmadi, 2012). For example, thermal conductivity of solid particles of Cu (copper), is 700 and 3,000 times greater than the thermal conductivities of water and engine oil respectively (Hassan et al., 2013). The addition of micro-sized solid materials to the base fluids was proposed decades ago. It was established that the micro-particles tend to settle from suspension; resulting in blocking channels, pipes, and heat exchangers. Moreover, accumulation of such abrasive solid particles causes erosion, corrosion in pipes, damage in pumps and other devices. Application of nanofluids that maintain suspended nano-sized particles in base fluids which would lessen the effect of erosion, corrosion, fouling and the pipe blockings.

1.2 Motivation

The motivation of the present research is clearly presented. Shell-and-tube TES systems have been globally drawn a huge attention because the energy demand is on a rise that caused to make the electricity rate higher. Shell-and-tube TES possesses other benefits that are the ecological advantages from its application. It was observed that the mentioned system application can assist in decreasing the total electricity production from the sources that may be ecologically malignant because TES helps to lower the energy demand during daytime. Decreasing of the peak electricity demand also causes decreasing of the total greenhouse gas emission due to the fact that a certain amount of electricity comes from oil, coal or natural gas fired power-plants.

Moreover, people consider the fact that in order to save money; they would better use electricity at daytime when the price is lower rather than that at the night time. TES application also helps to implement an extra heat load without changing the present systems of water heaters. The mentioned systems can be implanted and operated along with the present systems to help decreasing the extra heating loads which can be needed during specific nights and days. The mentioned ecological and economic problems create motivations to consider thermal energy storage while making huge heating systems. Although, not sufficient research has been conducted in this area in spite of its popularity, the researchers hope to pave the way for future studies through interpreting the charging and discharging processes of heat storage container by applying phase change material and nanofluids. The present research findings are expected to prompt the researchers and designers in shell-and-tube TES field to concentrate on the flow feature, heat transfer as well as thermodynamic characteristics to improve the overall operation and efficiency of the systems.

In recent years, the usage of the PCM latent heat as a thermal energy storage substance has interested areas like heat exchanger systems, solar energy systems, spacecraft, heating and cooling of buildings etc. Nevertheless, practical difficulties may occur in applying the latent heat method occasionally. Low thermal conductivity of the PCM, density change, stability of properties under extended cycling, sometimes phase segregation and sub-cooling of the PCMs are some reasons of these difficulties (Akgün, Aydın, & Kaygusuz, 2007).There have been significant researches done on STHX (shell-and- tube heat exchanger) which are shown in Chapter 2; however, there are some gaps in the previous works.

1.3 Objectives of Study

In this study the effect of changing some geometrical parameters of the horizontal cylindrical storage system for melting and solidification of paraffin during charging and discharging operating mode is investigated. This has led to the following research objectives for this project:

- To develop and construct a new storage unit with higher performance accommodating more PCM volume and considering the expanded PCM volume.
- To enhance the heat transfer of PCM by using the different concentrations of various nano fluids.
- To improve the heat transfer by increasing the contact surface area of heat exchanger tube.
- To investigate the effect of inlet HTF temperature and flow rate for higher performance.

A well-organized methodology is always compulsory to obtain the best work conceptual as outlined below:

- To have a most comprehensive Literature review for beginning the study.
- To prepare all the materials which are needed in the present case.
- To fabricate the samples with the mentioned process.
- To prepare documents and thesis.

The methodology of this research is shown in the following flowchart (Figure 1.2).

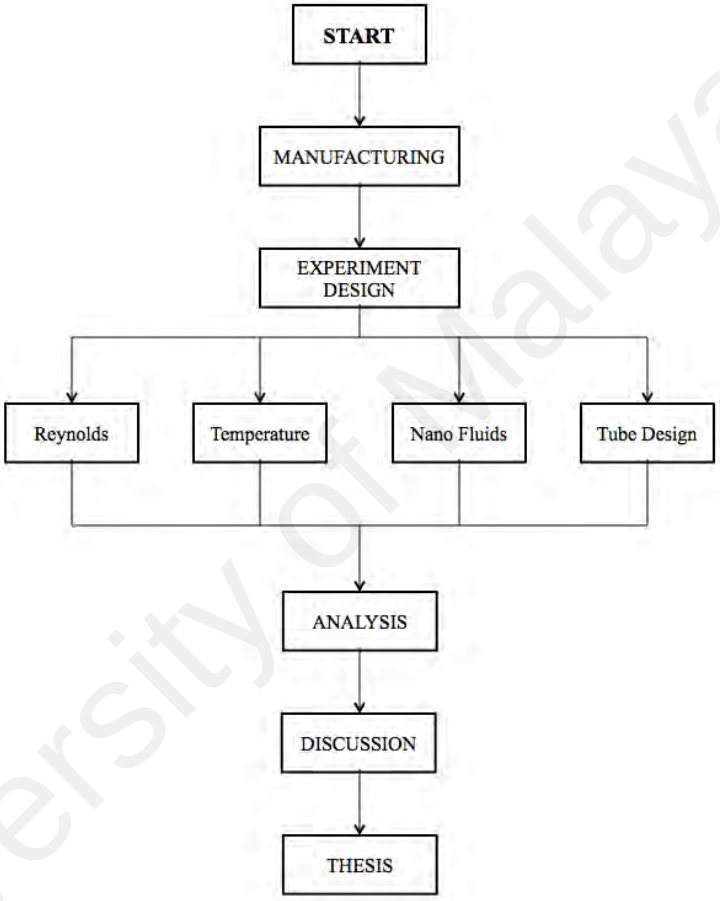

Figure 1.2: Flowchart of methodology

1.4 Aim of Study

The aim of this study is to design and fabricate a novel storage unit responding to the melting/solidification characteristics of the paraffin wax for improving the performance of latent heat energy storage by using full capacity of PCM container. Enhancement is achieved by a horizontal shell-tube integrated with radial fins, different nanofluids (TiO_2, MWCNT and GNP) with various concentrations (0, 0.05 and 0.1), different inlet temperatures (63°C, 70°C and 80°C) and various Reynolds numbers (1000, 1500 and

2000) on the interface together with time needed for the completion of charging and discharging of PCM.

1.5 Organization of this Dissertation

This dissertation adopts a university Malaya style guide to presentation, logically aimed and systematically rendered to enhance understanding of the research. The thesis is divided into five chapters as follows:

Chapter one highlights the background of the study, the problems existing in this area which build motivation for this project, and the objectives of this research.

Chapter two presents the literature review which covers geometries and materials used in STHX and experimental parameters for operating these systems. The effect of design on heat transfer performance and its impact on melting and solidification are also presented. This chapter shows that there have been many experimental and numerical studies regarding the consecutive charging/discharging operating mode of a LHESS. However, no work has been published on comparing the effect of geometrical parameters on charging/discharging operating mode for paraffin wax as a PCM in horizontal cylindrical container. This literature review has led to an informed decision on the design of the experimental STHX used in this thesis.

Chapter three explains the methodology for conducting this research project. Experimental setup described schematically and the geometry of the container, heat transfer enhancement designs, equipment and materials explained in details by adding some photographs, figures and tables.

Chapter four presents the experimental results which are analyzed then the patterns in the PCM behavior are identified.

Chapter five demonstrates the comprehensive conclusions along with recommendations for further work. The originality of this project is also summarized in this chapter.

CHAPTER 2: LITERATURE REVIEW

2.1 Introduction

The next part is in-depth review of materials explored in the present literature and their concentration effect on deep analysis of thermal energy storage. The sensible systems are going to be introduced just in brief but the main focus will be on systems using latent storage notions such as cool and warm thermal storage. A high number of studies can be found focusing on the sensible and latent methods employed for thermal energy storage. The thermal energy storage systems have attracted a huge interest to their design and optimization due to their environmental and economic advantages that improve their status as the first choice. Several methods have been employed where each of them could be largely categorized as numerical or analytical methods. Several research works have employed their experimental findings as a proof of their validity. Figure 2.1 shows a more in-depth flow diagram of several classifications of thermal energy storage studies that helps in understanding the flow of literature.

2.1.1 Thermal Energy Storage

Prior to explaining the basic points of TES, a distinguished resource should be presented to the readers to help them to approach any facet of Thermal energy storage (Dincer & Rosen, 2002). This thesis will provide a huge amount of information for those who like to seek knowledge about this field in both the undergraduate and graduate level.

There are two ways to store thermal energy which consists of the latent and the sensible storage. The first one deals with the change of energy in a material in the phase change time for example from a liquid to gas (water boiling) or liquid to solid (ice freezing). In the phase transition time, energy is discharged or absorbed by the process direction. The energy discharged/absorbed in the latent storage process which is done in a fixed temperature rate which helps to regulate the process with less effort. Although, knowing

the right PMC or phase change material to match with the particular processes is challenging, as some substances experience the phase transition just at the specific pressure and temperature.

Sensible thermal storage is observed as the stored energy in a material temperature change. *Specific heat* is the characteristic of all material simply defined as the energy used to convert one kilogram of any substance's temperature by one degree like 4.2 *kJ/kg.K* that is the specific heat of water in 5ºC meaning that in order to increase the temperature of 1 kg of water at 5ºC, 4.2 kilojoules of energy is needed. Therefore, energy storage can take place in any material temperature change, and sensible thermal energy storage is used for all applications, as the releasing and energy storage temperature is different. Although, storing the large amount of energy is an advantage of the sensible thermal energy storage. As an example, it can be mentioned that 334 kJ of energy is taken for freezing one kilogram of ice, though in order to store the same amount of energy, 79 kg of water is used to change the temperature one degree. There are advantages and disadvantages for each way of storing energy, but they both can be seen in thermal energy storage and are employed for both cool and warm TES.

2.1.2 Heat Storage

Solar heaters, geothermal storage methods and solar ponds are famous ways of storing warm thermal energy among the other methods. The benefit of warm TES is that it has gained by the way of an environmentally-friendly as well as excessive source like the sun and this source is affordable and green. The mismatched energy availability and demand of SDHW (Solar Domestic Hot Water) systems are the problems and an issue of limited availability of solar energy at night which needs to be addressed (Z. Liu, Wang, & Ma, 2006). Thermal energy storage (TES) is commonly used to bridge this gap between energy availability and demand. Commonly, the used sensible energy storage systems

such as hot water storage tanks require significant space which adds weight to the structural components. These space and weight requirements are barriers for further deployment of SDHW in buildings with limited space or structural limitations from the additional weight. Using phase change materials (PCMs) for TES can solve these problems by reducing the weight and space required for energy storage (Mehling & Cabeza, 2008). PCMs are used as energy storage mediums: energy is stored during melting and releasing at the solidification process. From an energy efficiency point of view, PCM storage systems (also called LHESS) have the advantage that their operation can be nearly isothermal (Fernandez, Martínez, Segarra, Martorell, & Cabeza, 2010).

The thermal storage technology based on the use of phase change materials (PCM) has recently raised an important practical interest. This is mainly due to the high-energy storage density during phase change within a very narrow temperature range. They can be employed to balance energy demand between daytime and nighttime. The latent thermal energy storage using a phase change material (PCM) has attracted attention in the energy storage area extensively because during the solidification and melting processes, PCMs have benefits of high energy storage density and isothermal operating characteristics such as charging and discharging heat at a nearly constant temperature. These advantages are good for efficient operation of thermal systems. TES can be broken into sensible and latent energy storage. Sensible energy is stored when the material temperature rises, and is released when the material temperature decreases. Sensible heat ($Q_{sensible}$) is proportional to the specific heat capacity of the material (C_p), the difference in temperature of the material from the initial temperature (T_i) to the final temperature (T_f) and the mass of material (m) given by:

$$Q_{Sensible} = m\, C_p(T_f - T_i) \qquad (2.1)$$

Latent heat is absorbed or released when a material undergoes a phase change at a relatively constant temperature; these materials are called PCMs. The amount of latent heat stored in a material (Q_{latent}) is proportional to the latent heat of fusion of the material (Δh_m) and the mass of material that undergoes a phase transition (m) given by:

$$Q_{latent} = m\, \Delta h_m \qquad (2.2)$$

PCMs also store sensible heat before and after the phase transition, therefore the total storage capacity of a LHESS from an initial temperature (T_i), to a final temperature (T_f) is given by (A. Sharma, Tyagi, Chen, & Buddhi, 2009):

$$Q_{pcm} = m\,[C_{ps}(T_m - T_i) + \Delta h_m + C_{pl}\,(T_f - T_m)] \qquad (2.3)$$

Where C_{ps} is the specific heat of the solid PCM, T_m is the melting temperature of the PCM, and C_{pl} is the specific heat of the liquid PCM. Over the small considered temperature range in the most LHESS (20 to 60 ºC temperature difference), the latent heat of some PCMs is several orders of magnitude larger than the specific heat, and many PCMs can store up to 14 times more energy per volume than water over the same temperature range (Agyenim, Eames, & Smyth, 2010). Available solar energy and hot water demands of residential homes are both time dependent and intermittent, however the energy source and demand times do not often match each other. For example, there may be a demand for domestic hot water at night when no solar energy is available. For this reason, a LHESS paired with SDHW has three possible operating modes:

1. Heat exchange by the hot HTF to the PCM, melting the PCM and charging the LHESS;
2. Heat exchange from the PCM to the domestic water, solidifying the PCM and discharging the LHESS;

3. Both 1 and 2 at the same time: Heat exchange from the hot HTF to the PCM, and heat exchange from the PCM to the domestic water at the same time, resulting in simultaneous charging and discharging.

The third operating mode occurs when there is a demand for domestic hot water at the same time that solar energy is available. Although charging and discharging are simultaneous in this operating mode, the time scales may differ with charging times of 6 to 8 hours (*i.e.* sunshine hours) and discharging times as short as 10 minutes (*i.e.* a shower). This simultaneous operating mode makes the system suitable for various time dependent energy sources, such as solar energy (Z. Liu et al., 2006). Direct heat transfer from the solar HTF to the domestic water may occur during the third operating mode, with additional energy being stored in, or recovered from, the PCM. Latent TES also plays a great role in heat storage. Paraffin waxes, with melting points well over that of water, can achieve relatively large latent heat of fusions, and as a result is used as a phase change material in many heat storage applications. These include solar water heaters and solar collectors, both of which are used in the heating industry. Paraffin along with many other materials including brines, eutectic salts and some acidic compounds make the excellent TES mediums, and the search continues more to suit individual purposes more precisely.

2.2 TES Systems and Applications – Overview

TES is also vital for various engineering usages. When the waste heat availability and application periods are not the same, it is necessary to have waste heat recovery system. Likewise, the systems including solar heat collectors, an influential medium is require to store energy for using at night or sunless days. There is a comprehensive review on few major storage mediums in the literature (Hasnain, 1998). Two major kinds of systems are found as latent and sensible systems. Sensible systems control the particular heat

materials which involve solid and liquid together. Though the latent systems conduct TES by the way of phase change and do not need large temperature disparity to store thermal energy and are able to be done in different PCMs.

2.2.1 Sensible TES Systems

The literature focusing on sensible thermal energy storage is compelling in spite of being irrelevant to the present research. Sensible thermal storage can be done in various mediums in either forms of solid and liquid. The former one is mostly in metals or rock form and involves alloys like zirconium oxide for high temperatures while the latter one includes molten salts, oils and water. (Nsofor, 2005). Despite the existing several studies considering on both forms, in the present study, two brief examples are presented: a rock bed and a solar pond which are both made to store solar energy (Karakilcik, Dincer, & Rosen, 2006) operated with high efficiency from a solar pond in Adana, Turkey that was brimmed by salty water in order to create three areas with various densities without being mingled. The upper area is the freshwater layer from the higher level of the pond and is fueled by rainwater and transfers it to make up the water loss resulted from the evaporation. In order to hinder the freshwater and the lower zone to be mingled, the middle layer is devised which is named insulation zone when the solar energy is retained as heat. The densest mixture that is the lower zone, which stores and absorbs the highest amount of solar heat in the heat exchangers of the solar pond and at the solar container bottom and the insulation areas. The best performance of thermal systems was observed in mid-summer as anticipated due to the fact that the ground level and solar radiation are at the utmost stage though temperature gradient are at very low level.

Choudhury, Chauhan, & Garg (1995) studied the efficiency of a solar air heater related to a rock bed thermal storage tool. A two-pass, solar air heater with a single cover is connected to the rock bed, though geometric design and functional factor are altered to

investigate its influence on the performance. Parameters like a charging time, air velocity, rock bed size, individual rock size as well as void fraction are investigated to explore their impact on the system's thermal performance. The charging period was observed as the most important impact on the total performance along with the optimal charging period arranged for 8 hours in the specific place of New Delhi. Several other applications are related to sensible thermal storage though the major concentration in the present study is to introduce latent TES systems.

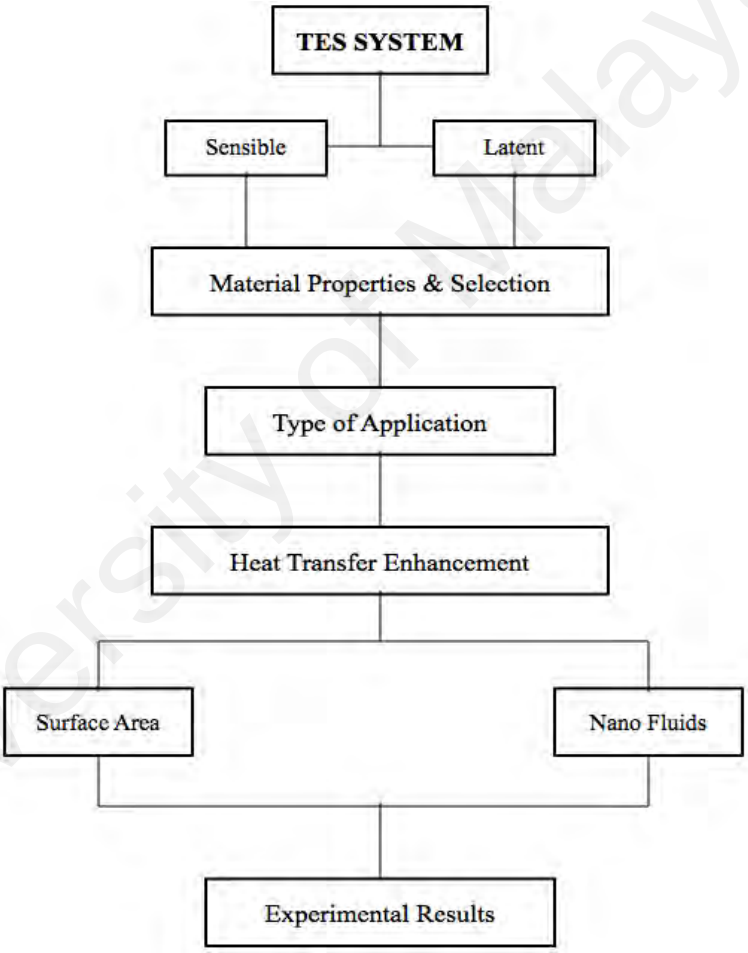

Figure 2.1: Literature review flowchart

2.2.2 Latent TES Systems

Latent TES systems have become much more viable for a high volumetric heat capacity. Latent systems can usually store much more thermal energy for a given volume, it requires less temperature gradient, and can be used for both hot and cold thermal energy

storage, depending on the material. A comprehensive review of the various types of systems can be found in Sharma and Sagara (S. D. Sharma & Sagara, 2005) where various applications and PCM innovations are discussed. In short, a few of the mentioned applications consist of space cooling and heating, solar water heating, solar cooking, waste recovery systems and greenhouse upkeep. The systems of Latent solar-water heating are the best example of the benefit of thermal energy kept in PCMs. Nallusamy *et al*. explored the efficiency of a solar collector paired with a storage container that is topped with the PCMs. Water was employed as the heat transfer fluid and the inlet temperature which has been guided to storage container was changed in order to explore the impacts of the bed porosity and the rate of the flow on the total efficiency of the system. Latent storage system was observed to tremendously decrease the size of the solar heat storage system. It was also found that such systems are employed for occasional application in which the latent heat is able to be employed in excellent way.

Lee and Jones found an ice-on-coil thermal energy storage unit highly suitable for residential and light commercial state. In the time of charging, in order to be used during the peak energy demand, the water inside the evaporator tubes is frozen by the chiller that is a vapor compression refrigeration cycle employing refrigerant R22. The unit was approved to be used altering condenser, evaporator temperatures as well as the factors like the ice-building rate, heating, cooling, compressor power as well as energy efficiency ratio and power computation are explored. The findings show that in all the factors, energy efficiency raised when the condenser temperature went down. It is easy to measure the efficiency of energy as the heat transfer rates can also be gained without difficulty that is considered as one of the advantages of thermal energy storage systems while trying to reduce the loss of energy. Cheralathan *et al* (2007) explored an ice refrigeration system in their research. TES is highly relied on the medium that it is stored on.

2.3 Phase Change Material Properties and Selection

PCMs are the backbone of LHESS design which can be broken into organic and inorganic PCM types. Organic materials including fatty acids and paraffin are the most commonly studied materials for PCM energy storage. Organic materials are known for congruent melting or melting and freezing repeatedly without phase segregation or degradation of their thermal and material properties. They are also self-nucleate, meaning they crystallize with little or no sub-cooling and are generally not corrosive (A. Sharma et al., 2009). Sub-cooling occurs when the liquid PCM reaches a temperature below the solidification temperature before crystallizing. Inorganic PCMs, which include salt hydrates, have a volumetric thermal storage density higher than most organic compounds due to higher latent heat and density. As well, salt hydrates go through relatively small volume changes during melting process. However, most salt hydrates have poor nucleating properties which result in sub-cooling of the liquid PCM prior to freezing (Abhat, 1983).

In some cases, a small amount of sub-cooling may not be an issue, however, large amounts of sub-cooling, which are seen in some inorganic PCMs, consider as a problem for some systems (Farid, Khudhair, Razack, & Al-Hallaj, 2004). Also, thermal cycling studies using a DSC showed that inorganic PCMs have a high level of thermal properties deviation by their quoted and experimental properties (Shukla, Buddhi, & Sawhney, 2009). PCM selection for FTHX depends on the desired application of the system. Some criteria to choose a PCM are as follows (Abhat, 1983; Agyenim et al., 2010):

- Melting point in the desired temperature range for the application to assure storage and release of heat at a useful temperature;
- High latent heat of fusion to achieve high storage density;
- High specific heat so that sensible heat storage effects may play a role;

- High thermal conductivity;
- Small volume changes during phase transition;
- Exhibit little or no sub-cooling during solidification;
- Possess chemical stability, no chemical decomposition and no destructive corrosion of materials used in the LHESS;
- Contain no poisonous, flammable or explosive elements;
- Reasonable price and easily accessible

According to the above criteria, a PCM can be selected, which could meet all or most of the requirements for a STHX. However, the PCM selection for a SDHW system should be done carefully in order to produce hot water in an acceptable range of temperatures and to minimize safety concerns (such as PCM leaking into the building water supply) in the event of an accident (El Qarnia, 2009). Out of the two types discussed, organic PCMs were shown to be more advantageous to use in a STHX because they are less corrosive (A. Sharma et al., 2009), have less sub-cooling and less deviation of thermal properties during melting and freezing cycles than inorganic PCMs (Sarı & Kaygusuz, 2002).

A PCM should fit the desired melting point as well as latent heat demanded by the system in order to use the latent heat release completely while melting (discharge time). For instance, water ice is not employed as the PCM by a solar collector which charges a hot water latent thermal energy system due to the fact that water is liquid in room temperature. Similarly, heavy metals like iron and copper cannot be employed as a PMC because their melting temperature is extremely high and it is not accessible in solar collector. That is the justification for including several PCM materials in the literature. To make short, paraffin waxes are the only material mentioned along with a short outline of other PCMs which are popular. A comprehensive description of more than 250 PCMs and their features can be seen in Sharma and Sagara's study (S. Sharma, Iwata, Kitano, & Sagara, 2005). The paraffin waxes were observed to have high thermal stability after

several cycles were repeated by the DSC, indicating little to zero degradation of the latent heat and phase transition temperature ranges (Zalba, Sanchez-valverde, & Marín, 2005). Dodecanoic acid or Lauric acid has been observed to possess a fitting melting temperature range by thermal energy storage applied for Solar Domestic Hot Water energy storage (40ºC to 50ºC for a SDHW system) (R. E. Murray & Groulx, 2011). The other characteristics of this system are included having stable thermal properties, being safe to employ with domestic water and is easily accessible and affordable.

2.3.1 Paraffin Waxes

Paraffin wax is found to be a great choice for thermal storage employing a larger temperature source. Paraffin is generally regarded as alkaline hydrocarbons with the formula *CnH2n+2*. On the other hand, paraffin waxes are solids in which n is in the range of 20 to 40 and possess a melting point which is fairly higher that makes them perfect for heat storage. Table 2.1 shows an outline of some paraffin wax characteristics.

Table 2.1: Some common paraffin wax properties

Name	Chemical Formula	Melting Point (°C)	Latent Heat (kJ/kg)
n-Eicosane	$C_{20}H_{42}$	37	247
n-Docosane	$C_{22}H_{46}$	44	249
n-Tetracosane	$C_{24}H_{50}$	51	255
n-Hexacosane	$C_{26}H_{54}$	56	257
n-Octacosane	$C_{28}H_{58}$	61	255
n-Triacontane	$C_{30}H_{62}$	65	252

Nallusamy et al. (2007) suggested a mixed sensible and latent heat thermal energy storage system coupled with a solar heat source for the aim of cooling and heating in their study. Paraffin storage is conducted by spherical capsules in which they employed water as the heat transfer fluid. Water transfers the solar heat energy to the phase change

material capsules and performs the role of sensible heat storage medium simultaneously. This mechanism is examined and compared to a traditional sensible heat storage system and the findings show that it is wiser to employ latent storage system for intermittent applications such as indoor heating and hot water heating. El-Kotb *et al*. (2006) conducted another research on paraffin application suggesting an insulated flat plate heat exchanger that applies paraffin as phase change material. Generally, Water is used as the heat transfer fluid that is quite popular to be used in the majority of paraffin systems due to have a large specific heat capacity as well as cost saving. A numerical model is designed and experimental information was used to prove its validity. One of the benefits of this model is the outlet and inlet flows which can be carefully observed while the heat transfer rates and solid/liquid boundaries are explored.

2.3.2 Water/Ice

Basically, water acts as storage medium in most of the cold thermal energy storage systems. Among the advantages of application of water are high volumetric heat capacity, high specific heat, low cost and high latent heat. Moreover, it is employed in many usages because it is non-volatile and stable. Along with encapsulated ice, it can be used in ice slurry systems (Wang and Kusumoto, 2001), ice-on-coil (Lee and Jones, 1996) and finned tube heat exchangers (Kayansayan and Acar, 2006). The mentioned systems will be fully presented in the following part, "Latent TES Methods". Table 2.2 compared the thermophysical characteristics of water with other popular phase change materials briefly.

2.3.3 Other Types of PCMs

As the list was found to be incomplete, few more phase changer materials were explored to more carefully parallel the growing number of thermal energy storage usages. Slight difference in their latent heat and melting temperatures can improve the system performance. Consequently, few researches have been conducted to study the thermal

efficiency based on them the properties of other kinds of phase change materials have been mentioned in the literature part. For instance, Sari and Kaygusuz (2002) had studied the thermal performance of Lauric acid PCM experimental. The solidification and melting processes were closely observed in a vertical double-pipe system and a few of the characteristics were reported such as the rates and nature of the heat transfer, solidification and melting times and temperature distribution. It is interesting to mention that conduction has a major impact on the heat transfer which is more than any other factor during melting and solidification. Sari and Kaygusuz (2002, 2005 and 2006) conducted related research to find out the features of several paraffin waxes and fatty acids and their usages to thermal energy storage. Other PCMs also exist to compare, such as eutectic mixtures and hydrated salts, though for the aim of low temperature-low cost analysis, Table 2.2 includes a list of few viable fatty acids and paraffin waxes as well as inorganic PCMs.

Table 2.2: Some common inorganic, fatty acid and paraffin PCMs for comparison

Name	Chemical Formula	Latent Heat (kJ/kg)	Melting Point (^{o}C)
Water	H_2O	333	0
Sulfuric Acid	H_2SO_4	100	10.4
Lauric Acid	$C_{12}H_{24}O_4$	178	42-44
n-Pentacosane	$C_{25}H_{52}$	238	54
Stearic Acid	$C_{18}H_{36}O_2$	202.5	69

2.4 Latent TES Methods

As previously stated, few various methods exist to store thermal energy in a PCM according to their usages. Several influential aspects related to these systems can be mentioned such as design simplicity, cost, performance level and ecological impact. Regarding the mentioned causes, sour specific thermal energy storage techniques are considered to be more practical and efficient compared to others and have been closely

investigated in the literature. The mentioned methods are called ice-on-coil, wax PCMs, ice slurry and encapsulated PCMs. Ice slurry and ice-on-coil techniques are employed for cold TES and the other two techniques for both cold and warm usages.

2.5 Experimental Studies

This section presents experimental setups commonly used by other researchers along with the results and conclusions made concerning STHX geometry, operating parameters, and heat transfer enhancement designs.

2.5.1 Experimental Setups

One of the most common experimental setups consists of a STHX with a HTF pipe passing through the center with hot and cold constant temperature water baths (with temperature controllers to limit fluctuations) from which the HTF is circulated to charge/discharge the system. Thermocouples are commonly placed throughout the PCM and on the storage container while PCs and data acquisition (DAQ) systems of various kinds are used to record and save data (Agyenim, Eames, & Smyth, 2009; Ettouney, El-Dessouky, & Al-Kandari, 2004; Jian-you, 2008; Sarı & Kaygusuz, 2002). Flow controls such as throttling valves are used to keep the HTF flow rate constant. Heat exchangers or radiators are used in some experimental setups to discharge the energy in the HTF that has not been collected by the PCM (Agyenim et al., 2010; Kaygusuz & Sari, 2005). Figure 2.2 shows the common setup for experimental studies of PCMs (Agyenim et al., 2009).

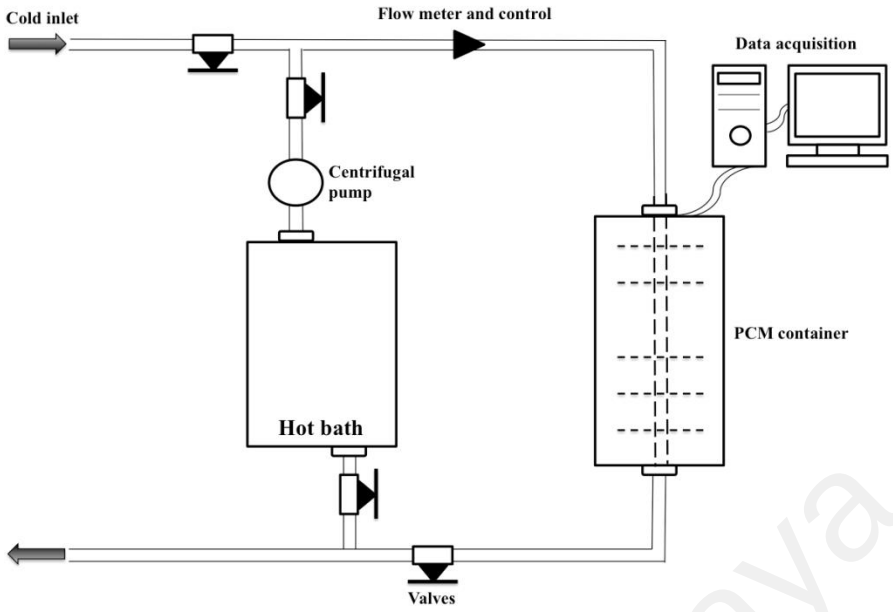

Figure 2.2: Typical experimental setup

An adjustment valve is applied in the piping section of the setup in order to control the Reynolds number. By using this, the effect of different Reynolds number on heat transfer is studied as shown in Figure 2.2.

2.5.2 Storage Geometry

Vertical cylindrical containers are the most common geometry for STHX. A figure showing the various types of PCM container geometries is given by (Agyenim & Hewitt, 2010).Vertical concentric pipe-in-pipe configurations with the HTF circulated inside the internal pipe through the PCM, which is in the annular space outside the metal HTF pipe, is a common configuration for consecutive charging/discharging experiments (Agyenim & Hewitt, 2010). Horizontal cylindrical LHESS has been used as well. In one experiment with a 1200 mm long, 375 mm diameter copper cylinder was used to hold RT-58 PCM, and a 65 mm diameter copper HTF pipe of the same length, with longitudinal fins for heat transfer, was placed centrally through the PCM (Agyenim & Hewitt, 2010). Although both vertical and horizontal cylindrical containers are common, there has been no direct comparison between them. A less common cylindrical container design is an inclined outer shell with the PCM in the annular space which is used for heat transfer enhancement

by natural convection. Results show, by use of paraffin wax PCM, an approximate 30 % decrease in the total melting time is noted in this configuration over a vertical outer shell (Akgün et al., 2007). Multi-tube arrays involve a cylindrical PCM container with two or more HTF tubes through the container. Multi-tubes result in significantly more melting than a single pipe-in-pipe geometry and experimental measurements have demonstrated earlier the onset of natural convection resulting in multiple convective cells which enhance melting (Agyenim et al., 2010). Multi-tube arrays were shown to enhance heat transfer for a horizontally oriented cylindrical container with $CaCl_2.6H_2O$ as the PCM (Kaygusuz, 1995).

Vertical multi-tube arrays were shown to be beneficial as well, due to the increased heat transfer surface area from the multiple HTF tubes, which results in higher heat fluxes. Higher heat fluxes in the vertically oriented container allow to increase the natural convection heat transfer (Hamada, Ohtsu, & Fukai, 2003). Although there are clear, advantages of this geometry, due to its more complicated nature, heat transfer and phase change behavior are more difficult to study experimentally. Rectangular flat plate containers were chosen for PCM storage by a research group because melting/solidification is symmetric about a plane at the center of the plate and the surface area to volume ratio for heat transfer is the largest compared with other geometries studied (Zalba et al., 2005). Experimental results for a stainless steel container, 100 mm wide, 100 mm thick, and 20 mm high, have shown that a rectangular container requires only half of the melting time of a cylindrical container with the same volume and heat transfer area (Zivkovic & Fujii, 2001).

Spherical containers are not as commonly used for LHESS but the research has been done on micro-encapsulated PCMs inside other LHESS geometries. Encapsulated PCMs which have a barrier protecting the PCM from harmful interaction with the environment

provide sufficient surface area for heat transfer and provide structural stability. Microencapsulation is not commonly used because it is more expensive and the matrix reduces the heat transfer through the PCM in order to limit the natural convection (Regin, Solanki, & Saini, 2008). Researchers have also studied experimental systems in which PCMs are built directly into solar collectors (ALVA S, Gonzalez, & Dukhan, 2006; E. B. S. Mettawee & G. M. R. Assassa, 2006). In these cases, PCM has a direct contact with the energy source (i.e. the solar collector) which has been shown to enhance the energy storage rate. It was found, using of this type of setup has a smaller solar collector surface area for heat collection and larger PCM surface area for heat transfer, which results in lower outlet HTF temperatures and more energy storage in the PCM, but it also increases cost of the LHESS due to the requirement of a larger amount of PCM (Koca, Oztop, Koyun, & Varol, 2008).

2.5.3 System Operating Parameters

Some operating parameters can be adjusted to achieve optimum operation and storage capacity of a STHX. These parameters include the HTF temperature at the inlet of the LHESS, the flow rate and HTF direction (Castell et al., 2008). Of the parameters studied experimentally, an increase in the HTF inlet temperature has been shown as lead to a decrease in the melting time (Akgün et al., 2007) and an increase in the amount of energy that can be stored (Agyenim & Hewitt, 2010; Jian-you, 2008). In one experiment where Dodecanoic acid was filled the annular space between the PCM container and the HTF pipe, the average heat transfer rates were found to enhance when the inlet HTF temperature was increased during melting and the average heat transfer rates decreased while the inlet HTF temperature was decreased during solidification (Sarı & Kaygusuz, 2002). Also, at lower flow rates during charging, the PCM temperatures took longer to increase, resulting in lower energy storage rates (Jian-you, 2008; E. B. S. Mettawee & G. M. R. Assassa, 2006). It was shown for a vertical pipe-in-pipe LHESS configuration that

natural convection effects played a major role during melting when the HTF entered the container from the bottom of the LHESS but were not significant while the HTF entered by the top of the container (Ettouney et al., 2004). Furthermore, in a 1200 mm long and 90 mm diameter vertically oriented pipe-in-pipe STHX configuration with $CaCl_2$ as the PCM, using air as the HTF had shown the increased results of reliability by allowing the longer cycle durations (Bajnoczy, Gagyi Palffy, & Prépostffy, 1999).

2.6 Heat Transfer in a Shell-and-Tube Heat Exchanger

Many researchers have shown the advantages of using PCMs for energy storage. STHX operating parameters such as flow rates and temperatures of HTFs have been explored as well by both numerical and experimental studies. Previous works published on LHESS have guided the design of the experimental STHX used in this thesis. This literature review clearly demonstrates the need for experimental works in studying the operating parameters such as flow rates, charging time and changing fin spacing in charging and discharging mode of a STHX to use in a SDHW system. The melting or solidification periods of a particular PCM must be known in order to design a latent heat storage unit. The operating circumstances and the storage configurations also must be known in order to forecast the heat transfer coefficients during the phase change process.

It is seen that two kinds of storage configurations were studied in the literature in which one of them is the shell and tube type heat exchanger. In this kind of heat storage unit, the PCM is kept in the shell and the heat transfer fluid is allowed to flow in the tubes (Y. Zhang & Faghri, 1996a). The second configuration is a rigid capsule in which the PCM is put in this capsule and the heat transfer fluid flows in a tube surrounding the capsule. The shell and tube type heat exchanger is considered as the most promising configuration as a latent heat storage system that provides high efficiency for a minimum volume (Erek, Ilken, & Acar, 2005). Ismail and Alves (1986) presented a theoretical model of the shell

and tube type heat exchanger for storing energy. A similar problem is also modeled by (Yrn Cao & Faghri, 1991). In this model, the circulating fluid carried out the heat charging and the recovery processes. The shell wall of the storage unit was presumed to be adiabatic for both of these models. The energy storage model in a shell and tube type heat exchanger was also examined by Bellecci et al. (Bellecci & Conti, 1993) where they used the enthalpy model to solve the problem. Y Cao et al. had (Y. Cao, Faghri, & Juhasz, 1991) searched the latent heat energy storage systems for annular and countercurrent flows separately. Also, they stated that the storage system with the countercurrent flow is an efficient method to absorb heat energy (Erek et al., 2005).

Generally, increasing the heat transfer surface area by using finned surfaces is one of the techniques used in order to enhance the amount of energy storage. Therefore, a great number of researches both experimental and theoretical were done in order to explore the effect of fins with rectangular cross section on the rate of melting and solidification. In this case, Bathelt and Viskanta (1981) carried out a study of the solidification around a horizontal finned tube with four different fin spacing. L. Cabeza et al. have (L. Cabeza, Mehling, Hiebler, & Ziegler, 2002) experimentally researched the forms of the frozen layer on finned tubes where the finned tubes were situated vertically in those experiments. Jegadheeswaran et al. (Jegadheeswaran & Pohekar, 2009) theoretically examined the solidification within two concentric cylinders which had longitudinal fins. In that study, a relation regarding the percent of solidification to the fin thickness and length, the number of fins, the Stefan and Fourier numbers of the problem were represented. In another study, (Sasaguchi, Kusano, & Viskanta, 1997) theoretically investigated the melting event on the same geometry. The noteworthy effect of the natural convection on melting was stated in this study. Lacroix (Lacroix, 1993) represented a theoretical model in order to estimate the transient behavior of a shell and tube heat exchanger by placing the PCM on the shell side and heat transfer fluid circulating through the finned tube (Erek

et al., 2005). In this regard, the fact that heat transfer in a latent thermal energy storage system can be increased by placing internally finned tubes which was showed by (Y. Zhang & Faghri, 1996a). In this study, fully developed velocity profile of the heat transfer fluid in the tube is considered. Erek et al. (Erek et al., 2005) developed a two-dimensional numerical model to predict the effect of fin dimensions and operation parameters (fin space, fin diameter, Re number, and heat transfer fluid inlet temperature) on the melting/solidification processes of PCM in the shell-and-tube type heat exchanger.

Balikowski and Mollendorf (Balikowski & Mollendorf, 2007) studied the effect of using a spined pipe tube and smooth pipe heat exchanger with two types of PCMs on the charging/discharging of heat exchanger with different PCMs in the annular gap. Stritih (U. Stritih, 2004) added a rectangular external fin to enhance heat transfer during melting/solidification of a latent heat storage for thermal applications in buildings. B len et al. (B len, Takgil, & Kaygusuz, 2008) investigated the melting/ solidification characteristics of ($CaCl_2.6H_2O$) as a PCM in a two-concentric pipe energy storage system. Different designs and operation parameters were studied including the number of fins inside the PCM, mass flow rate and inlet heat transfer fluid (HTF) temperature. However, in recent years study on the tube-in-shell PCM storage geometries is considered as a significant issue in this research field. For a vertical tube-in-shell storage geometry, there are numerous studies which comprehensively investigated both experimentally and numerically the transient melting and solidification behaviors of paraffin in a vertical shell-in-tube latent thermal energy storage unit (Jesumathy, Udayakumar, & Suresh, 2012; Shmueli, Ziskind, & Letan, 2010; Trp, Lenic, & Frankovic, 2006).

However, the horizontal tube-in-shell storage geometry has achieved great attention in solar energy application (T. Zhang, Tang, Lu, Wang, & Sun, 2015). In another research, Bathelt and Viskanta (Bathelt, Viskanta, & Leidenfrost, 1979) investigated the heat

transfer of n-paraffin during melting from a horizontal cylindrical heat source with a uniform surface heat flux and surface temperature. They reported that melting behavior in the upper half of the annulus is much more enhanced than that in the lower half because of the ascending melt flow due to the natural convection. Cao and Faghri (Yiding Cao & Faghri, 1990) numerically studied performance of a horizontal thermal energy module. In a similar numerical study, Cao et al. (Yrn Cao & Faghri, 1991) investigated latent heat thermal energy storage system with both annular and countercurrent flows. Zhang and Faghri (Y. Zhang & Faghri, 1996b) obtained a semi-analytical solution for the melting behavior of PCM loaded in a horizontal tube-in-shell system.

Seeniraj et al. (Seeniraj & Narasimhan, 2008) numerically studied performance of a latent heat energy storage system with both finned-tube and multiple PCM by employing the enthalpy method. Dutta et al. (Dutta, Atta, & Dutta, 2008) studied melting of paraffin wax in a horizontal annulus both experimentally and numerically. Ezan et al. (Ezan, Ozdogan, & Erek, 2011) investigated energetic and exergetic performances of horizontal latent energy storage systems both for charging and discharging processes. Ismail and Lino (Ismail & Lino, 2011) experimentally studied enhancement of the melting process through the usage of fins and turbulence promoters in a horizontal tube-in-shell storage system. Hosseini et al. (Hosseini, Ranjbar, Sedighi, & Rahimi, 2012) experimentally studied the role of buoyancy effects on the PCM melting in the horizontal tube-in-shell storage unit. The surveys in the presented literature indicate that the main constraint of previous studies is the use of the maximum 80% capacity of the PCM container in vertical and horizontal tube-in-shell PCM storage geometries. To the best of our knowledge, no research has been carried out on investigation of thermal energy storage performance of PCM that is using the full capacity of PCM container in processes, charging and discharging latent heat energy.

2.7 Limitation of Phase Change Materials

Over the last three decades, the thermal energy storage of phase-change materials (PCMs) have been intensively studied by numerous researchers because of their high thermal energy and their potential to apply in different engineering fields such as thermal storage of building structures (Cossi, Rega, Scalmani, & Barone, 2003; Zhou, Zhao, & Tian, 2012), building equipment such as domestic hot water, heating and cooling systems (Arkar & Medved, 2007; Hawlader, Uddin, & Khin, 2003), electronic products (Nemykin, Makarova, Grosland, Hadt, & Koposov, 2007; Sato & Sakaki, 2004), drying technology (Al-Abidi, Mat, Sopian, Sulaiman, & Mohammad, 2013; Çakmak & Yıldız, 2011), waste heat recovery (Maruoka & Akiyama, 2003; Maruoka, Sato, Yagi, & Akiyama, 2002), refrigeration and cold storage (Uroš Stritih & Butala, 2010), solar air collectors (E.-B. S. Mettawee & G. M. Assassa, 2006; Wang, Tang, & Zhang, 2012) and solar cookers (Roy et al., 2015; S. Sharma et al., 2005) with wide temperatures ranges.

Using the PCM as thermal energy storage is critical due to the mismatch between energy supply and demand is eliminated and also the efficiency of solar energy systems is improved. However, PCMs have limited use as thermal energy storage devices because of their low thermal conductivity. This disadvantage lengthens the time necessary to complete the melting and solidification processes. Several researchers investigated heat transfer enhancement in PCMs using various techniques such as insertion of a metal matrix in the PCM (Lafdi, Mesalhy, & Elgafy, 2008; Liang, Chen, Sun, Zhu, & Li, 2014), bubble agitation in PCMs (Mohamed, 2005), PCM dispersed with high-conductivity particles (Sundarraj, Maity, Roy, & Taylor, 2014; Tang, Sun, Yu, & Wang, 2014), multiple families of PCMs in LHTES, multi-tubes and specially the use of finned tubes (Al-Abidi et al., 2013; Mat, Al-Abidi, Sopian, Sulaiman, & Mohammad, 2013).

2.8 Heat Transfer Enhancement of PCMs

Regarding the low thermal conductivity of PCMs, designs to enhance heat transfer were identified in order to increase energy storage rates and decrease charging time and extend discharging time of a LHESS (Mettawee & Assassa, 2007). Many different methods were studied to increase the heat transfer through PCMs. These methods include extended fins, multi-tube arrays, bubble agitation, metal rings, metal matrixes and brushes and encapsulation (Jegadheeswaran & Pohekar, 2009). These studies were performed to determine which of these heat transfer enhancement methods are the most advantageous and the use of fins and high conductivity matrixes were shown to be the most attractive options (Kenisarin & Mahkamov, 2007). Comparing three different enhancement techniques including internal longitudinal fins, lessening rings and bubble agitation, showed that lessening rings and fins are acceptable in situations where solidification enhancement is required; and the bubble agitation is useful only when melting enhancement is required (Velraj, Seeniraj, Hafner, Faber, & Schwarzer, 1999). Varieties of fin configurations were studied and found to be an effective and inexpensive way to enhance heat transfer. When heat is being transferred between the PCM and HTF, fins could be either on the PCM side or on the HTF side.

Fins are usually placed on the side that has the lowest thermal conductivity because this will result in higher fin efficiency, so normally fins extend into the PCM. Fins can be either vertical (longitudinal in the case of a cylindrical container) or horizontal (radial in the case of a cylindrical container). Radial fins were experimentally shown to aid conduction heat transfer and result in the largest increase in heat transfer rates during the solidification process whereas longitudinal fins have the most increase in heat transfer during melting (Nagano, 2004). This is because of the radial fins inhibit natural convection for the case of vertical cylindrical systems during the melting process whereas longitudinal fins do not (Nagano, 2004). In an analytical study, radial fins were found to

be the most effective fin type (Lacroix, 1993), however most experimental results show that longitudinal fins are the best to decrease the time required for PCM melting and solidification (Agyenim et al., 2009; R. Murray et al., 2011). The presence of fins also decreases the overall PCM volume in the system, thus the total storage capacity is decreased. Therefore the advantages of fin additions may be outweighed by the disadvantages (U. Stritih, 2004). For example, a simple increase in the number of fins on the PCM side has been shown to result in insufficient enhancement of heat transfer to compensate the reduced PCM volume for energy storage (Nagano, 2004).

Using longer fins were also shown to decrease the solidification time of the PCM and to promote a higher natural convection heat transfer coefficient over a smaller change in temperature (Castell et al., 2008). A combined numerical and experimental study suggested that a metallic tube fitted with four or five longitudinal fins with a radial length around twice the tube diameter is the best compromise among the efficiency, increase in the heat flow rate, and loss of available storage capacity. The effectiveness of fins at enhancing the heat transfer also depends on the mechanism of heat transfer (melting or solidification). For example, fins were shown to be more effective during solidification than melting in a rectangular container because natural convection, which is dominant during melting, is reduced by the addition of these fins (U. Stritih, 2004). The effects of carbon fiber chips and carbon brushes as additives to a PCM used in a LHESS were studied. The results showed that the addition of carbon fiber chips (fiber diameter 10 μm, fiber length 5 mm) results in a higher effective thermal conductivity of the bulk PCM for the vertically arranged cylindrical container made of acrylic resin with n-octadecane PCM (Hamada et al., 2003). However, the thermal resistance near the heat transfer surface was higher than that of the carbon brushes (brush diameter 110 mm, axial length 60 mm); therefore, the overall heat transfer rate for the fiber chips was lower in comparison with the carbon brushes, even though the effective thermal conductivity of the bulk PCM with

the fiber chips is higher (Hamada et al., 2003). Another study is compared stainless steel pieces, copper pieces and a new PCM-graphite composite material, all inside a rectangular storage tank with dimensions of 107 mm height, 105 mm width, and 430 mm length. Graphite composites were found to increase more heat transfer over stainless steel or copper tube. This is because the effect of inserting metal pieces into the PCM is only useful if the metallic material has very high conductivity to make up for the storage capacity loss due to the decreased volume of PCM (L. Cabeza et al., 2002).

Using an experimental setup which combines storing latent and sensible heat using a combination of PCM and water inside a storage container is beneficial for SDHW applications (Canbazoğlu, Şahinaslan, Ekmekyapar, Aksoy, & Akarsu, 2005). In a system with energy input from a flat plate solar collector, a combined storage system using water and paraffin wax (with the wax inside aluminum bottles in the vertical cylindrical storage container), kept the storage water temperature over 45ºC under all operational and climatic conditions (Al-Hinti et al., 2010). However, a one hour time lag was noticed between the peak solar radiation and the peak water temperature in the tank. It was demonstrated that in cases of high domestic water consumption during evening hours, the existence of the PCM partially recovers the water temperature and extends the effective operational time of the system (Al-Hinti et al., 2010). As well, the rate of energy storage, the mass of hot water produced and the heat accumulated in the storage tank were several times greater when using PCM in the storage tank than that of conventional solar energy system using a heat storage tank with just water (Canbazoğlu et al., 2005). The system comprised of a granular PCM–graphite compound (90 vol.% of sodium acetate and 10 vol.% graphite) in aluminum bottles at the top of a water storage tank connected to flat plate solar collectors. The energy density of the storage container increase of 57% with four PCM bottles to 78% with six PCM bottles: more PCM inside the storage tank results in a higher energy density (L. F. Cabeza, Ibanez, Sole, Roca, & Nogués, 2006). Along

with the advantages already discussed, thermal stratification can be employed to improve the efficiency of storage tanks. This is because the PCM at an intermediate temperature in the middle of the storage tank (not high enough temperature to heat the top layer) transfers energy to heat the lower, colder layers (Mehling, Cabeza, Hippeli, & Hiebler, 2003). Energy density improvements of 20 to 45 % were shown by using a cylindrical tank with a diameter of 20 cm and a height of 120 cm. This type of heat storage is a good use of low-temperature heat and/or waste heat (Mehling et al., 2003). However, if the thermal conductivity of the PCM container material is low, the actual melting time of the PCM is longer than the theoretical melting time and therefore, the cylindrical container materials and dimensions should be selected carefully (Kaygusuz & Sari, 2005).

One way optimize the latent heat that can be stored in a system is to use multiple PCMs with various melting temperatures so that latent energy is collected over a broader range of temperatures. If the phase change temperature of the PCM corresponds to a variety of solar conditions, a phase transition will occur on all days when the solar gain exceeds a certain value (Bajnoczy et al., 1999). An increased cumulative storage capacity was shown in a cylindrical LHESS, 1200 mm long and 90 mm in diameter, with a two-grade heat storage system (a combination of 60 to 30 ºC using $CaCl_2.4H_2O$ and 30 to 20 ºC using $CaCl_2.6H_2O$) compared to a single-grade system (using only $CaCl_2.6H_2O$) (Bajnoczy et al., 1999). Therefore, improvements in charging and discharging rates were observed in a LHESS using three PCMs with various melting temperatures (Watanabe et al., 1993). By wide spread application of heat transfer in industry, the demand for efficiency has significantly risen, which resulted in development of recent inventive methods. Improving the efficiency of heat treatment devices which has enhanced the energy consumption on one hand and has reduced the size of such devices on the other hand resulted the material and production costs which have to be reduced. Such enhancements were possible through increasing the surface area in contact per unit

volume which causes devastating pressure drops and requires more powerful pumps. In addition to that, the price of heat transfer equipment escalates. Nanotechnology advancements in general along with application of nanofluids as heat transfer medium are breakthrough in the past two decades.

2.9 The Application of Nano-fluids in Forced Convection Heat Transfer

Choi, in 1995 was the first to present the concept of nanofluids (Choi & Eastman, 1995). Nanofluids are basically heat conducting fluids which consists of a base fluid incorporating suspended particles in the range of 1~100 nm. Meanwhile solid particles have better thermal conductivity compared to conventional base fluid, as a result the addition of solid nanoparticles is expected to increase thermal conductivity of the nanofluid (Abouali & Ahmadi, 2012; Afshar, Shams, Nainian, & Ahmadi, 2012). For example, thermal conductivity of solid particle of Cu (copper) is 700 and 3,000 times greater than the thermal conductivity of water or engine oil as liquids, respectively (Hassan et al., 2013). The addition of micro-sized solid materials to the base fluids was proposed decades ago. It was established that the micro-particles tend to settle from suspension; resulting in blocking channels, pipes and heat exchangers. Moreover, accumulation of such abrasive solid particles causes erosion, corrosion in pipes, damage in pumps and other devices. Application of nanofluids that maintain suspended nano-sized particles in base fluids would lessen the effect of erosion, corrosion, fouling and the pipe blockings.

2.9.1 Experimental Studies in Tubes and Ducts

Pak and Cho (1998) was the first to present studies on nanofluids convection heat transfer and fluid flow through a tube with 10.66 mm diameter namely “dispersed fluid with submicron particles”, with sufficient size about 13 nm and 27 nm for being named after as nanofluid. Considerable rise in heat transfer coefficient were observed in turbulent

regime with suspending particles. In addition, it was observed that the Dittus–Boelter formulation for pure water as well as a water/nanoparticles fluid flow can be applicable in this experiment. The increase in the heat transfer coefficient was 45% and 75% with 1.34% and 2.78% Al_2O_3 nanoparticles accordingly. It is apparent that this phenomenon is not dependent on the increase in conductivity solely and the resulting enhancement in the heat transfer through convection cannot be attributed to the rise only in the nanofluid conductivity. However, their overall depiction is gloomy. It is identified that the friction factor of Darcy is following the Kays correlation. Therefore, due to the viscosity increment, considerable frictional pressure drop would occur. Meaning that, even though nanofluid heat transfer coefficient rises, substantial pressure drop occurs consequently.

Applications of convection heat transfer always involve the challenge of heat transfer enhancement versus undesired resulting pressure drop. Boundary layer interruption, more complete turbulent flow creation or other similar heat transfer enhancement methods have relative pressure penalty which results in requirement of a higher pumping power that may counterbalance heat transfer enhancement effects. Better picture can be obtained by comparing enhancements of heat transfer at the pumping power identical to the prior works. Pak and Cho (1998) stated that for γ-Al_2O_3/water and TiO_2/water nanofluids with constant average velocity about 3% to 12% heat transfer coefficient decline was obtained in comparison with pure water. Regarding this, pure slightly bigger (≈100 nm) copper particles and a carefully designed test loops were used in this experiment (Figure 2.3) (Li et al., 2003). The graph of heat transfer coefficient measurement versus the velocity demonstrates a great increment in convection heat transfer using nanofluids. On the one hand, this result opposes Pak and Cho (1998) interpretation for fluid which flows constantly at an average velocity in which the heat transfer coefficient would decline as low as 12% when containing nanofluids. Conversely, Li et al. (2003) showed a 40% rise in heat transfer coefficient for the same velocity. These researchers explained this conflict

between their work and Pak and Cho (1998) study shows in this case that the high increase in viscosity could have suppressed the turbulence which has resulted in reduction of the heat transfer.

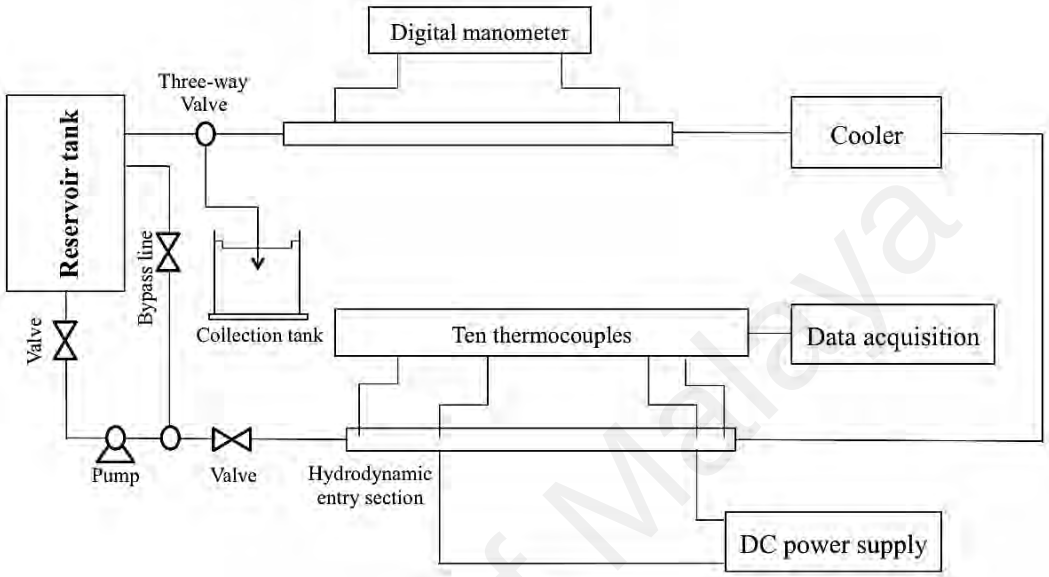

Figure 2.3: Convection test loop.

Therefore, they specified that the volume fractions, the dimension of the particle as well as material characteristics are significant. Moreover, having designed the experimental system appropriately, a considerable increase in coefficient of heat transfer is obtainable. Further essential investigations on convection heat transfer in nanofluids were conducted by Wen and Ding (2004) which is important in different aspects. Predominantly, it appeared to be the primary research in which to observe the effect of the entry-length. Longer hydrodynamic and thermal entering sections are often found in the laminar flows. In these sections of the flow, the heat transfer coefficient is higher because the boundary layer is thinner. The local heat transfer coefficient through the tube during laminar flow was measured by Wen and Ding (2004). Different water/γ-Al_2O_3 nanofluids were used to flow through a 4.5 mm internal diameter with 970 mm length copper tube in their study. Considerable increase in convective heat transfer coefficient was observable all throughout. This increase was greatest at the entry-length section and

it was further enhanced as the concentration of the particle increased. This confirms that both steady entrance section and other heat transfer enhancement systems like boundary layer interruptions as well as creation of artificial entrance can be used as "smart" choice to augment heat transfer. Investigations on a test rig which was similar to previous experimental setups were conducted by Yang, Zhang, Grulke, Anderson and Wu (2005) wherein tubes with 4.57 mm inner diameter and 457 mm (i.e., 100 diameters) length were used. A significant feature of the issued test loop was the small holdup fluid volume and application of water with high temperature to heat instead of heating by electricity.

The second characteristic is rather more significant because of the fact that Kabelac and Kuhnke (2006) research demonstrated that heating by electricity can affect motions of nanofluids particle and it makes possible that particles carry electrical charge. Four dissimilar experimental fluids with diverse combinations of two base fluids and graphite nanoparticles, ranging between 2% to 2.5% concentration were tested by Yang et al. (2005). Used particles were disk-shaped with 20 to 40 nm diameter and 1 to 2 nm thicknesses. Yang et al. (2005) concluded that loading of particles, source of nanoparticles, temperature and base fluid influence the results of heat transfer. However, multiple data deviations in different papers are obtained compared with the Yang et al. (2005) research . This may happen due to the particles shape (disk shape) and their major dimension which is their diameter, being rather large. This disqualifies them to be named as nanoparticles and creates the uncertainty whether this work can be categorized as nanofluid at all. Zeinali Heris, Etemad, and Nasr Esfahany (2006) study has resulted in similar conclusions as obtained by Li et al. (2003). Moreover, the experiment was performed using a copper tube with 6 mm diameter for water/Al_2O_3 as well as water/CuO nanofluids. The higher enhancement in convective heat transfer was reported for Al_2O_3-based nanofluid compared to water/CuO nanofluid. As a result, two major observations

in this effort are as follows; heat transfer enhances considerably with particle volume fraction augmentation as well as enhancements are more at greater Peclet numbers.

Altogether, it seems that size distribution, particle source, preparation method, dispersion technique, value of pH and many other factors are accountable for the divergent trends in data collected experimentally between Li et al. (2003), Wen and Ding (2004) and Zeinali Heris et al. (2006) on one hand and Pak and Cho (1998) and Yang et al. (2005) on the other. Another experiment on convection which contains carbon nanotube (CNTs) as nanoparticles was conducted by Ding, Alias, Wen, and Williams (2006). Multi-walled carbon nanotubes (MWCNTs) followed by a setup which consisted of a 4.5 mm inner diameter tube were used in that study (Figure 2.4) (Ding et al., 2006). The tube was electrically heated and the rotors with high speed (at about 24,000 rpm) were used in order to disperse the nanomaterials in base fluid to avoid CNTs agglomeration. Measuring the thermal conductivity of the nanofluids showed 50% thermal conductivity enhancement by adding 0.7% CNT to base fluid. It appeared that temperature tremendously influence conductivity with just 10% increase in suspension temperature. Their work also showed great improvement with respect to convective heat transfer. The enhancements were tested by factors such as concentration of particle, Reynolds number, axial distance and pH value. At Re=800, about 350% enhancement were observed for convective heat transfer coefficient. Furthermore, the enhancement was found to increase abruptly above a certain Reynolds number which was then related to shear thinning behavior of the working fluid.

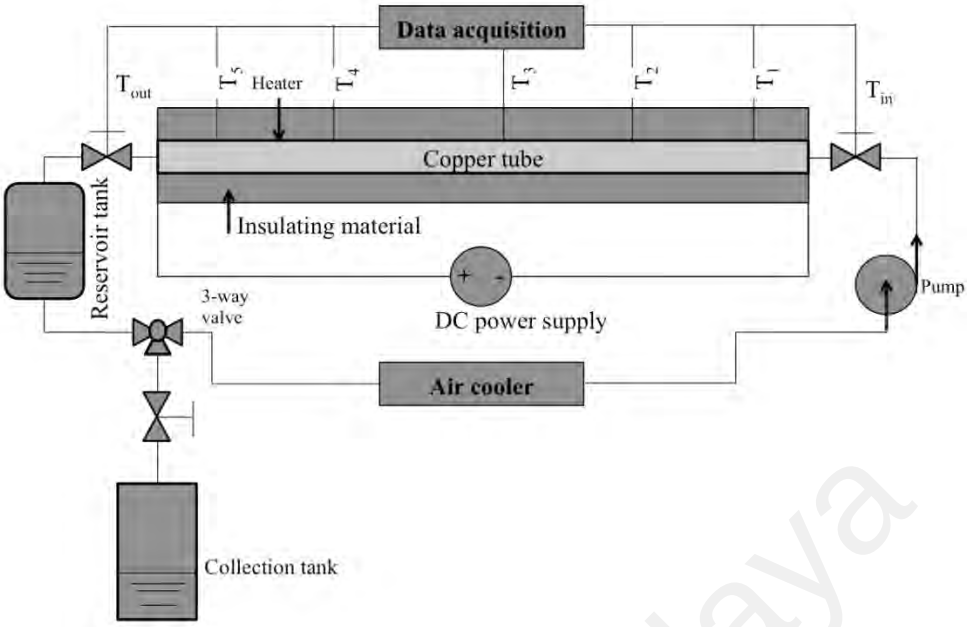

Figure 2.4: The schematic of experimental setup.

Turbulent convective heat transfer of dilute Al_2O_3/water nanofluid through a circular pipe was experimentally studied by Fotukian and Nasr Esfahany (2010) as it can be seen in Figure 2.5 which demonstrates their experimental setup (Fotukian & Nasr Esfahany, 2010). The tests were performed on Al_2O_3/water nanofluids with 0.03%, 0.054% as well as 0.135% loading and the Reynolds number variation was from 6000 to 31000. Data obtained from experiments illustrated that adding minor quantity of nanoparticles to pure water considerably enhances the heat transfer. The maximum value of 48% rise in the heat transfer coefficient in comparison with pure water was obtained for 0.054% volume density at Re=10000. Addition of further nanoparticle concentration did not enhance heat transfer in turbulent section. Consequently, the ratio of heat transfer coefficient of pure water to nanofluid enhanced by increasing the Reynolds number. That's while, for Re= 2000 and nanofluid volume concentration equal to 0.135%, a rise of 30% in pressure drop was observed in comparison with pure water.

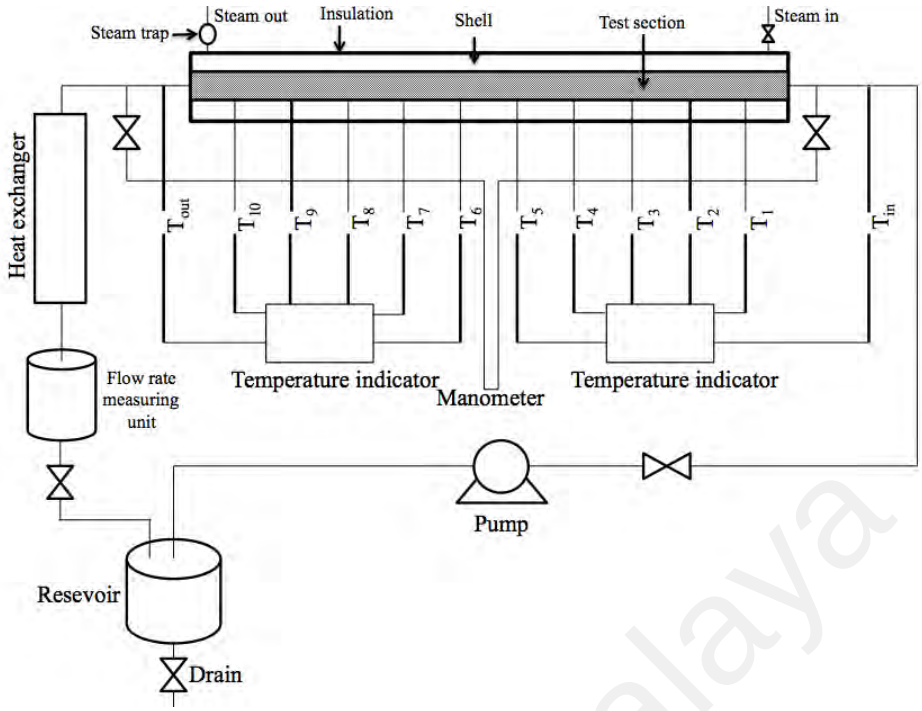

Figure 2.5: Experimental apparatus for water–Al_2O_3 nanofluid convection study.

Vajjha, Das, and Kulkarni (2010) experimentally investigated the forced convective heat transfer of nanofluids comprised of aluminum oxide, copper oxide and silicon dioxide dispersed in ethylene glycol and water in the fully developed turbulent regime. They also introduced an experimental correlation for Nusselt number for the above mentioned nanofluids. The heat transfer enhancement of low volume concentration Al_2O_3 nanofluid with longitudinal strip inserts in a circular tube were experimentally investigated by Sundar and Sharma (2010) (Figure 2.6) (Sundar & Sharma, 2010). The main objective of the study was to investigate Al_2O_3/water nanofluid convection heat transfer and friction factor with various aspect ratios. Experimentations were performed by water and nanofluid Reynolds number in the range between 3000 and 22000, alumina volume concentration (φ) 0 %≤ φ ≤ 0.5% and longitudinal strip aspect ratio (AR) in the range between 1 and 18. The friction factor of 0.5% volume concentration nanofluid with longitudinal strip insert with aspect ratio of 1 is 5.5 times more at Re=3000 and 3.6 times greater at Re=22000 compared with pure water or nanofluid flowing through a normal tube. The heat transfer coefficient of 0.5% volume concentration Al_2O_3 nanofluid with

longitudinal strip insert with aspect ratio of AR = 1 was 50.12% and 55.73% higher at Reynolds number of 3000 and 22000, respectively when compared to the same nanofluid. These enhancements were 76.20% and 80.19%, in comparison with pure water flowing in a normal tube.

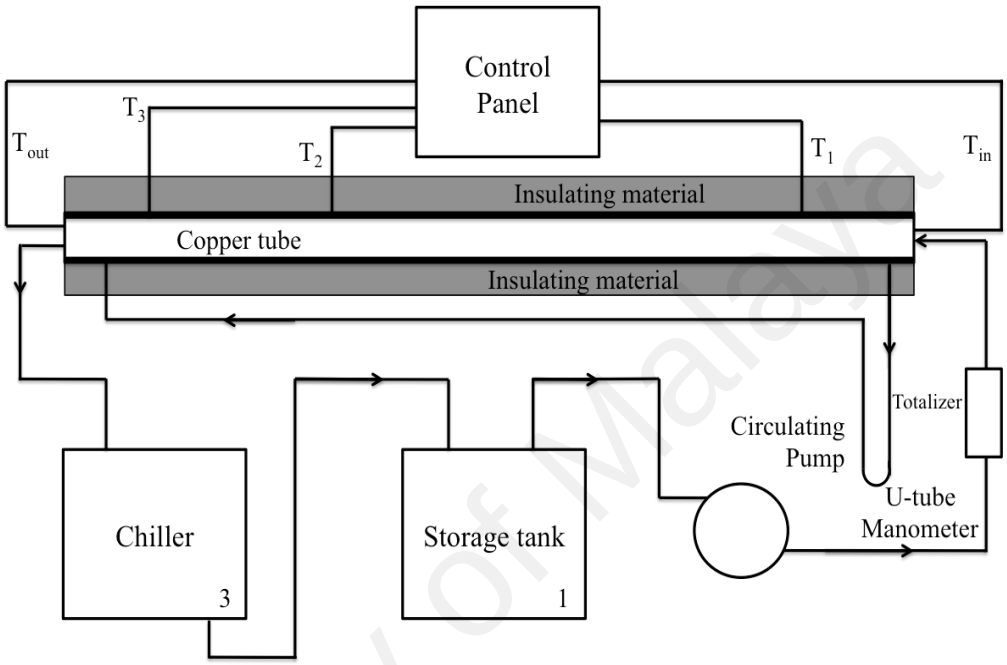

Figure 2.6: Schematic diagram of the experimental setup.

Nanofluid heat transfer was tested through annular duct by Nasiri, Etemad, and Bagheri (2011). Figure 2.7 demonstrates the schematic of their experimental setup (Nasiri et al., 2011). The selected nanofluids were Al_2O_3 and TiO_2 using water as the base fluid. Reynolds number for the two nanofluids ranged from 4000 to 13000 and the volume concentrations of two types of nanofluids were selected equal to 0.1%, 0.5%, 1.0% and 1.5%. The Nusselt numbers of the two nanofluids were greater than those of the base fluid and more enhancements were obtained by nanoparticle concentration augmentation. At Peclet number of about 24400, the enhancements of Nusselt number for Al_2O_3/water nanofluid with concentration of 0.1%, 0.5%, 1.0% and 1.5% were 2.2%, 9%, 17% and 23.8%, respectively. At Peclet number of 53200, the Nusselt number enhancement for TiO_2/water nanofluid with particle concentration of 0.1%, 0.5%, 1.0% and 1.5% were

1%, 2%, 5.1% and 10.1%, respectively. Relative heat transfer coefficient was enhanced by nanoparticle concentration augmentation for both nanofluids. This could be because of the presence of the Brownian motion, nanofluid thermal conductivity, thinner boundary layer thickness, nanoparticle migration in nanofluid and probable slip velocity at adjacent to the walls. Comparison between the two nanofluids also showed similar properties for both working fluids in equal particle concentration. This could be corresponded to the greater thermal conductivity and smaller Al_2O_3 particle size in Al_2O_3/water nanofluid.

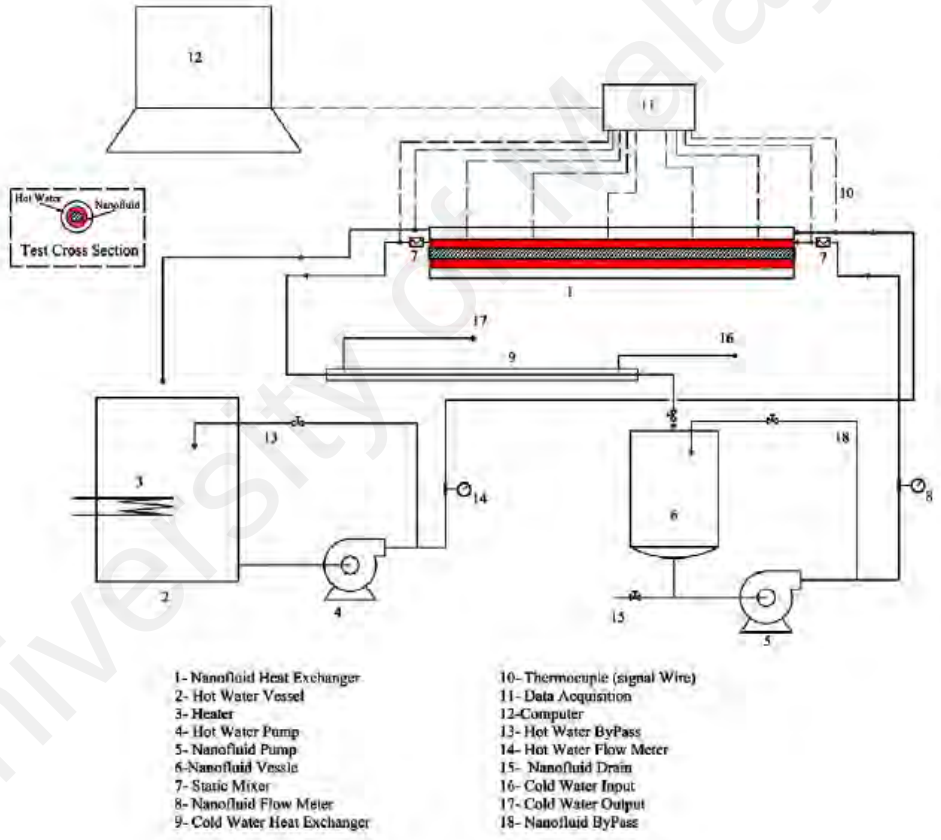

Figure 2.7: The schematic of experimental setup.

2.9.2 Inside Heat Exchangers:

Variety of heat exchangers has been widely employed in different engineering applications. Examples are double pipe or plate heat exchangers used in power production and recovery, food processing, chemical industry and mechanical appliances such as air

conditions, refrigerators and ventilators (Layton, Reap, Bras, & Weissburg, 2012; M. Liu, Lin, & Wang, 2011). In recent years, efforts have been made to enhance heat transfer performance of heat exchangers. The applied methods mostly include creation of turbulent flow (Maddah, Aghayari, Farokhi, Jahanizadeh, & Ashtary, 2014; Maddah, Alizadeh, Ghasemi, & Alwi, 2014), use of fins, twisters and baffles (Azmi et al., 2014; Karmo, Ajib, & Khateeb, 2013; Mohammed, Hasan, & Wahid, 2013). An obstacle in heat transfer improvement of heat exchangers is the limited thermal properties of conventional coolants. Nevertheless, improvement of the thermal efficiency of a plate heat exchanger would require an augmentation in the thermal capability of the working fluid (Dwivedi & Das, 2007) which was taken into account by Choi and Eastman (1995) who introduced nanofluids for the first time.

Nano fluids enhance the heat transfer because (a) nanoparticles increase the thermal conductivity of the operating fluid which eventually enhances the heat transfer efficiency of the system (Goodarzi et al., 2014) and (b) as the temperature increases, the Brownian motion of nanoparticles increases which improves the convective heat transfer of the fluid (Malvandi & Ganji, 2014). Many attempts have been performed in the field of nanofluids by different researches in recent years (Hedayati, Malvandi, Kaffash, & Ganji, 2015; Karimipour et al., 2014). Some of these works are concentrated on nanofluid usages in various classes of heat exchangers (Anoop, Cox, & Sadr, 2013; Khoshvaght-Aliabadi, Zamzamian, & Hormozi, 2014; Tiwari, Ghosh, & Sarkar, 2013). Pantzali, Kanaris, Antoniadis, Mouza, and Paras (2009) studied numerically and experimentally the influence of 4 vol. % CuO/water nanofluids on the efficiency of a miniature plate heat exchanger with modulated surface. Their study reveals that increase in heat transfer is higher at lower flow rates. Results reveal that for a certain heat load, the desired volumetric flow rate for nanofluid is less than that for water, which leads to less pressure drop and therefore lower pumping power. Kwon et al. (2011) evaluated the heat transfer

coefficient and pressure drop through a plate heat exchanger utilizing two different water based nanofluids containing Al_2O_3 and ZnO nanoparticles. The experimental results were presented for pure water and concentrations of 1%, 3%, and 6% of Al_2O_3 nanofluids while the concentration of ZnO nanofluids was 1%. Their findings for Al_2O_3 /water nanofluids elucidate that by using the volume fraction of 6%, the overall heat transfer coefficient is maximized whereas the overall heat transfer coefficient associated with the concentration of 3% is lower than concentration of 1%. In addition, they reported that there is no significant difference between the overall heat transfer coefficient of ZnO and Al_2O_3 nanofluids at the same concentration where the Reynolds number is approximately between 150 and 350.

The authors observed that the pressure drop is increased by particle loading. Also, they recorded a linear rise in pressure drop with respect to volumetric flow rate. Turbulent convective heat transfer of nanofluids in a corrugated plate heat exchanger has been studied by Pandey and Nema (2012). The nanofluids comprised aluminum oxides nanoparticles in water as base fluid in various concentrations. Given a heat duty, the results indicated that the required flow rate for nanofluid is lower than that for water, while pressure drop is higher for nanofluid. Kabeel, El Maaty, and El Samadony (2013) tested Al_2O_3 nanofluids in a corrugated plate heat exchanger. It was found that increasing the nanomaterial concentration dramatically increased the heat transfer coefficient and transmitted power. At a given Reynolds number, the maximum rise in heat transfer coefficient was 13% with 9.8% uncertainty. This increment was even lower when constant flow rates were considered. Hence, there was doubt about the influence of nanofluids on improving heat transfer in the heat exchanger in this study. Taws, Nguyen, Galanis, and Gherasim (2012) tested the CuO/water nanofluid in a chevron-type with two-channel PHE experimentally. Through the experiments, they determined the forced convection heat transfer of the nanofluid and hydraulic characteristics of the heat

exchanger. Nanofluid was applied in volume concentrations of 2% and 4.65% as well as different Reynolds numbers with a maximum value of 1000. As a result, the friction factor appeared higher for nanofluids than water at a certain Reynolds number. Calculating the Nusselt number for 2% nanofluid concentration revealed no noticeable increment in heat transfer. It is considerable that nanofluid with 4.65% concentration actually decreased the heat transfer. These findings were incongruent with the results of Elias, Saidur, Rahim, Sohel, and Mahbubul (2014) who found a significant rise in heat transfer coefficient and heat transfer rate by using 0-1% Al_2O_3 and SiO_2 nanofluid concentrations. Khairul et al. (2014) obtained the same results as Elias et al. (2014) by using CuO nanofluid of up to 1.5% in a corrugated plate heat exchanger.

Chun, Kang, and Kim (2008) experimentally analyzed convection heat transfer coefficient of nanofluids (alumina nanoparticles and transformer oil) through a double pipe heat exchanger system under laminar flow regime. The experimental results showed that the surface properties of nanoparticles, particle loading and particle shape are the key factors to enhance the heat transfer properties of nanofluids. Influence of TiO_2/water nanofluid on pressure drop and heat transfer was investigated by Abbasian Arani and Amani (2012). In their study, the size of the particles chosen was 30 nm. The volume fraction of 0.002, 0.02 and the Reynolds number ranging from 8000 to 51000 were selected to conduct the experiments. The test section was a horizontal double tube counter-flow heat exchanger (Figure 2.8) (Abbasian Arani & Amani, 2012). From their results, it can be obtained that increase of volume fraction of nanoparticles or Reynolds number would result in increase of Nusselt number. Meantime, all nanofluids obtain greater Nusselt number in comparison to distilled water. It has been established that by utilization of the nanofluid at higher Reynolds numbers - above 30,000- more power compared to lower Reynolds numbers are required to encounter the pressure drop of nanofluid as enhancements in the Nusselt number for all Reynolds numbers are rather

similar. It was observed that using nanofluids with greater Reynolds numbers is less beneficial than usage of nanofluids with lower Reynolds numbers. It was obtained that optimum thermal performance factor equal to 1.8 is gained with the application of the water/TiO_2 nanofluid having 0.02% volume fraction and at Reynolds number equal to 47,000.

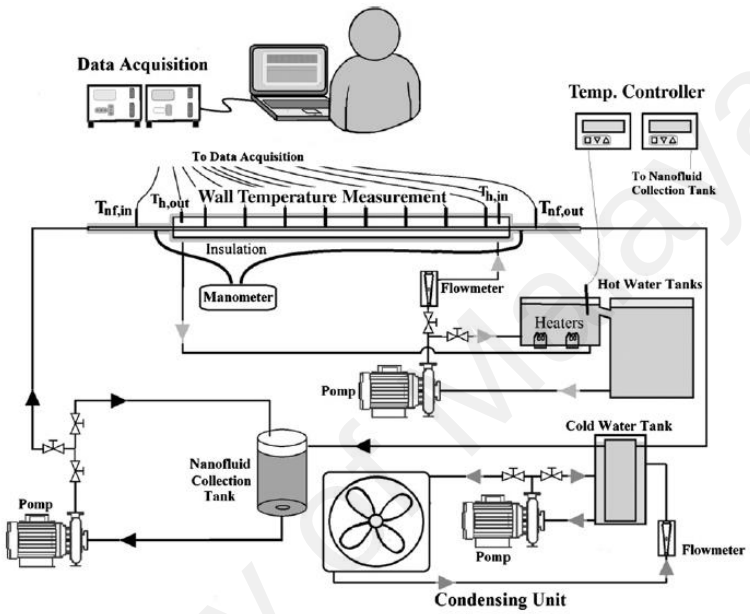

Figure 2.8: Schematic diagram of the experimental apparatus.

Duangthongsuk and Wongwises (2009) used TiO_2/water nanofluid in a horizontal counter flow double tube heat exchanger to test the hydrothermal properties of the nanofluid. Their conclusion was that the increase in mass flow rate of either hot fluid or nanofluid provides enhancement in the heat transfer coefficient of the nanofluid. This coefficient also increases with the reduction in nanofluid temperature. Convective heat transfer coefficient of two nanofluids were experimentally investigated in two types of heat exchangers by Zamzamian, Oskouie, Doosthoseini, Joneidi, and Pazouki (2011). The nanofluids were comprised of Al_2O_3 and CuO nanoparticles in ethylene glycol as a base fluid and examined in double pipe as well as plate heat exchangers. It was found that convective heat transfer coefficient of nanofluids is increased by the increment of

nanofluids temperature. This result conformed with the results of Akhtari, Haghshenasfard, and Talaie (2013), while differed from what is concluded by Duangthongsuk and Wongwises (2009). Heat transfer properties of CuO/water and TiO_2/water nanofluids were numerically examined in a double tube helical heat exchanger by Huminic and Huminic (2011). The result shows that the use of nanofluids in laminar condition considerably improves the convective heat transfer; and the increment is higher when particle concentration increases. This was similar to the findings of Chandra Sekhara Reddy and Vasudeva Rao (2014). However, Wu, Wang, and Sunden (2013) found different results when examined laminar and turbulent flow of nanofluids in a double-pipe helically coiled heat exchanger. They used Al_2O_3/water nanofluid with weight concentration percentage from 0.78 to 7.04 at a fixed flow velocity. Percentage enhancement of heat transfer was insignificant in both the flow conditions, ranging between 0.37% and 3.43%.

2.10 Numerical and Analytical Methods

Predicting the behavior of phase change systems using numerical analysis is difficult due to its inherent non-linear nature at moving interfaces and the transient characteristics of the process. Several methods are used to solve the phase change problem, the most common being the enthalpy method (Trp et al., 2006). By introducing an enthalpy method, the phase-change problem becomes much simpler since the governing equation is the same for two phases, the interface conditions are automatically achieved and it creates a mushy zone between the two phases and a fixed grid which can be used. In this method, the enthalpy is defined as a function of temperature (Dutil, Rousse, Salah, Lassue, & Zalewski, 2011; Ogoh & Groulx, 2012) and physical properties which vary linearly with the temperature in the solid-liquid phase region (A. Sharma et al., 2009). The majority of numerical and analytical studies are based on the assumption that conduction is the major mechanism of heat transfer and convection can be neglected in

the melted PCM (Trp et al., 2006). Some researchers have shown by using of experimental and numerical comparisons that the effects of natural convection within the liquid PCM can be ignored in the thin rectangular PCM containers (Zivkovic & Fujii, 2001) and for the low heat fluxes (Shatikian, Ziskind, & Letan, 2008). It has been shown that an analytical model generates more precise results for the solid–liquid interface location in the cases when the ratio of side lengths is much smaller or much larger than unity (Lamberg, 2004). However, other researchers have shown that for the spherical capsules, experimental and numerical results match more closely when natural convection is numerically accounted in the melted PCM and a fixed temperature range (such as 1 K) is used for phase change (Regin, Solanki, & Saini, 2006).

Therefore, the PCM container geometry is an important consideration when deciding whether to model natural convection in the melted PCM and has an influence on the accuracy of the model. Natural convection in the melted PCM can be modeled using an effective thermal conductivity which takes into account the additional heat transfer by convection (El Qarnia, 2009) or by using physical properties (viscosity and density) that vary as a function of PCM temperature (R. E. Murray & Groulx, 2011). By using the later method, the PCM is modeled as a fluid, with the viscosity infinitely larger when the PCM is below the melting temperature, which causes it to act as a solid (R. Murray et al., 2011). Along with the experimental setups discussed, numerical models have been used to study LHESS designs and operating parameters. It was shown numerically that more latent heat is significantly stored during the melting process in the multi-tube arrays than the single pipe in-pipe configurations. Consequently, this increases the energy storage capacity of the PCM (Farid et al., 2004). Microencapsulation was studied numerically but most works found that the matrix reduces the heat transfer through the PCM because it limits natural convection. This, along with the increased expense of microencapsulation, has made it less common. Similarly to the experimental case, PCMs of a variety of melting

temperatures in the same storage container were studied. A five-grade PCM model was compared to a single-grade PCM model using a single pass shell and tube heat exchanger of the same length in both cases and more isothermal operation was found with the five PCM model. Also, the five PCM model was shown to facilitate the PCM melting at the HTF outlet, where less melting is normally observed due to the temperature drop in the HTF relative to the PCM melting temperature (Seeniraj & Lakshmi Narasimhan, 2008). It was shown experimentally that at lower flow rates, the PCM temperatures take longer to increase in the storage system and heat transfer rates are lower (Jian-you, 2008). This was verified with a numerical model which showed that increasing of the flow rate enhanced the heat transfer rate and the volume fraction of the melted PCM over time (Lacroix, 1993).

The direction of HTF flow also has an impact on the heat transfer rates. For consecutive charging/discharging experiments, it was found that introducing the hot and cold fluid from the same end of a horizontal storage container resulted in a 5 % increase in the heat transfer rate over introducing the hot and cold fluid from opposite ends of the container (Gong & Mujumdar, 1997). Varieties of fin configurations were studied numerically as well. Numerical simulations have indicated that an optimal number of fins should be used to improve the overall system performance and proper geometrical fin design which has a strong influence on the solidification rate of the PCM. Numerical studies differ from experimental results when it comes to rise by increasing the size (thickness as well as height) and the number of the longitudinal fins on the HTF side (Y. Zhang & Faghri, 1996a). This goes against the results found experimentally where the presence of fins decreases the overall PCM volume in the system thus decreasing the total storage capacity (U. Stritih, 2004). Differing from experimental studies, Sasaguchi found by using a numerical model that the performance of the LHESS unit is almost the same for any fin configuration with the same surface area (Sasaguchi, Yoshida, & Nakashima,

1990). In this case, natural convection was included in the numerical model that differing it from most LHESS models fin studies. In the model used by Zhang & Faghri, natural convection was neglected and a single melting point was used for the PCM, which could have generated the differing results (Y. Zhang & Faghri, 1996b).

2.11 Summary of Literature

Based on the literatures and most of the similar studies, the main gap which directed us to design and manufacture a novel test rig addresses the problems which most of the researches are struggling with. This design provides a phase change material that fully surrounds or covers whole of the finned-tube with symmetric position during both charging and solidification of the phase change material. It will remarkably enhance the savings of energy of the energy storage device between 15-30%.

Briefly, significant findings from the literature review are as follows:

- Organic PCMs with melting temperatures in the suitable range for the application (40 to 50 ºC for a SDHW system) are best for use in LHESS.
- Charging and discharging modes of a heat exchanger with PCM storage could be in practice. In this work, a finned tube heat exchanger has been used, which differs from previous works, the container installed in a vacuum area and paraffin wax as a PCM utilized. Details of these experiments discussed in Chapter 3.
- Increasing HTF inlet temperature results in increment of the rate of energy storage.
- Longitudinal fins are best for enhancing heat transfer in horizontal FTHX setups.
- Increasing of the heat transfer surface area of fins is only advantageous if it does not interfere with natural convection in the melted PCM.

- Investigate the effect of fin spacing change and the variations of the Reynolds number on the PCM system performance.

The above findings from the literature will aid in the design choices made for the FTHX used in this thesis. The aim of this study is to design and fabricate a novel storage unit responding to the melting/solidification characteristics of the paraffin wax for improving the performance of latent heat energy storage by using full capacity of PCM container and using of the nano fluids as a HTF to enhance the heat transfer rate. Enhancement is achieved by a horizontal shell-tube integrated with or without fins and the various Reynolds numbers (1000, 1250, 1500, 1750 and 2000) on the interface together with time needed for completion of charging and discharging of the PCM.

CHAPTER 3: METHODOLOGY

This chapter provides a detailed account of the setup design, temperature measurement system as well as materials and experimental procedure.

3.1 Setup Design

In this thesis, two separated setups have been realized in order to deliver a complete analysis about the PCM behavior in both radial and axial directions for two states of heat transfer (conduction, convection). Setup A is mostly dedicated to the analysis associated to the axial and setup B is able to evaluate the heat transfer for both axial and radial for the copper tube. All experiments on this research were performed on the experimental energy storage unit which is schematically shown in Figure 3.1 and Figure 3.2. Setup A is the revised and modified setup of SAMAN which has been proposed in 2012 to improve the performance and reduce the errors in the experiment. In setup A, two different current sources for two processes of melting and solidification are used. In addition, instead of flowmeter and pump, valve and beaker have been realized. As seen in Fig.3.1, utilizing warm and cold sources prevents wasting of energy in the solidification process and provides a condition that after finishing the melting process, the solidification process starts without any delay. However, in previous design, much time was wasted to transfer the hot HTF to cold HTF source.

During this time, melted PCM starts to transfer heat outside which is the waste noticeable energy resulting in changing of PCM behavior. It also affects the solidification process time. Moreover, using of a digital flow rate helps to set the current conveniently with high accuracy and provide the ability to monitor the flow line of heat transfer throughout the entire process. This ability was not offered by the previous setups since the values are set manually before the start of experiment which induces considerable errors. Furthermore, using a pump in the flow line for this setup helps the flow more

unified. The accuracy of this setup will be obvious by observing the numerical results of this setup which is in the next section.

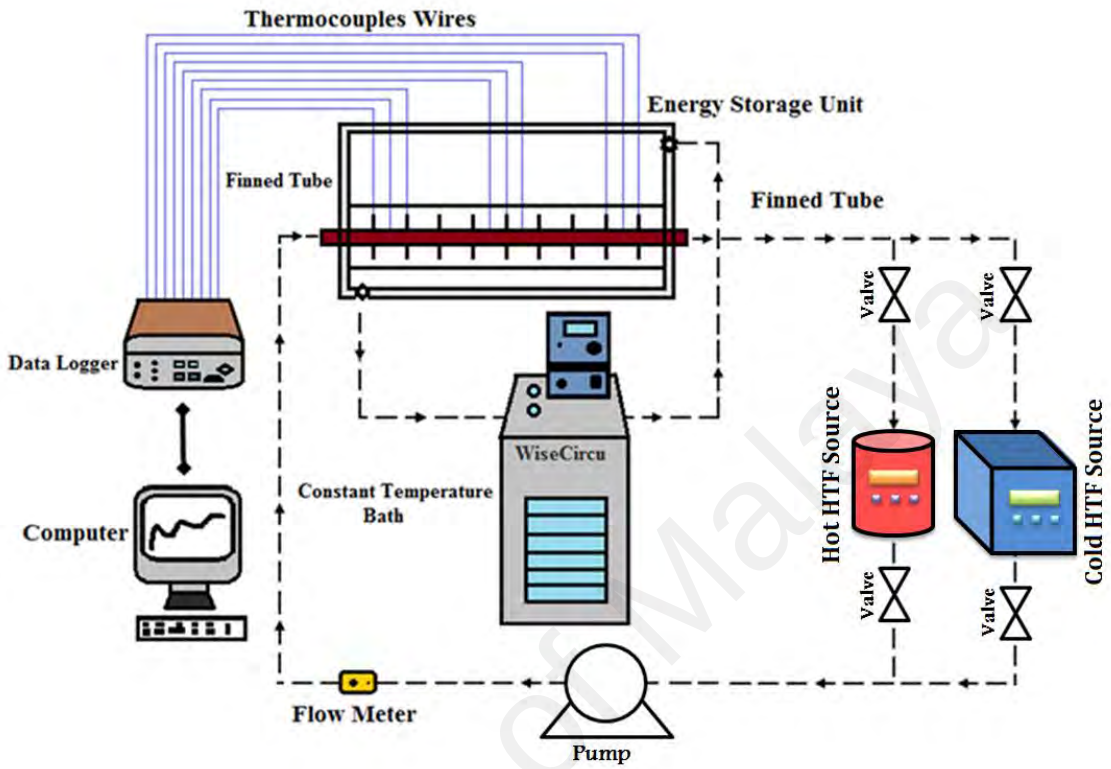

Figure 3.1: The flow line of the heat transfer for setup A

Figure 3.2 and Figure 3.3 show the energy storage tank and thermocouple wires and also represent the flow line of the heat transfer fluid. Setup B has the ability to analyze the changing of PCM behavior in the melting and solidification process in radial and axial directions and the results of setup A and B can be compared accordingly.

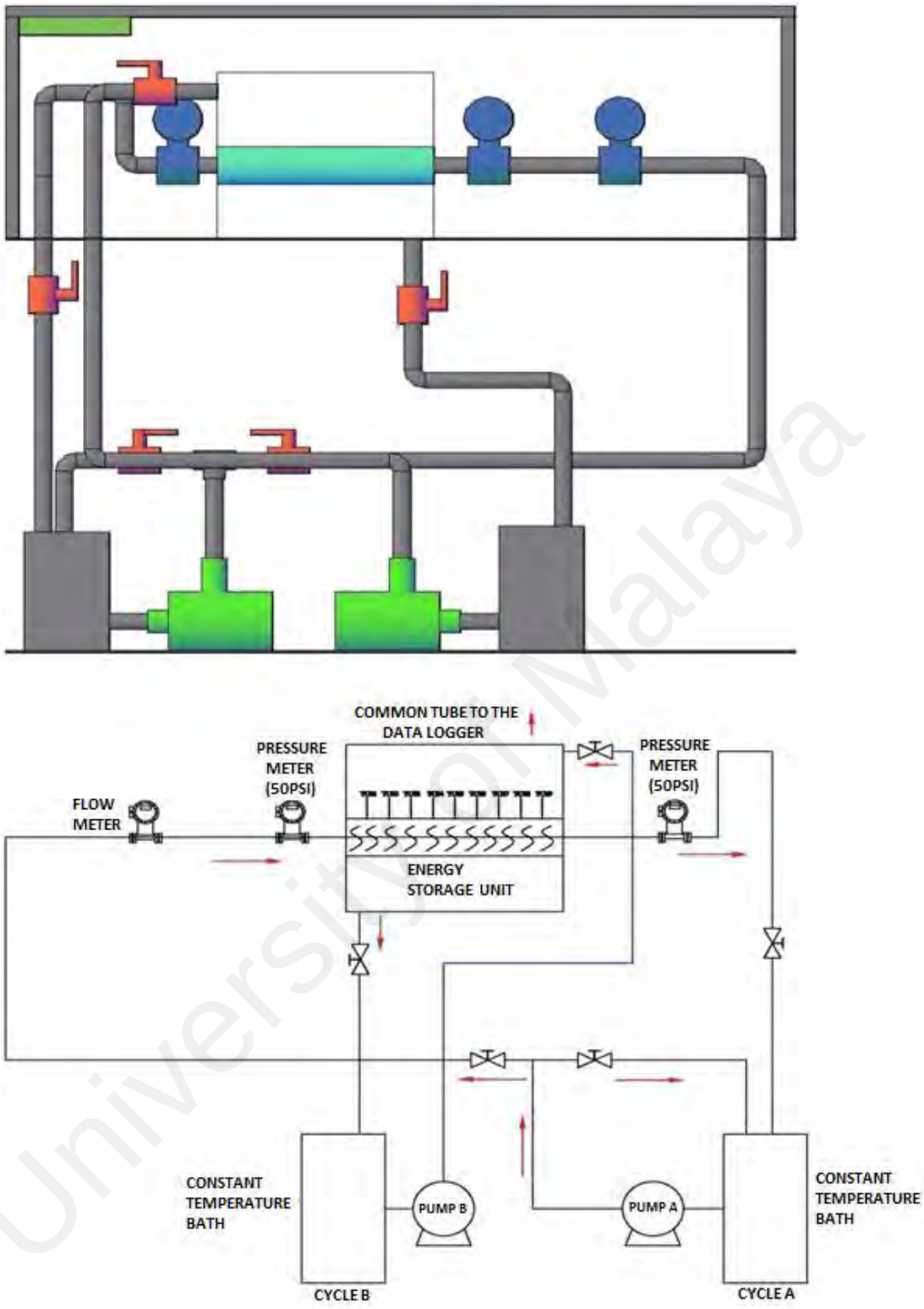

Figure 3.2: The flow line of the heat transfer for setup B.

Figure 3.3: The test rig of experimental setup.

Experimental units (setup A and setup B) mainly consist of these systems:

1. Thermal bath

2. The flow system

3. Energy storage unit

4. Temperature measurement system

5. Computer system

These systems are introduced and presented in the following sections of this chapter with all numbered elements of the setup that shown in Figure 3.1 and Figure 3.2.

3.1.1 Thermal Bath

There are two thermal baths which are shown in Figure 3.2. They were employed to ensure the heat transfer fluid at a certain temperature at the inlet of the test section. The thermal bath with the sensitivity of ±0.1°C as well as the flow rate of 20L/min worked as a source of energy in melting and solidification process (Figure 3.4). The first one is

applied to keep the temperature of the vacuum container between 53°C and 55°C. The second one is used to circulate heat transfer fluid in the range of 47°C and 63°C. The fluid circulates the whole setup with the aid of a pump inside the device. These constant temperature baths includes a thermostat which keeps the temperature of the heat transfer fluid in the reservoir within the desired range.

Figure 3.4: Thermal bath.

The flow rate of the heat transfer fluid was controlled by 5 valves. Two valves, which are shown in Figure 3.2, were at the entrance and exit of the bath to open or close the fluid circulation. The function of the valve, which installed after the exit valve of the constant temperature bath, was to adjust the flow rate. This valve is demonstrated in Figure 3.2 which shows the flow pipeline. By adjusting this valve, the flow rate was increased or decreased. By opening full that valve and closing the entrance valve, all of the circulating heat transfer fluid was transferred into a flowmeter. In addition, there are two other valves which are installed on two sides of the container in different levels for circulating the water inside the unit storage to vacuum the area. The heat transfer fluid was supposed to solidify and liquidate the phase change material by transferring its thermal energy during the solidification and melting processes of the experiments. For

this purpose, the temperature of 60°C was set in the constant temperature bath for melting. In solidification parts of the experiments, the temperature was decreased to 46°C in order to melt the solidified phase change material. The heat transfer fluid was chosen water for all the experiments. Some thermophysical properties of water at the temperatures of 60°C and 46°C are shown in Table 3.1 with the flow rate values measured during the experiments, the values of density and viscosity were used to calculate Reynolds numbers of the heat transfer fluid.

Table 3.1: Thermophysical properties of water.

T (ºC)	P (Kg/m^3)	μ
47	989.76	0.4274
63	983	0.467

3.1.2 The Flow System

As shown in Figure 3.2, the flow section of the experimental setup includes a hydrodynamic entry section. Fully developed flow conditions for the heat transfer fluid must be provided to ensure the accuracy of the experimental results at the inlet of the energy storage unit. Therefore, the hydrodynamic entry section was long enough to satisfy this necessity at both laminar and turbulent flows of heat transfer fluid (Kays). As shown in Figure 3.2, pipe was raised 150 mm at the return of the flow line and 150 mm away from the exit of the energy storage unit. It was chosen because of the fact that the heat transfer fluid cannot completely fill the piping system especially at low Reynolds numbers. So, such an operation was made in order to remove this risk. The entry length and the return piping sections of the apparatus were made of UPVC tubing, which had 15 mm inner, 2.6 mm thickness that is shown in Figure 3.5. The whole length of the flow system including the entry section was approximately 450 mm. To provide isolation of

the flow system, the whole piping was insulated by a 20 mm thick tube covering foam rubber.

Figure 3.5: Photograph of the UPVC pipe used for the flow of the HTF.

3.1.3 Energy Storage Unit

The dimensions of the energy storage unit were 300mm x 520mm x 400mm. Energy storage unit also included a cylindrical tube with inner and outer diameters of 62mm and 66mm, respectively. The length of the mentioned tube is 520mm, which is installed at the distance of 150mm from bottom, left and right faces of the unit storage. The tube is integrated with two parallel rectangular plates with dimensions of 520mm x 320mm. These plates are located at the top of the tube and the distance between them is equal to 20mm. Fin tube heat exchanger and PCM are placed inside of this part. To watch the solidification and melting around the finned tube, the front, back and the bottom faces of the storage unit were 10mm thick acrylic. The other lateral faces were 3mm thick acrylic. All the surfaces were covered with 3mm thick Styrofoam layers. A central window with the 200mm x 60 mm dimensions, which is shown in Figure 3.6 and Figure 3.7, were formed at Styrofoam layer covering the acrylic surfaces.

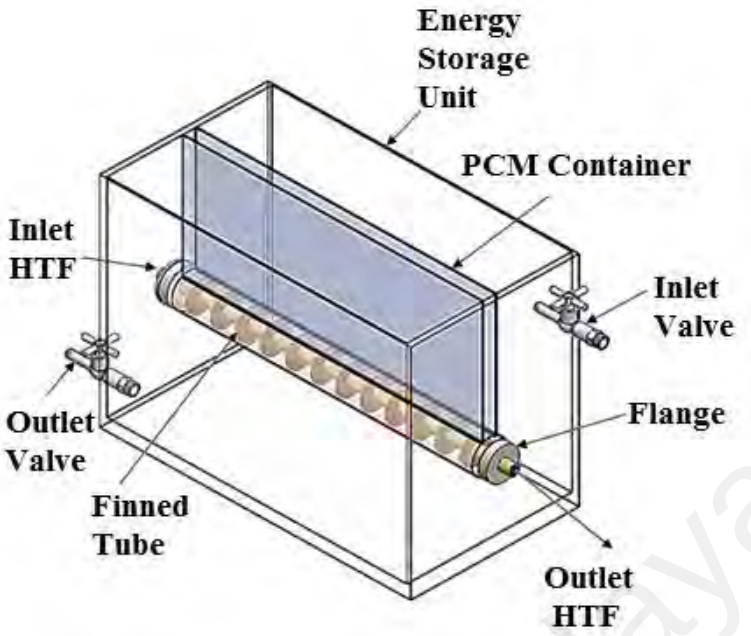

Figure 3.6: Lateral view of the energy storage unit for setup A.

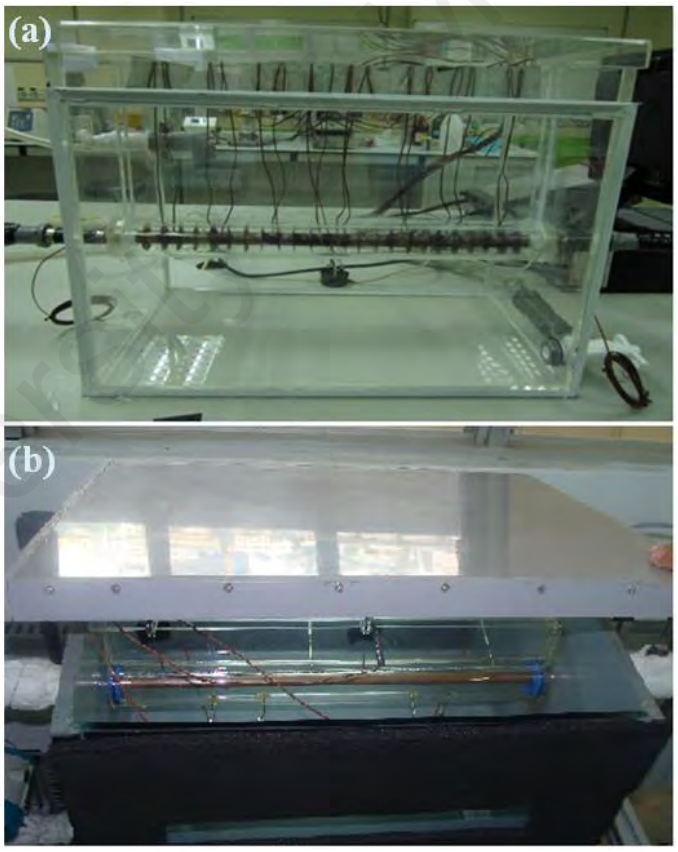

Figure 3.7: Energy storage tank a) setup A b) setup B.

Owing to these openings, momentary photographs of solidification and melting of the phase change material could be taken by a digital camera with the help of a light source. These pictures of melted and solidified phase change material around the finned tube were

transferred from the digital camera to a computer. Energy storage unit included the finned tube, vacuum tube and the phase change material. Paraffin wax was selected as a phase change material for the experiments. The thermophysical properties of paraffin wax are shown in Table 3.2.

Table 3.2: Thermophysical properties of PCM.

Properties	Tube material	Phase change material	
		Solid	Liquid
ρ (kg/m^3)	8800	0.790	0.916
Cp (j/kg.K)	420	n.a	n.a
K (W/m.K)	52	0.167	0.346
α (m^2/s)	1.4×10^{-5}	n.a	n.a
L (kJ/kg)	n.a	160	160
T(ºC)	n.a	53	57

In this study, 3 different types of tubes were used in the experiments. Table 3.3 shows the geometrical parameters of all of the tubes tested. As demonstrated in this table, each tube was numbered to define any tubes easily as can be seen in the following sections of this thesis. The finned tubes had circular fins of constant thickness. All of them had the same length of 620 mm and their inner and outer diameters were 15 mm and 20 mm respectively. Nevertheless, their fin spacing was different. The parameters for the tubes shown in this table were indicated as a layout in Table 3.3. Copper alloy cylinders were used in the production of the tubes .In Table 3.2, the thermophysical properties of this alloy were given. While producing the tubes, at first the finned surface of the alloy cylinders was an integral piece. The tube is an ordinary one to which fins are attached by oxy acetylene welding. This is due to budget shortage and in future works integrated finned tubes will replace the current ones. By producing in this way, the risk of a possible thermal contact resistance between the tube base and the fin was removed.

Table 3.3: Geometrical parameters of the tubes used in this study.

Tube No.	*NF	D_i (mm)	D_o (mm)	D_f (mm)	t (mm)	W (mm)	S (mm^2)
I	0	15	20	20	0	-	30565
II	24	15	20	40	0.5	20	48356
III	48	15	20	40	0.5	10	93572

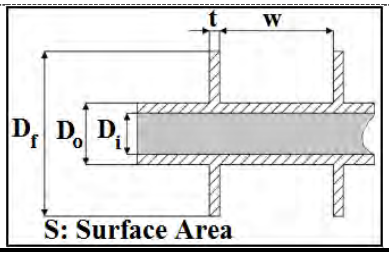

The finned tube was situated at the midsection of the energy storage unit and connected to the flow system to fulfill thermally symmetrical conditions in the storage tank. The system was tested for possible leaks after completing the assembly. The photographs of some of the tubes used in the experiments are shown in Figure 3.8.

Figure 3.8: (a) The tube I (without fin), (b) The tube II (24 finned) and (c) The tube III (48 finned).

3.1.4 Temperature Measurement System

Temperature measurement system consists of thermocouples and data logger. This section is divided into 3 parts, the first and the second parts discuss about the modality of installation of thermocouples and the third part debates on how to record and save the data in data logger. In this study, thermocouples of type K were used. Calibration of the thermocouples were done to ensure the measured temperatures were correct.

3.2 Thermocouples Design A

It is essential to measure the temperatures of the finned tube wall, the fin tip and base tube for accurate determination of the heat transfer to the phase change material. As shown in Figure 3.9, temperatures at 18 different points in the system were measured and recorded during the experiments. So, 18 thermocouples were used for all of the tubes used in the experiments. Figure 3.9 demonstrates a model of thermocouple arrangement for both tubes (tube II and III). Two thermocouples were installed to measure the heat transfer fluid temperatures at the inlet and outlet of the finned tube. Thermocouple installations for each of the tubes were at different distances but they had same arrangement. All thermocouples were installed to the tubes by oxy-acetylene welding. All these points can be seen in Figure 3.9. The reason of using much more thermocouples among fins is to have more temperature data for rising accuracy in drawing graphs.

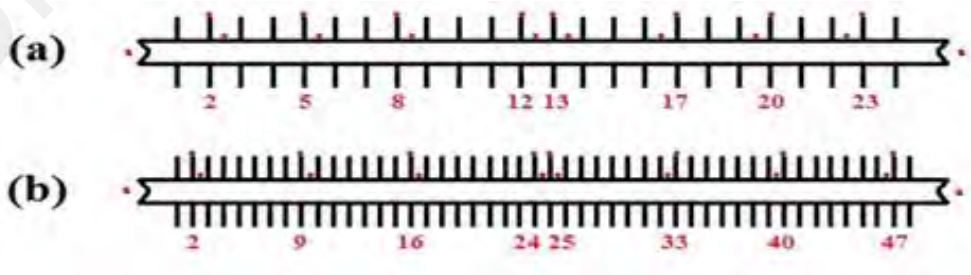

Figure 3.9: (a) Installation of the thermocouples for tube II (b) Installation of the thermocouples for tube III

3.3 Thermocouples Design B

As it is obvious in the Figure 3.10, eight thermocouples are used in this part. The thermocouples have been installed radially with the different angles and distances from the copper tube and with the same linear distance of each other on the tube. The purpose of this design is to study the symmetry of the experiment and discus on variations in distance and angles on the melting and solidification levels.

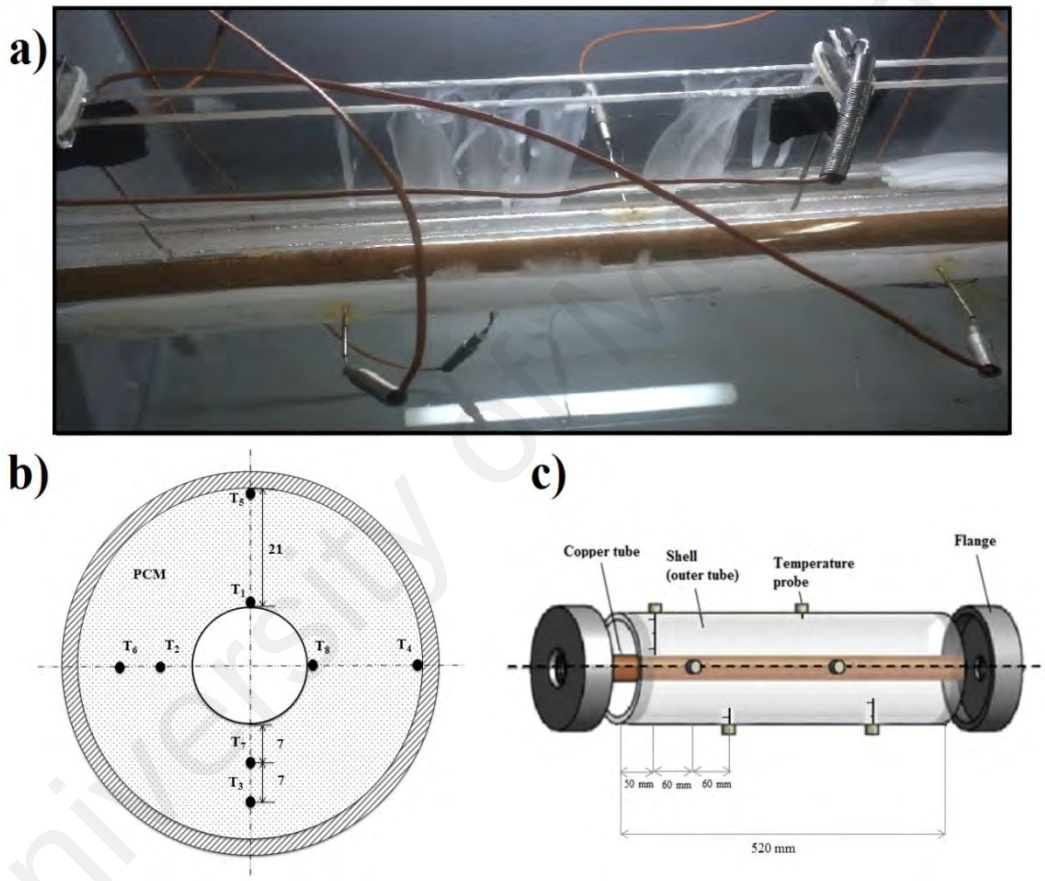

Figure 3.10: Installation of the thermocouples for tube I (a) Visual photo (b) Cross section view (c) 3D view.

As it is obvious in the above table, all the thermocouples are the same in pairs with regards to the inclination angle or the gap between the thermocouples and copper tube surface. This means that T_1 with T_5 is same due to their angle and T_1 with T_8 is similar because of the distance.

Table 3.4: Radial and axial distance of the thermocouples relative to copper tube.

Thermocouple	Inclination Angle (Degree)	Gap between thermocouple and copper tube (mm)
T_1	0	0
T_2	90	7
T_3	180	14
T_4	270	21
T_5	0	21
T_6	90	14
T_7	180	7
T_8	270	0

3.4 Measurement Device

In this study, type K thermocouples were used and calibration of the thermocouples had been done. It was learned that the measured temperature values were correct. Because of the large number of temperatures to be measured, the output record of the data was recorded by the help of a GRAPHTEC data logger with an accuracy of ±1°C and this data logger, which is shown in Figure 3.11, were measured the millivolt outputs of the thermocouples. The signals output of the data logger were transmitted and recorded in a personal computer. For this process, the "GRAPHTEC" software was used. The temperature values were scanned by the data logger every 5 seconds during both solidification and melting processes. These values could be observed on the computer screen simultaneously by the GRAPHTEC software. Also, the inlet and outlet temperatures of the heat transfer fluid could be seen graphically, so the inlet temperature of the water could be kept constant.

Figure 3.11: GRAPHTEC Data logger.

3.5 Computer System

As previously mentioned, the data scanned by the data logger were recorded on a personal computer during the experiments. The values scanned every 5 seconds were be able to watched simultaneously on the computer screen by using of GRAPHTEC Data Logger software as shown in Figure 3.12. In addition, the inlet and the outlet temperatures of the heat transfer fluid were able to view graphically to ensure the inlet temperature at constant.

Figure 3.12: A view of GRAPHTEC Data Logger software.

3.6 Importance of the Setup Design

The significant limitation in tube-in-shell PCM storage is volumetric expansion/shrinkage of PCM during charging and discharging process. Therefore, the PCM is not completely filled to the brim in the cavities. The previous researchers reported that the container must be filled up to 75% to 80% of container capacity. It is well known that the heat transfer equation in the heat exchangers is defined by symmetric model.

Thus, the PCM behavior is not controllable around the finned tube and it cannot follow the symmetric pattern. Therefore, the reported results were not verified by the numerical methods. Here in the unique geometry of tube-in-shell heat exchanger was designed to overcome this issue. Figure 3.6 shows an air-gap which is provided by adding two rectangular plates in top of the container in order to account for the volumetric expansion/shrinkage during melting and solidification process. It can be observed that during the PCM melting, its volume expands and squeezes consecutively by being trapped in the air. The natural convection of air in this air-gap results in the PCM temperature at the top section which is a negative point in this unit storage. Thus, to decrease the negative impact of natural convection between the air gap and PCM, the condition near the vacuum was provided by placing the tube-in-shell storage in isolated rectangular container.

3.7 Material and Method

The pristine Graphene Nanoplatelets (GNP) with diameter of 0.5–3 μm and thickness of 0.55–3.74 nm and Multi-walled carbon nanotubes (MWCNT) with diameter of 20-30 nm and length less than 30 μm were obtained from Neutrino Company. Sodium dodecyl sulfate (SDS), TiO_2, sulfuric acid (H_2SO_4, 98%) and nitric acid (HNO_3, 68%), all with ACS quality were purchased from Sigma–Aldrich. SDS used as a surfactant for synthesizing non-covalent nanofluids and mixture of HNO_3 and H_2SO_4 for covalent samples. Graphene Nanoplatelets (GNP) or Multi-walled carbon nanotubes (MWCNT) are first covalently functionalized with carboxyl groups. Pristine GNP or MWCNT is sonicated with a mixture of H_2SO_4–HNO_3 acids in volume ratio of 3:1 for 12h at 60 °C and then followed by string for 36h at the same condition to synthesize carboxylated GNP (GNP-COOH) or MWCNT (MWCNT-COOH). The suspension is centrifuged at 11000 rpm with di-water to separate completely and supernatant reach PH around 3-4 simultaneously. The sample is then placed in the oven for 48h at 50 °C to dry. To prepare stable suspension in water, the given amount of GNP-COOH or MWCNT-COOH is

poured into the water and sonicated for half an hour. To prepare non-covalently TiO_2/water, the given amount of TiO_2 and SDS (weight ratio of 1:2) poured into the water and sonicated for 3h.

3.8 Experimental Procedure

Firstly, the thermocouples were installed to one of the finned tubes to be tested for starting a particular set of experiments. Then the finned tube with the thermocouples on it was assembled to the cylindrical storage tank of the phase change material (paraffin) was poured into the energy storage tank at a temperature of 53-57ºC. Then, a preheating process was performed by circulating the warm water in rectangular storage. By applying this process, the temperature of the paraffin was increased more and became closer to 53-57ºC. This range of temperature causes the paraffin holding in mushy zone. To make a more homogeneous temperature distribution in (around) the paraffin, the outlet valve of unit storage was close at the start of circulating and warm water with 55 ºC pouring from inlet valve to rectangular box, after the water reached to 300 mm height in the box, the outlet valve was then opened to start to circulation of the warm water.

After this process, inlet valve was closed and outlet valve still open until the height of water 200 mm decreased. The total amount of the water stored into the tank was at a 100 mm height of the rectangular box. HTF at a predetermined flow rate was circulated through the system. After adjustment of the flow rate by the specific valve which is described in the previous part, the circulation of the water was stopped by closing the valves. Both the constant temperatures were regulated for the desired inlet temperature at 66ºC. Then, the water at the specified inlet temperature was let abruptly in order to maintain 63 °C at the inlet by using the heat loss along the pipe into the test section by opening the outlet valve of the thermal bath. For each experiment, this procedure was repeated and melting process started. By the completion of melting, the circulation of the

water was stopped by closing the outlet valve of the bath so that the thermal bath temperature can reach at 47 °C. Then, the circulation was started again. Different inlet temperatures were studied for 3 different tubes: one tube without fin (#1), tube with 24 fins (#2) and tube with 48 finned tubes (#3). In the previous part, all of these tubes were numbered in order to express easily. Various values of Reynolds numbers were considered, 1000, 1500 and 2000 of heat transfer fluids for each tube.

3.9 Determination of Charged and Discharged Heat Thermal Energy

For the solidification part of the experimental run, the amount of negative energy stored comprises latent heat of solidification and sensible heat of both solid and melt paraffin. So, the total energy stored is,

$$E_{total} = E_{sensible,l} + E_{sensible,s} + E_{latent,s} \quad (3.1)$$

Where,

$$E_{sensible,l} = m_l C_{p,l}(T_i - T_f) \quad (3.2)$$

$$E_{sensible,s} = m_s C_{p,s}(T_s - T_{fr}) \quad (3.3)$$

$$E_{latent,s} = m_s L \quad (3.4)$$

In the solidification process, (3.3) and (3.4) were used in order to determine the stored energy. Since the initial temperature of the paraffin, *Ti*, was almost equal to 53°C, equation (3.2) can be used for computing the stored heat energy. Nevertheless, the equation (3.3) could not be directly used for sensible heat of liquid.

CHAPTER 4: RESULTS AND DISSCUSIONS

4.1 Introduction

This part of the thesis is divided in to two main parts, A (with 24 and 48 fins) and B (without fins), containing a comparative study was done based on the thermal performance assessment of the LHSU. All the thermocouples are embedded linearly in part A but radially with the different distances from the copper tube in part B. The impact of flow rate, the number of fins on PCM melting as well as solidification processes regarding the first arrangement of thermocouples were investigated in part A. Furthermore, the effects of inlet temperature (T_i = 70 and 80 °C), three kind of Nano fluids (TiO_2, CNT and GNP) with different weight percentages (0, 0.05 and 0.1 wt. %) as the HTF on PCM melting and solidification processes are demonstrated in part B. In the both parts, all the experiments were performed for Reynolds number within the range of 1000 to 2000 in the laminar regions.

4.2 Result and Discussions, Part A

4.2.1 Thermal analysis of LHSU

Based on the phase transition of paraffin as a PCM, Figure 4.1 (a and b) show three separate regions (charging and discharging processes) which are named (i) the solid PCM region (region A), (ii) solid-liquid phase transition state (region B) and (iii) the liquid PCM (region C). Figure 4.1a shows that the temperature of PCM at region A rises up rapidly when the PCM starts to melt. This fact is relevant to the large amount of temperature gradient at the start of experiment since PCM temperature is lowest during charging process. Continuously, in region B, the temperature gradient dramatically decreased as compared with region A. At this region, phase transition and interface of solid- liquid which is named mushy zone was started. In region C, the temperature gradient of PCM decreases to 50% as compared with the section B and the PCM gets completely molten while the temperature difference between PCM and HTF reaches to

its minimum amount in the charging process. It is well known that as the heat transfer rate is a function of the temperature difference between the HTF and the PCM, the highest and the lowest heat transfer rate are expected at region A and C respectively. Figure 4.1b shows the different regions for discharging process. In this process, the HTF needs to flow in opposite directions to achieve the same effects. To summarize, during the discharging process the molten PCM solidifies and releases heat which causes to increase the temperature of HTF. The PCM temperature reduces rapidly till it reaches the freezing point of PCM (52°C, region C and B). This is because of the larger temperature difference between the HTF tube and PCM. As the PCM starts to solidify, the solidified PCM layer near the tube provides thermal conduction resistance and thus reduces the heat transfer rate.

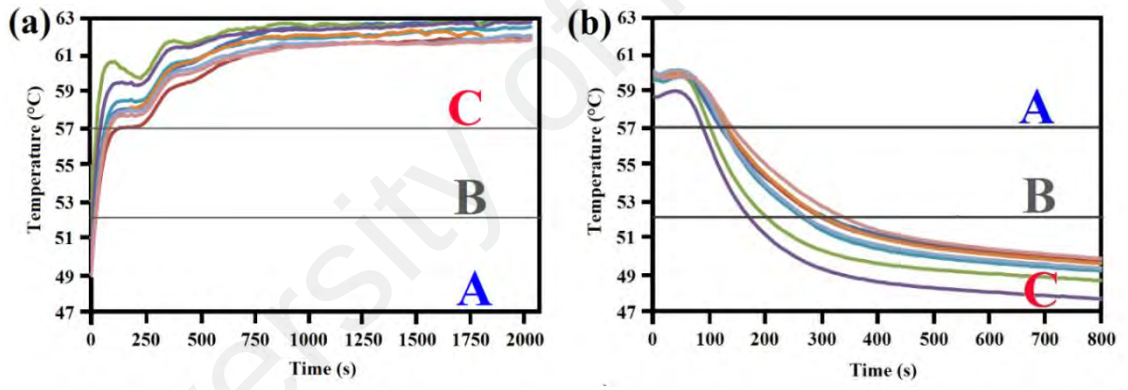

Figure 4.1: Phase transition of paraffin for tube #2 at Re=1000 (a) melting process and (b) solidification process.

4.2.2 Charging Process

Figure 4.2 shows an example of melting process of paraffin wax at different times on tube#2 (24 fins) and tube#3 (48 fins) for the same Reynolds Number (Re = 1000). Melting begins peripherally near the HTF tube wall and continues to spread radially outwards. When the charging process is initiated, the PCMs close to the HTF tube wall surface reach the melt and causes to form a thin layer of liquid in the narrow melting area due to heat transfer and the conduction of finned tubes (Figure 4.2(a and e)). The rapid melting of the PCMs caused mostly near the walls because of greater temperature differences of PCM

in the surrounding areas of the tube wall. It can be inferred that the phase front moves faster in the radial direction near the left annulus as compared to the right side. Tubes#1 in comparison with tube#2, a conical path or traverse of the interface which can be visualized in the PCM during charging process (Figure 4.2(b and f)). This signifies the fact that the shape of the melting front is not influenced by added extra fins. Only the motion of the melting front is increased due to augmentation in heat transfer by adding extra fins. As can be seen that un-melted PCM inside shell of tube #1 took a longer time to melt as compared to tube#2 because convection circulation is formed away from the bottom side of the inside tube, as shown in Figure 4. 2 (c, d, g and h). Melting process in tube#2 significantly improved and became more homogenous due to the wider contact surface.

On the other hand, as the liquid fraction increased in the upper part of the tube as shown in the Figure 4.2, the hotter liquid of PCM was pushed upward to the top of the tubes because of natural convection effects driven by buoyancy. Moreover, the solid part of the PCM was squeezed down to the bottom of the tube because of heavier density. The natural convection has a greater effect in the upper regions of the annular storage container. Aydin et al. (A. A. Aydın & Okutan, 2011; O. Aydın, Akgün, & Kaygusuz, 2007) reported a comprehensive description of the physical attributes displayed by PCM in the charging process whereby two areas coexist. These two areas are the solid phase of non-melted PCM and liquid phase of melted PCM. Due to buoyancy forces produced by the density gradients that resulted from temperature differences, the melted PCM recirculation is spurred by the heat transfer through convection when the solid matrix of PCM melts. The heating and mixing of the molten PCM are elevated by recirculation inside the test section and the fact that it takes less time for the areas closer to the upper regions to reach melting temperature than lower regions. However, it is worth noting that PCM has a lower density in the molten phase compared to the solid phase.

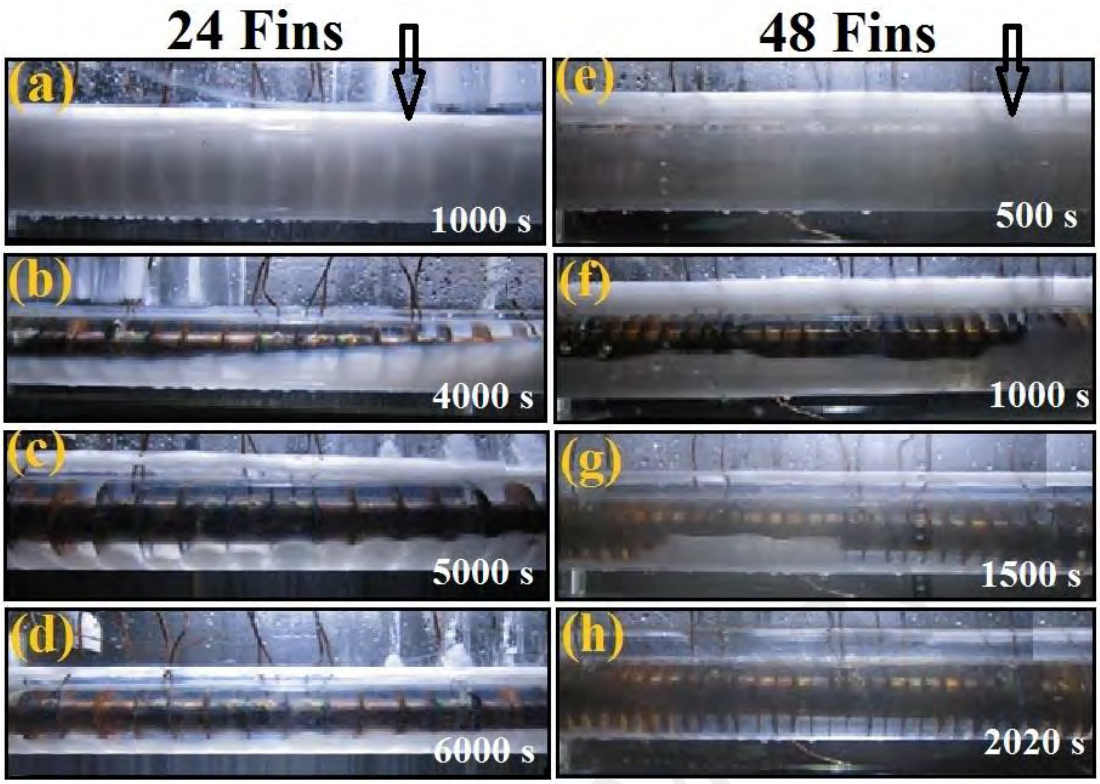

Figure 4.2: Melting Process at Re=1000 for tube #2 at (a) 1000s, (b) 4000s, (c) 5000s, (d) 6000s and for tube #3 at (e) 500s, (f) 1000s, (g) 1500s, (h) 2020s.

4.2.3 Discharging Process

Discharging process was carried out by circulating the cold water through the system after reversing the heat transfer direction between HTF and PCM. Figure 4.3 depicts the results for Re=1000 as an example. It is found that the molten Paraffin starts to solidify due to the release of latent heat stored in the liquid PCM. Figure 4.3 (a and e) shows the initial solidification of PCM at the early stage of process. The observation shows the forming of solid crystal of PCM around the finned tubes. Moreover, Figure 4.3 (b and f) indicates that the points closer to the inlet part and HTF wall solidified faster than the other areas because the heat transfer takes place uniformly along the radial distance. Thus, the solidification front moves in radial direction parallel to the axis of the test section for both tubes. By examining Figure 4.3, it is found that the PCM solidified around the finned tubes is thicker at the bottom than at the top near the start of the discharge process. This is due to the natural convection taking place in the liquid PCM. In the melting zone, the relatively cold PCM moves downward due to the gravity effect along with a decrease

temperature in the lower portion. After a primary period of time, during which solid PCM layer thickness increases, the natural convection effect decreases. The elliptic shape of the frozen PCM gradually changes to approximately circular shape. This may indicate that the heat transfer is dominated by conduction.

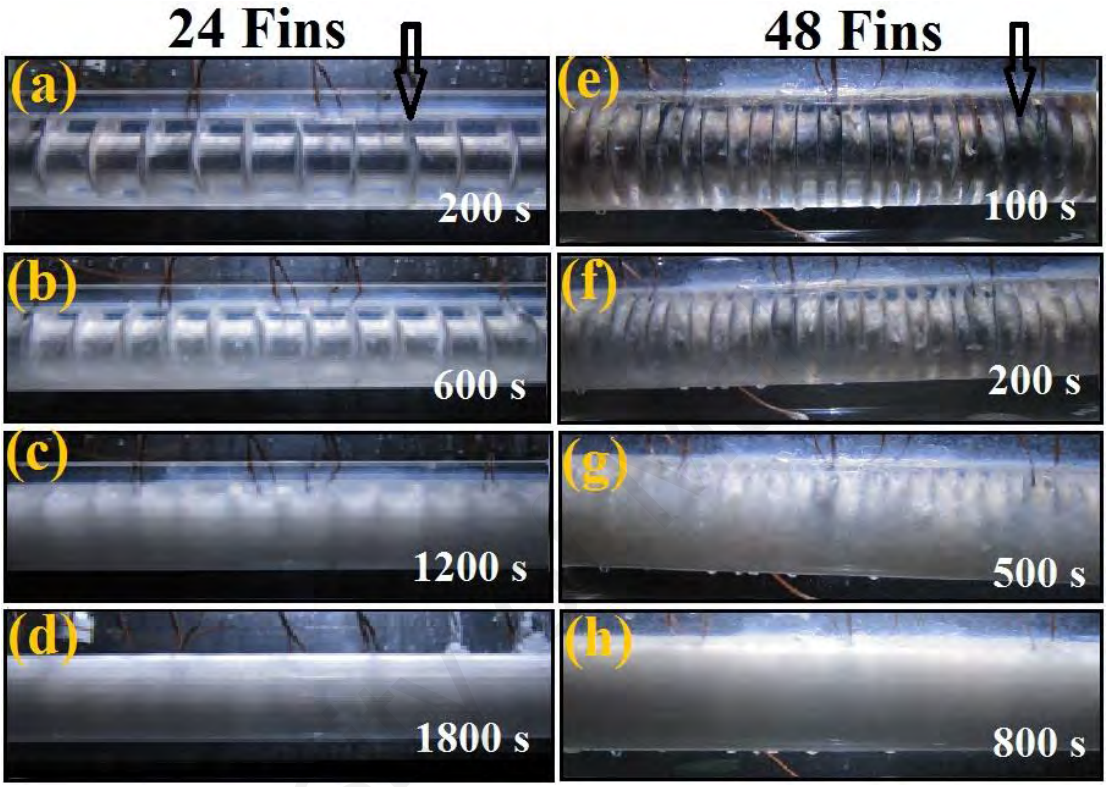

Figure 4.3: Solidification Process at Re=1000 for tube #2at (a) 200s, (b) 600s, (c) 1200s, and (d) 1800s and for tube #3 at (e) 100s, (f) 200s, (g) 500s, (h) 800.

4.2.4 Influence of Fin Number on Charging and Discharging

The temperature distribution of PCM near the tube, the variation of average PCM temperature with time and the effects of fin density on the time with constant diameter and constant working fluid temperatures at different fluid flow rates during the charging are shown in Figure 4.4. It can be seen that the PCM takes a short time to reach the melting temperature in tube with 48 fins as compared to 24 fins. A rapid increase in PCM temperature in tube with 48 fins occurs because of the radial finned tube which is able to transfer heat from HTF quickly. The higher heat transfer rate induced by the presence of fins near the HTF tube causes faster melting of PCM. The fluctuations observed in Figure

4.4 (a) refer to the change of density of PCMs during the melting and solidification process. This phenomenon plays a crucial role even in different Reynolds numbers of HTF as well as different fin numbers (Figure 4.4 (b-f)), but in higher Reynold and fin numbers, the fluctuation is seen less due to the increasing of the rate of heat transfer.

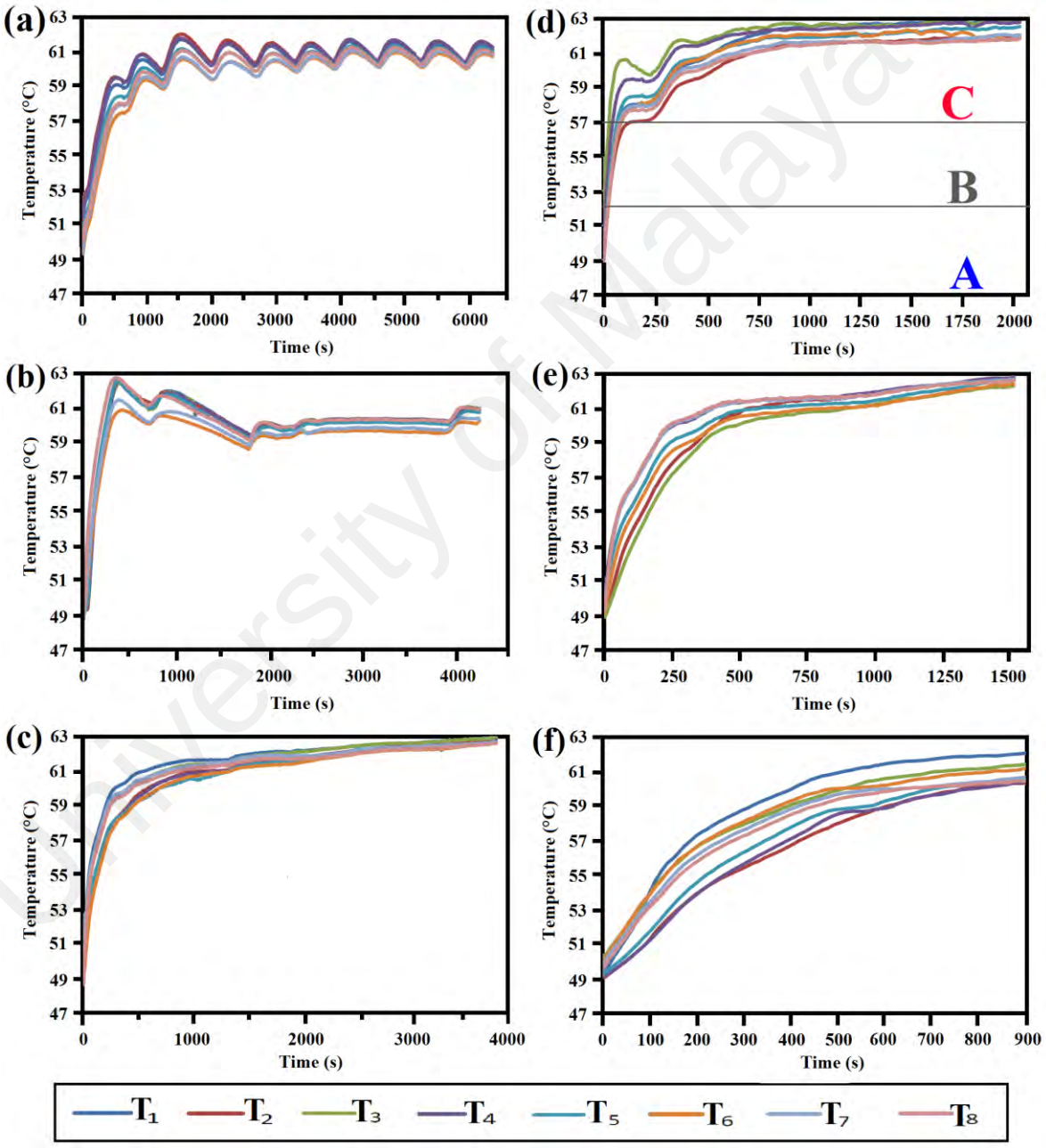

Figure 4.4: Temperature measurement records in the melting process for tube #2at a) Re=1000, b) Re=1500, c) Re=2000 and for tube #3at d) Re=1000, e) Re=1500, f) Re=2000.

Thus, the total melting time in tube with 48 fins is reduced as compared to the system with 24 fins. Moreover, by increasing the number of fins, the temperature difference among the fins would be less. As the fin spacing decreases, the heat transfer coefficient increases because of the interaction of the boundary layers developed on two adjacent fins. This interaction is at the origin of the decrement in the velocity gradients in the boundary layer, leading to a convective heat transfer drop on the fin. Therefore, the gradient temperature fluctuations began faster for tube with 48 fins. For example, at Re=1000 the times are 470s and 60s for tube with 24 and 48 fins respectively. It is clear that the fluctuation of gradient temperature decreased and became smooth with increasing fin density. The interesting point about the above issue is that the results were the same with all Reynolds numbers. According to the Figure 4.4 (a and d), the melting time is reduced from 6300s to 2200s due to the number of fins. Also, Figure 4.4(c and f) shows a reduction in melting time from 3800s to 900s. It is due to the fins which accelerate the heat transfer rate from the surface of HTF tube to the PCM for all flow rates of HTF.

Figure 4.5 presents the temperature temporal variation distribution at the lengthy points which are similarly distanced from the tube wall of HTF for discharging process. It can be seen from Figure 4.5 (a-b, b-e and c-f) for the same Reynolds number, the solidification rate is improved with the extra fins. Further, due to the provision of the radial fins, a better thermal contact is established between the liquid PCM and the heat transfer surface. Moreover, the intense reduction in the PCM temperature in initial time is observed and continuously the time taken to reach the steady state condition is reduced significantly. This happens with the provision of 48 fins as compared to a system with 24 fins for all mass flow rates of HTF. The reason is the initial impact and effectiveness of natural convection on heat transfer. Also, the reduction of the thermal resistance of the solid PCM between the heat transfer surface and liquid PCM is occurred. Therefore, time taken for the average PCM temperature to reach 47°C is reduced from 1700s, 1100s and

950s for 24 fins to 800s, 650s and 480s for 48 fins at Reynolds number 1000, 1500 and 2000 respectively. In brief, the percentage decrement of melting time due to the provision of fins are 19.08%, 23.20% and 24.52% for HTF flow rate at Re=1000, 1500 and 2000 respectively.

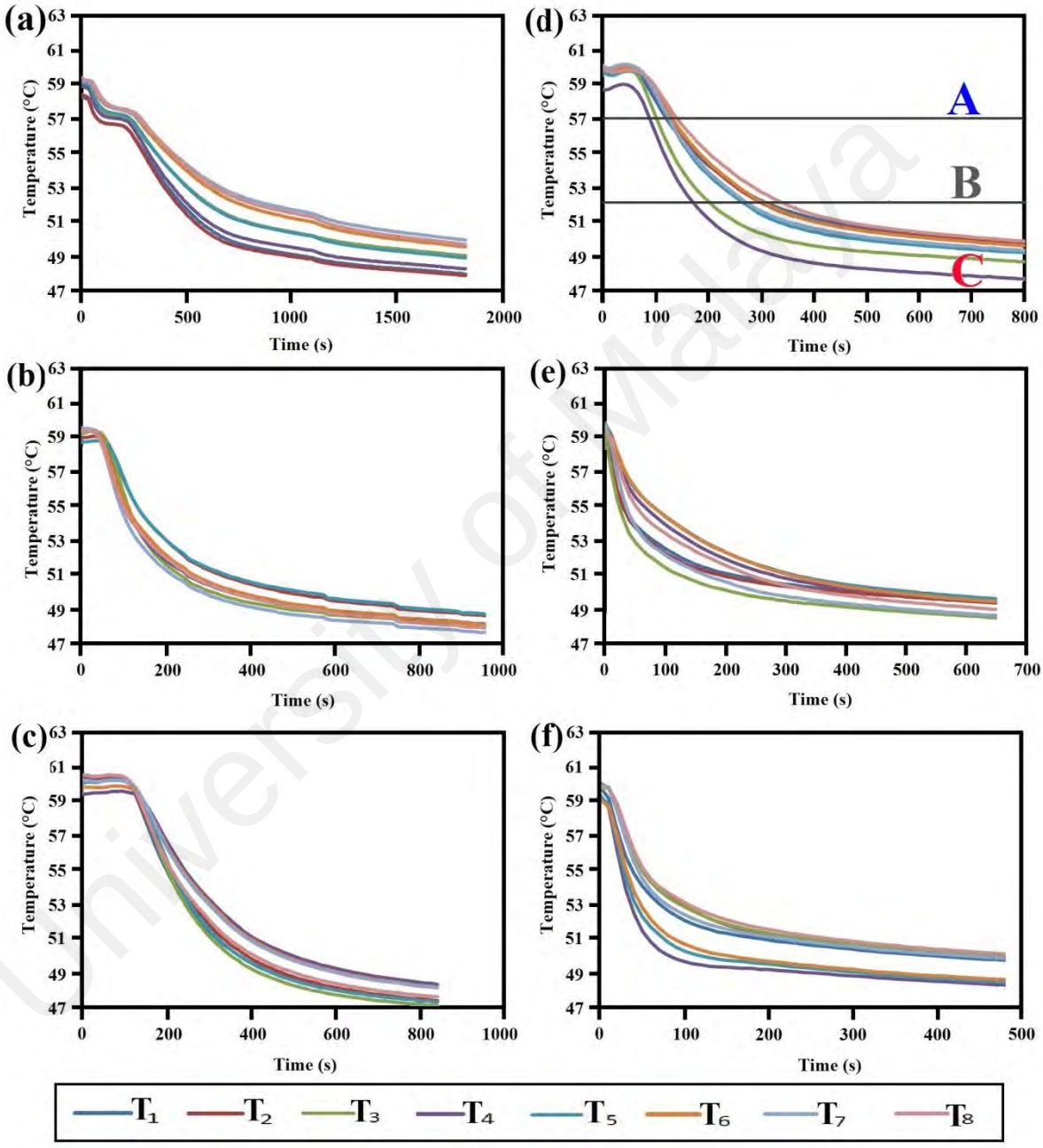

Figure 4.5: Temperature measurement records in the solidification process for tube #2 at a) Re=1000, b) Re=1500, c) Re=2000 and for tube #3 at d) Re=1000, e) Re=1500, f) Re=2000.

It is also observed that the temporal variation of PCM temperature near the inner tube for both the cases with 24 and 48 fins is similar. However, the solidification time is decreased between 40% and 55% when the fin density is increased depending on flow rate. It was observed that the effect of fin density is more highlighted in the melting part for all experiments. Therefore, the provision of extra fins on the PCM side should be considered to enhance the natural convection during charging and conduction during the discharging.

4.2.5 Influence of HTF Flow Rate on Charging and Discharging

The influence of flow rates of HTF on the charging time required for the system with 24 and 48 fins is shown in Figure 4.4. As can be seen, at the low flow rate (low Reynolds number), the lower heat transfer coefficient was occurred on the working fluid side which leads to extended melting time while the reverse effect was found at high flow rate. The Figure 4.4 also expresses the temporal variation of PCM temperature at the test unit for varying flow rates of HTF i.e., Re= 1000, 1500 and 2000 and 63°C of fluid inlet temperature. It can be observed from Figure 4.4 that the time taken to reach the steady state condition is reduced with the increase in HTF flow rate. The reduction in time is nominal with the increase in HTF flow rate. Thus the increase in HTF flow rates has little influence on total melting time for shell and tube type finned LHSU.

At higher HTF flow rates, the residence time for the HTF is less and the heat transfer surface of HTF tube remains almost at isothermal (Dirichlet) condition. Influence of flow rates of HTF on temporal variation of PCM temperature during the discharging process is shown in Figure 4.5 for both the cases- with 24 and 48 fins. In tube with 24 fins, temperature drop of PCM is started with a delay, which is decreased by increasing Reynolds number. Doubling the Reynolds number in the tube#2 and tube#3 will decrement the time by 50% and 40% respectively. From Figure 4.5, it is evident that by increasing flow rate, less fluctuation is observed in the graph and the negative slope

becomes deeper. Towards the end of the solidification process the interface position is nearly unchanged and the heat flow nearly stops, that is, complete solidification is achieved as indicated by the last points on the curve. It is noticed that the influence of flow rate of HTF on temperature distribution is same for both the cases.

4.2.6 Comparison between Reynolds Number and Fin Number

It can be concluded that the effect of Reynolds number and fin density are close to each other. The results generally showed that the increment of the fin density and Reynolds number have increased the amount of charging thermal energy during melting process. Since in this experiment the amount of paraffin mass was fixed, it can be understood that by increasing the fin density and Reynolds number, the charging time reduced and the amount of stored energy and heat transfer enhanced. Neglecting heat losses to the surroundings from the sides, the upper and the lower parts of the storage container, the rate of heat transfer from HTF to PCM will be equal to enthalpy change of HTF between inlet and outlet, which is equal to:

$$\mathbf{Q = \dot{m} c_{HTF} (T_i - T_o)} \quad (4.1)$$

Where, $\dot{m}$ is the mass flow rate of the HTF, c_{HTF} is the specific heat of the HTF and T_i and T_o are the inlet and outlet temperatures of the HTF respectively. Figure 4.6 indicates the heat discharge rate (HDR) of solidification for different Reynolds numbers. At the beginning of the solidification process, due to the large temperature difference between PCM and HTF, the heat discharge rate is at a maximum level. Later, the heat transfer rate gradually decreases as the PCM temperature value approaches to the temperature of water. Regarding a fixed PCM amount, time would play a significant role in this case. It is observed that the HDR for Reynolds numbers of 1500 and 2000 are quite close to each other and drastically drop until 480s, signifying a decrease of 80%.

However, in Re=1000 the heat discharge rate is slower, which means it takes longer time (1800s) to reach 80% HDR loss.

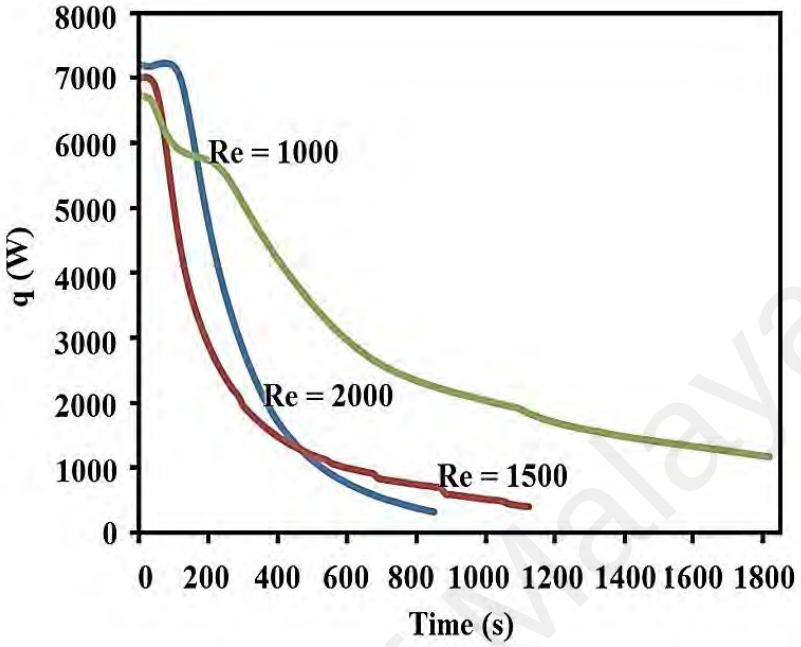

Figure 4.6: Heat discharge rate for solidification process.

4.2.7 Comparison of the CFD model with the Experimental Data

The FLUENT commercial code based on finite volume method, which has been used in some previous works (Oon et al., 2014; M. R. Safaei, Goshayeshi, Razavi, & Goodarzi, 2011; Yarmand, Gharehkhani, Kazi, Sadeghinezhad, & Safaei, 2014), was applied to solve the Reynolds Averaged Navier-Stokes (RANS) equations. This method is based on a particular type of the residual weighting approach. In this approach, the computational zone is divided into finite control volumes as each node is covered by a control volume. Eventually, the differential equation is integrated on each finite volume. The second-order upwind method was chosen for the discretization of all terms, while the SIMPLE algorithm was employed for pressure-velocity coupling. The solution was converged when the residuals for all the equations dropped below 10^{-6} (M. Safaei, Goodarzi, & Mohammadi, 2011).

Figures 4.7 (a and c) depict the results of Re = 1000 as an example of normal behavior of a transition. As witnessed, melting begins peripherally, near the HTF tube's wall and it continues to spread radially outwards. When the charging process is initiated, the PCMs close to the HTF tube wall surface reach the melting point, which is due to the conduction of the finned-tube.

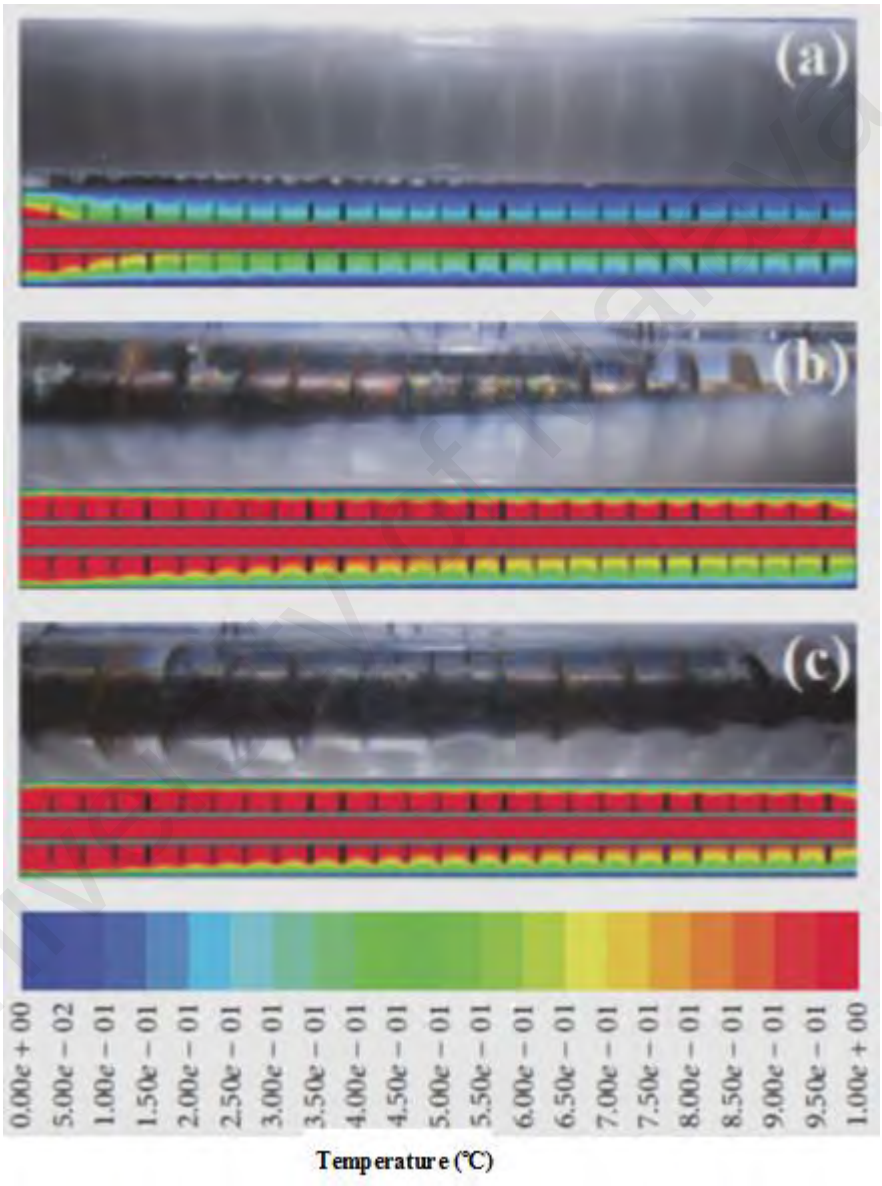

Figure 4.7: Melting process for Re = 1000 at (a) 1000 s, (b) 3500 s, and (c) 6000 s.

The rapid melting of the PCMs near the walls is mostly because of greater temperature differences of PCM in the surrounding areas of the tube wall. Nevertheless, it is worth noting that the melting behavior of PCMs in the upper areas differs from those in the

lower regions. The molten PCM moves up towards the top areas of the storage container due to the natural convection. The melting region extends radially upward. As a result, the areas in the upper sections attain melting temperature more rapidly than the lower parts. The natural convection has a greater effect in the upper regions of the annular storage container. Aydin et al. {Aydın, 2007} offered a good and comprehensive description of the physical attributes displayed by PCM in the charging process whereby two areas coexist. These two areas are the solid phase non melted PCM and liquid phase melted PCM. Due to buoyancy forces produced by the density gradients which resulted from differences in temperature, the melted PCM recirculation is spurred by the heat transfer through convection when the PCM solid matrix melts.

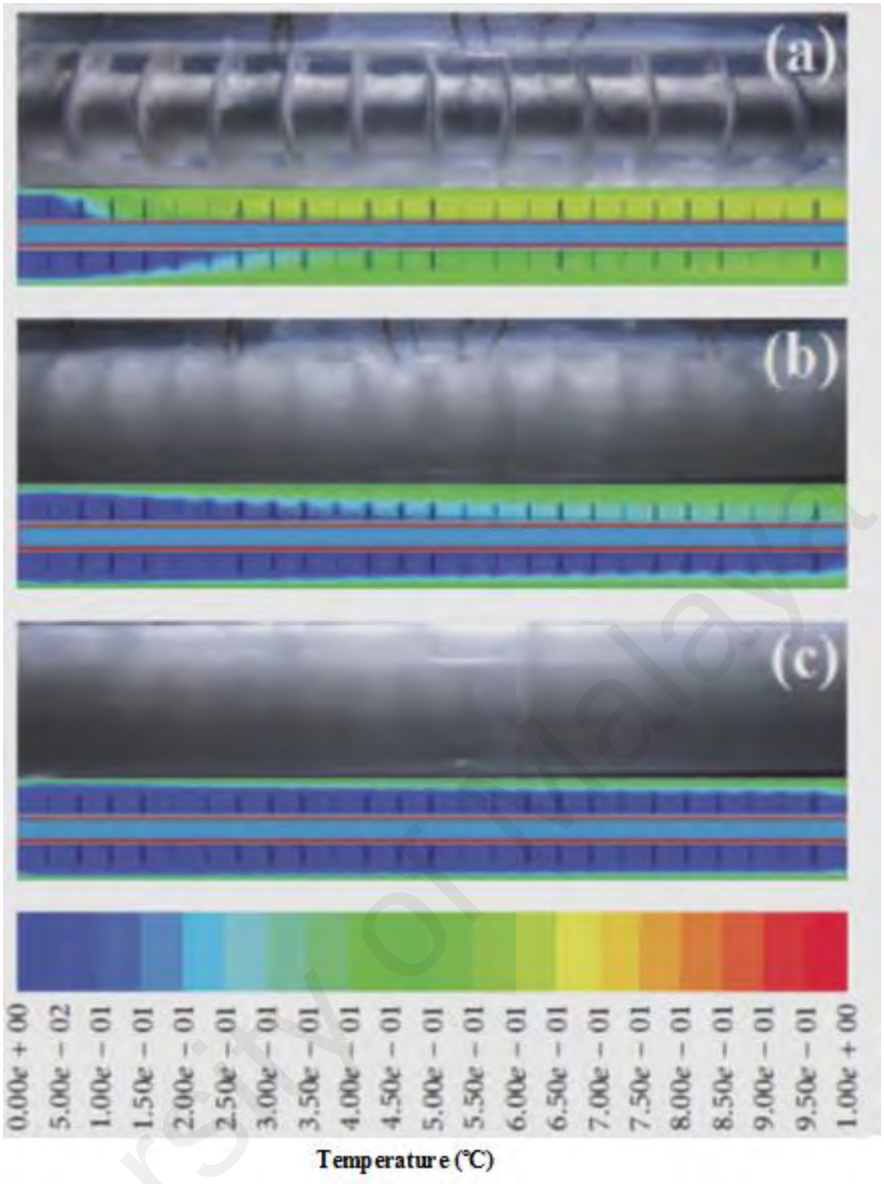

Figure 4.8: Solidification process for Re = 1000 at (a) 200 s, (b) 1000 s, and (c) 1800 s.

The heating and mixing of the molten PCM are elevated by recirculation inside the test section and the fact is that it takes less time for the areas closer to the upper regions to reach melting temperature than lower regions. However, it is worth noting that PCM has a lower density in the molten phase compared to the solid phase. In cases with larger operation, the PCM molten area spreads to cover larger areas of the PCM container. In line with the assumptions, the melting will increase with rising Reynolds number. Experimentations on the discharging process were carried out by reversing the heat transfer direction between HTF and PCM. Hereby, the cold water was circulated through

the system. It is then introduced to a sudden temperature change in the circulating system during the discharging process as a result of the high temperature differences between HTF and PCM. Regarding the transfer of sensible heat taking place within the solid PCM, volume increases until complete solidification occurs at solidification temperature. In accordance with the expectations, the points closer to the inlet part and HTF wall solidified faster than the other areas.

The PCM temperature at particular positions reduces slowly with time, as demonstrated before; temporal variation becomes almost uniform after some time due to the initial impact and effectiveness of natural convection on heat transfer. After that, conduction becomes the only dominating mechanism in heat transfer, with lower convection impacts in contrast to the melting or charging instances. This happens due to the melted PCM circulation quantity that is influenced by the decreasing natural convection with the increase in time as a result of the outward HTF tube's solidification. In the same vein, the process of solidification will speed up with increasing Reynolds number in the discharging process. For a clearer explanation, Figures 4.8 (a, b and c) depict the results for Re = 1000 where the ordinary and normal behavior of a transmission occurs. It is clear that solidification occurred homogeneously with increasing time.

4.2.8 Signal to Noise Ratio and ANOVA

4.2.8.1 S/N Ratio

A performance statistic known as the Signal-to-Noise ratio (SNR) is employed in Taguchi methods that results in the predictive performance of a process or product when variables such as noise factors are present. The factors with the maximum SNR outcome must be chosen because it suggests process improvement and product performance. Analysis methods consist of SNR analysis to achieve design and process robustness, the analysis of variance to determine the key process and design parameters as well as the

main interactions and the performance prediction at the best condition. Then, a confidence interval can be created around the anticipated mean performance. The calculations and equations in the SNR are acquired from the system of experimental design by Taguchi. The type of measured quality characteristic has effect on the selection of a suitable S/N Ratio. Several Signals were employed to Noise ratio for multiple quality characteristics, which is the resultant from the quality loss function of Taguchi.

The selection of quality characteristics to measure the experimental output which influences the number of experiments have to be carried out to be statistically meaningful. These outputs can be variable or attribute in nature. Variable characteristics such as exergy, efficiency, viscosity and strength, generally provide more information than attribute characteristics such as "good or bad," "pass or fail." Variable characteristics require fewer experiments or samples than characteristics that are attributing in nature to achieve the same level of statistical significance. The quality characteristic for the experiment should be related as closely as possible to the product basic engineering mechanism. In Taguchi methods of experimental design, the following three types of quality characteristics are generally considered:

- Smaller-the-better quality characteristics: This is used to measure characteristics such as melting time, melting temperature, heat lost and other defects. It is used where the smaller value is desired. Where y_i= observed response value and n = number of replications (Kapur & Chen, 1988; Liao, Huang, & Su, 1997; Genchi Taguchi, Chowdhury, & Taguchi, 2000; Genichi Taguchi, Chowdhury, & Wu, 2005).

$$S/\mathrm{N}\,ratio = -10\log(\frac{1}{n}\sum_{i=1}^{n} y_i^2) \qquad (4.2)$$

- Larger-the-better quality characteristics: This measures characteristics such as efficiency, exergy and thermal conductivity. It is used where the larger value is desired (Kapur & Chen, 1988; Liao et al., 1997; Genchi Taguchi et al., 2000; Genichi Taguchi et al., 2005).

$$S/Nratio = -10\log(\frac{1}{n}\sum_{i=1}^{n} \frac{1}{y_i^2}) \qquad (4.3)$$

- Nominal-is-the-best quality characteristics: This is used to measure characteristics such as melting time and solidification time. It is used where the nominal or target value and variation about that value is minimum (Kapur & Chen, 1988; Liao et al., 1997; Genchi Taguchi et al., 2000; Genichi Taguchi et al., 2005).

$$S/Nratio = 10\log\frac{\bar{y}_i^{\,2}}{S_{y_i}^2} \tag{4.4}$$

Experimenters should define the measurement process including understanding what, where and how to measure the test setup prior to the experiment in order to understand the contribution of variation accounted by the measurement system. Every measurement has some uncertainty that can be attributed to key inputs such as gages, parts, operators, methods and environment. These sources of variation may bias the experiment and so the measurement system must be capable, stable, robust and insensitive to operator or environmental changes.

Table 4.1: Result of experiments for melting time and solidification time in three repeat ion and Signal to noise ratio for each response separately.

No	Fin Number	Reynolds Number	Melting Time(s)	Solidification Time(s)	SNRA Melting	SNRA Solidification
1	24		6350	1720		
2	24	1000	6510	1685	29.1231	40.50367
3	24		6249	1740		
4	24		4250	760		
5	24	1500	4339	745	22.0498	37.01594
6	24		4182	775		
7	24		3759	550		
8	24	2000	3838	539	19.2391	35.94991
9	24		3699	560		
10	48		1850	730		
11	48	1000	1839	718	21.7082	29.78709
12	48		1866	743		
13	48		1540	650		
14	48	1500	1531	640	20.7021	28.19599
15	48		1553	662		
16	48		1200	480		
17	48	2000	1193	472	18.0714	26.01115
18	48		1204	489		

Table 4.1 shows the signal to noise ratio values for melting time and solidification time. With reference to the Table 4.1, response tables for melting time and solidification time extracted and listed in Table 4.2 and Table 4.3 respectively. Moreover, the main plots are prepared for each response table and have shown in the Figures 4.9 and 4.10.

Table 4.2: Response table for S/N ratios "Smaller is better" for the melting time.

Level	Fin	Re
1	-37.83	-35.15
2	-28.00	-32.61
3		-30.98
Delta	9.83	4.17
Rank	1	2

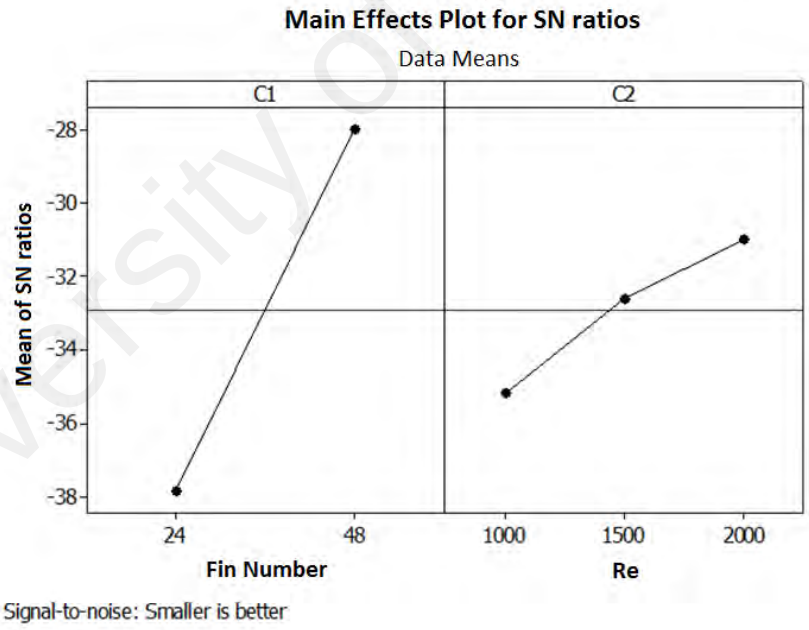

Figure 4.9: Effect of the control factors on melting time.

With reference to the Figures 4.9 and Figure 4.10, the best combinations for melting and solidification are (48 fin, Re=2000) and (24 fin, Re=1000) respectively, which with the mentioned combinations, the minimum and the maximum values for the response will be achieved separately.

Table 4.3: Response table for S/N ratios "larger is better" for solidification.

Level	Fin	Re
1	23.47	25.41
2	20.16	21.37
3		18.65
Delta	3.31	6.76
Rank	2	1

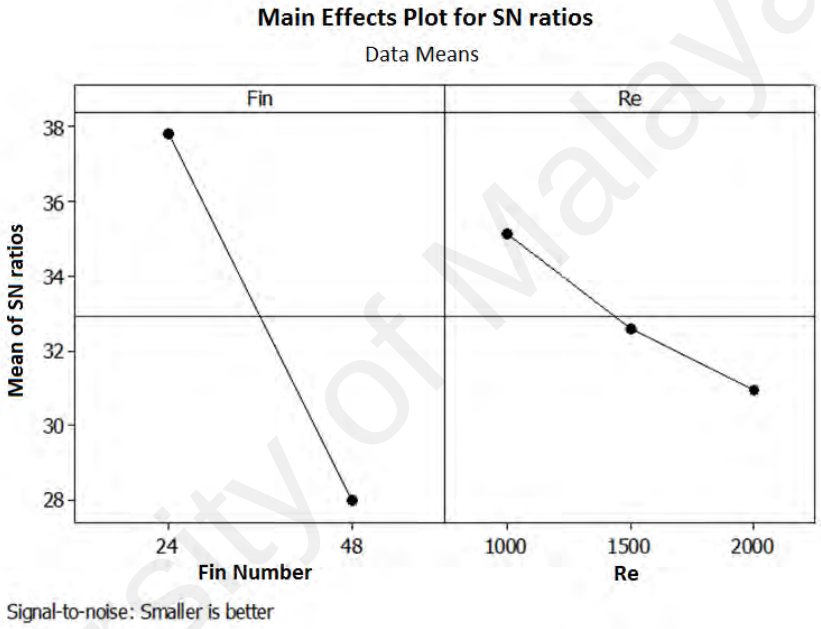

Figure 4.10: Effect of the control factors on solidification time.

4.2.8.2 Analysis of variance

ANOVA is a statistically based, objective decision-making tool for detecting any differences in the average performance of groups of tested items (Kurt, Bagci, & Kaynak, 2009). Generally, ANOVA helps in formally testing the significance of all main factors and their interactions by comparing the mean square against an estimate of the experimental errors at specific confidence levels. This is accomplished by separating the total variability of the S/N ratios, which is measured by the sum of the squared deviations from the total mean S/N ratio, into the contributions by each of the design parameters and

the errors. First, the total sum of squared deviations SST from the total mean S/N ratio η_m can be calculated as (i, 2009):

$$SS_T = \sum_{i=1}^{n} (\eta_i - \eta_m)^2 \tag{4.5}$$

Where, n is the number of experiments in the orthogonal array and η_i is the mean S/N ratio for the i_{th} experiment. The percentage contribution P can be calculated as:

$$P = \frac{SS_d}{SS_T} \tag{4.6}$$

Where, SS_d is the sum of the squared deviations. The ANOVA results are illustrated in Table 4.4 and Table 4.5. Statistically, there is a tool called an F test, named after Fisher (PJ. & (1996)), to see which design parameters have a significant effect on the quality characteristic. In the analysis, the F-ratio is a ratio of the mean square error to the residual error and is traditionally used to determine the significance of a factor.

Table 4.4: Analysis of variance table for S/N ratio of melting time.

Source	DF	Seq SS	Adj SS	Adj MS	F	P
C1	1	144.900	144.900	144.900	318.77	0.003
C2	2	17.626	17.626	8.813	19.39	0.049
Residual	Error	2	0.909	0.909	0.455	
Total	5	163.435				

Regression Model and equation for melting time = 175 - 2.27*(Fin Number) - 0.0271*(Reynolds)

Table 4.5: Analysis of variance table for SN ratio of solidification time.

Source	DF	Seq SS	Adj SS	Adj MS	F	P
C1	1	16.43	16.43	16.429	2.60	0.248
C2	2	46.29	46.29	23.147	3.66	0.215
Residual	Error	2	12.65	12.65	6.326	
Total	5	75.38				

Regression Model and equation for solidification time = 41.0 - 0.269*(Fin Numbers) - 0.0118*(Reynolds)

4.2.8.3 Data Pre-processing (Normalized the Values)

Data pre-processing is normally required since the range and unit in one data sequence may vary from the others. It is also essential when the sequence scatter range is too large or the directions of the target in the sequences are different. It means data pre-processing transfers the original sequence to a comparable sequence. Dependent on the characteristics of a data sequence, there are various methodologies of available data pre-processing for the GRA (Fung, 2003; Tosun, 2006). Based on target values, there are three different equations to normalize the sequence value. If the target value of the original sequence is infinite, then it has two characteristics, “higher the best” and “smaller the best” or if there is a definite target value (desired value) to be achieved, “nominal the best”. The original sequence can be normalized as follows for “smaller the best”, “higher the best” and “nominal the best” by equations 4.7, 4.8 and 4.9 respectively.

$$X_i^*(k) = \frac{\max x_i^{(0)}(k) - x_i^{(0)}(k)}{\max x_i^{(0)}(k) - \min x_i^{(0)}(k)} \tag{4.7}$$

$$X_i^*(k) = \frac{x_i^{(0)}(k) - \min x_i^{(0)}(k)}{\max x_i^{(0)}(k) - \min x_i^{(0)}(k)} \tag{4.8}$$

$$X_i^*(k) = \frac{(x_i^{(0)}(k) - x_t) - \min(x_i^{(0)}(k) - x_t)}{\max(x_i^{(0)}(k) - x_t) - \min(x_i^{(0)}(k) - x_t)} \quad (4.9)$$

Where, i = 1,2,..,m; k = 1,2,…,n and m are the number of experimental data items. Also, n is the number of parameters and $x_i^{(0)}(k)$ denotes the original sequence, $X_i^*(k)$ the sequence after the data pre-processing, $\max x_i^{(0)}(k)$ the largest value of $x_i^{(0)}(k)$, $\min x_i^{(0)}(k)$ the smallest value of $x_i^{(0)}(k)$ and x_t are the desired values.------Pl. Check

4.2.8.4 Grey Relational Coefficient

In grey relational analysis, the relevancy measure between two systems or two sequences is defined as the grey relational grade. When only one sequence, x0 (k), is available as the reference sequence and all other sequences serve as comparison sequences, it is called a local grey relation measurement. After data pre-processing is carried out, the grey relation coefficient $\gamma(x_0^*(k), x_i^*(k))$ for the k^{th} performance characteristics in the i^{th} experiment can be expressed as (Gaitonde, Karnik, Achyutha, & Siddeswarappa, 2008; Haq, Marimuthu, & Jeyapaul, 2008):

$$\boldsymbol{\gamma(x_0^*(k), x_i^*(k)) = \frac{\Delta_{min} + \xi.\Delta_{max}}{\Delta_{0i}(k) + \xi.\Delta_{max}}} \quad (4.10)$$

According to the above equation, $x_0^*(k)$ denotes the reference sequence and $x_i^*(k)$ denotes the comparability sequence. Also, ξ is distinguishing or identification coefficient: ξ ∈ [0, 1] (the value may be adjusted based on the actual system requirements). A value of ξ is the smaller and the distinguished ability is the larger. ξ = 0.5 is generally used. Δ_{0i} is the deviation sequence of the reference sequence and the comparability sequence.

$\Delta_{0i} = \|x_0^*(k) - x_i^*(k)\|$ The absolute value of differences between$x_0(k)$ and $x_i(k)$

$\Delta_{min} = \min_{\forall j \in i} \min_{\forall k} \|x_0^*(k) - x_j^*(k)\|$ Is the smallest value of $x_i(k)$

$\Delta_{max} = \max_{\forall j \in i} \max_{\forall k} \left\| x_0^*(k) - x_j^*(k) \right\|$ Is the largest value of $x_i(k)$

4.2.8.5 Grey Relational Grade

After the grey relational coefficient is derived, it is usual to take average value of the grey relational coefficients as the grey relational degree.

$$\overline{\boldsymbol{\gamma}} = \frac{\mathbf{1}}{\boldsymbol{k}} \sum_{\boldsymbol{i=1}}^{\boldsymbol{m}} \boldsymbol{\gamma_{ij}} \tag{4.11}$$

Where, $\bar{\gamma}$ is the grey relational grade for j^{th} experimental and k is the number of performance characteristics. The values of grey relational coefficient and grey relational grade are calculated from the Equations 4.2 and 4.3 then they are listed in Table 4.6.

Table 4.6: Full results of the experiments, normalized value, GRC and GRG values

Fin NO.	Re	Melting Time (s)	Solidification Time (s)	Normalized		Grey coefficient		Grade
				Melting	Solidification	Melting	Solidification	
24	1000	6350	1720	0.016	0.975	0.337	0.952	0.645
24	1500	6510	1685	0.773	0.578	0.688	0.542	0.615
24	2000	6249	1740	0.939	0.485	0.891	0.493	0.692
24	1000	4250	760	0.043	1.000	0.343	1.000	0.672
24	1500	4339	745	0.785	0.595	0.700	0.552	0.626
24	2000	4182	775	0.948	0.500	0.905	0.500	0.703
24	1000	3759	550	0.000	0.956	0.333	0.918	0.626
24	1500	3838	539	0.761	0.565	0.677	0.535	0.606
24	2000	3699	560	0.930	0.474	0.878	0.487	0.682
48	1000	1850	730	0.797	0.124	0.711	0.363	0.537
48	1500	1839	718	0.860	0.066	0.781	0.349	0.565
48	2000	1866	743	0.994	0.001	0.988	0.334	0.661
48	1000	1540	650	0.806	0.122	0.721	0.363	0.542
48	1500	1531	640	0.868	0.064	0.791	0.348	0.570
48	2000	1553	662	1.000	0.000	1.000	0.333	0.667
48	1000	1200	480	0.786	0.127	0.700	0.364	0.532
48	1500	1193	472	0.850	0.068	0.769	0.349	0.559
48	2000	1204	489	0.987	0.002	0.974	0.334	0.654

According to the Table 4.6 from the grey relational grade, the response table was prepared. Table 4.7 is the response table for both the two control factors and their levels which show that fin number has the most effect on optimizing the results and after that the flow rate of HTF.

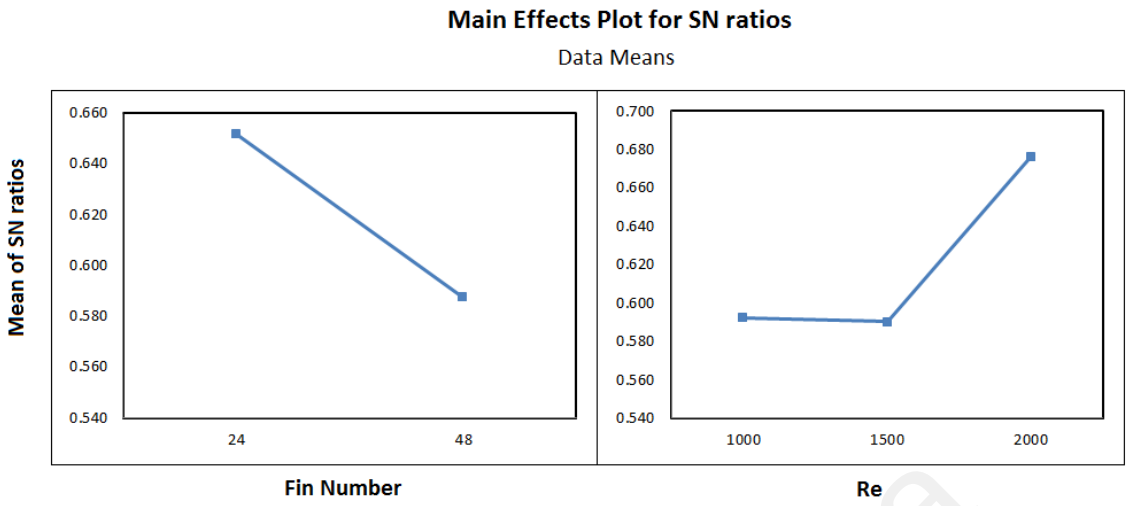

Figure 4.11: Effect of the control factors on solidification and melting time simultaneously.

Table 4.7: Response table for gray grade.

	Fin No	Re
level 1	0.652	0.592
level 2	0.587	0.590
level 3		0.676
delta	0.064	0.086
rank	2	1

Considering Table 4.7, the best combination to achieve optimum result is Re=1000 and 48 fins. Although, this combination was tested three times, to confirm the result of this combination, a new experiment with this condition was implemented as a validation test. There remains a very close agreement between initial experimental results and confirmation test results which show the accuracy of the experimental conditions.

4.3 Result and Discussions, Part B

4.3.1 Melting Process

Temporal variation of temperature at different radial points given in Figure 4.12, Figure 4.13, Figure 4.14 and Figure 4.15 are obtained for different inlet temperatures, various types of HTF and HTF flow rates considered. For the brevity, only the results for specific conditions are depicted in figures, which represent a typical transient behavior. As can be seen, melting starts peripherally near the HTF tube wall. Then, it extends to the radially outwards. After the initiation of the charging process, all the points close to the HTF tube surface reaches to the melting temperature, i.e. the PCM in the region close to the HTF tube wall immediately melts, as result of conduction. It is mainly due to the higher HTF-PCM temperature difference at the vicinity of the tube wall that makes the PCM near the walls to melt faster. However, melting behavior dramatically differs for the points located in the upper region than those located in the lower region. The molten PCM ascends to the top part of the storage container as a result of natural convection currents. The melt region extends radially upward. Consequently, the points in the upper region reach the melting temperatures earlier than those in the lower region.

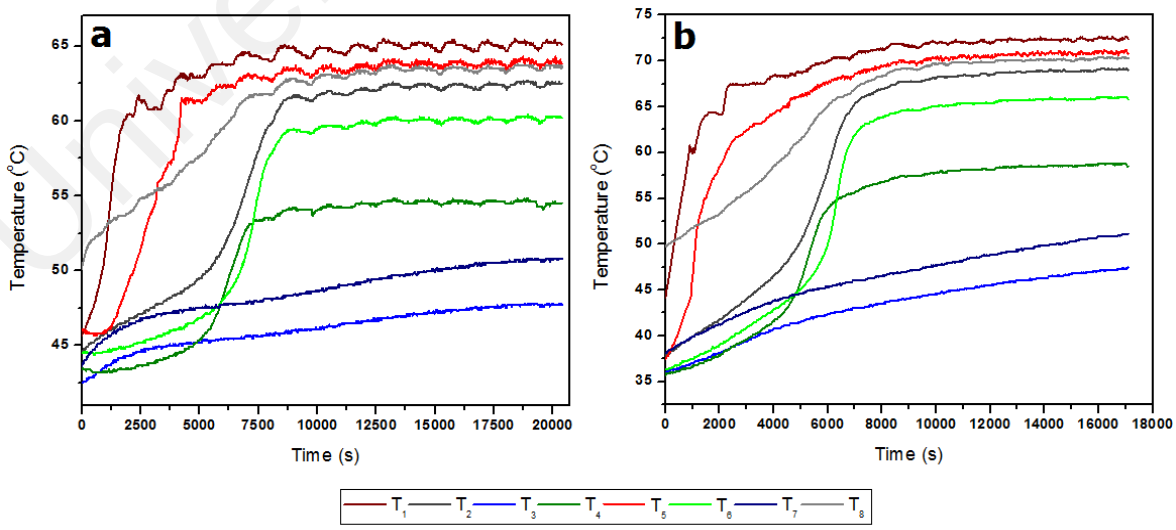

Figure 4.12: Temperature measurement records in the melting process for tube #1 with Distilled Water as HTF at a) Re=1500(Temp=70), b) Re=2000 (Temp=80).

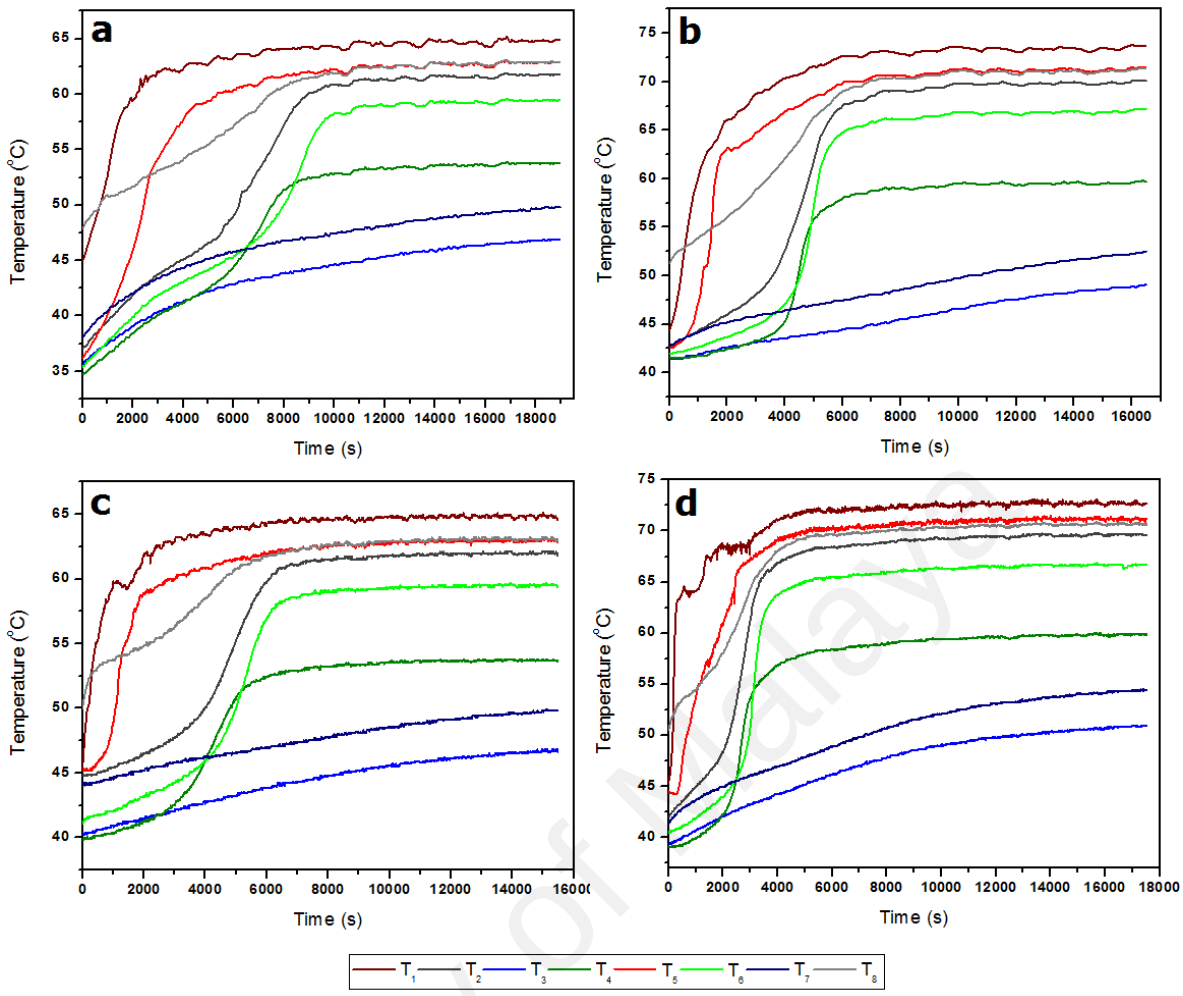

Figure 4.13: Temperature measurement records in the melting process for tube #1 with TiO_2 (0.05 %wt) as HTF at a) Re=1000(Temp=70), b) Re=1500 (Temp=80) with TiO_2 (0.1 %wt) as HTF at c) Re=1000(Temp=80), d) Re=2000 (Temp=70).

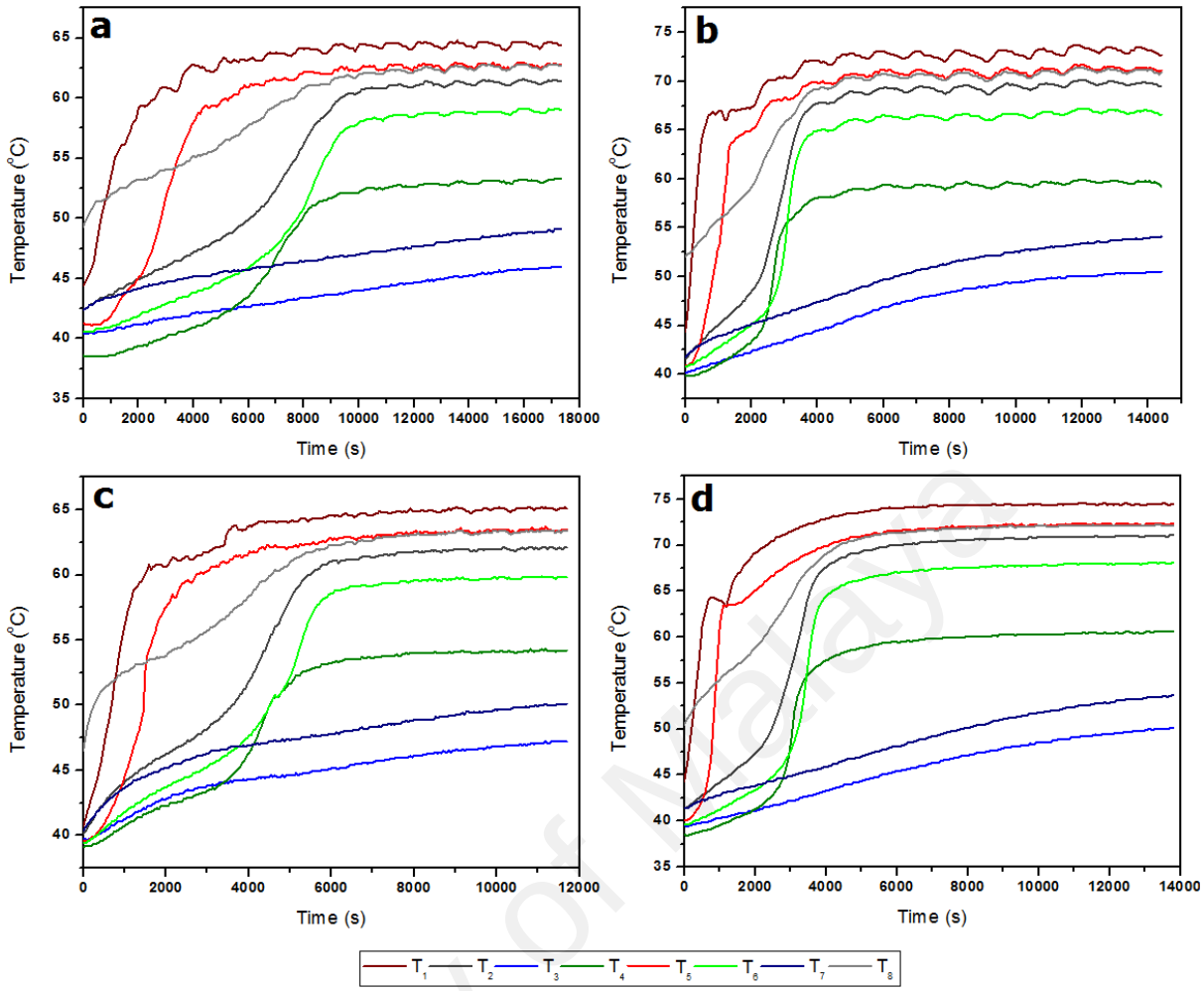

Figure 4.14: Temperature measurement records in the melting process for tube #1 with CNT (0.05 %wt) as a HTF at a) Re=1000 (Temp=70), b) Re=1500 (Temp=80) and with CNT (0.1 %wt) as HTF at c) Re=1000 (Temp=80), d) Re=2000 (Temp=70).

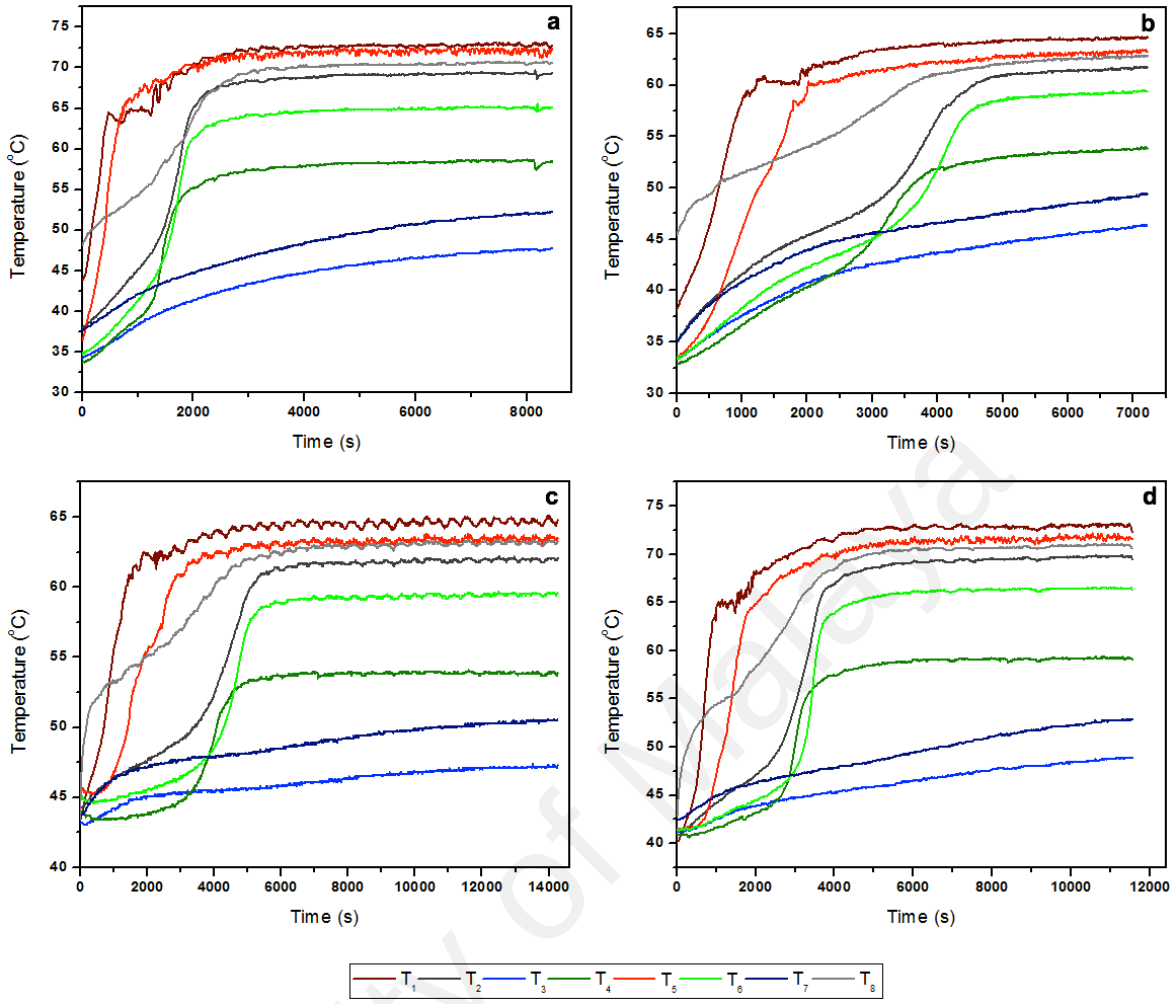

Figure 4.15: Temperature measurement records in the melting process for tube #1 with GNP (0.05 %wt) as a HTF at a) Re=1000 (Temp=70), b) Re=1500 (Temp=80) and with GNP (0.1 %wt) as HTF at c) Re=1000 (Temp=80), d) Re=2000 (Temp=70).

This is much clearer by visual photo of PCM behavior in melting process that given in Figure 4.16. This figure clearly illustrates evolution of temperature at the radial points located radially at equal distance from the HTF tube wall. The radial temperature of the PCM at the specified radial position gradually increases by time. As can be observed, the main mechanism is initially conduction in heat transfer. The next dominant mechanism is natural convection which is highly effective at the upper section of the annular storage tank. Aydın et al. [1] clarified the physical features of PCM in the charging process. In the charging processes, the melted PCM in the liquid phase and the non-melted PCM in the solid phase are the regions that exist together. In the solid region, the heat transfer process inside is attributed to the conduction which is inside the PCM solid matrix. It

should be mentioned that this region gets the heat from the melted wax is through convention. The heat transfer convention system conducts the recirculation in the melted PCM after its solid matrix melts. This can be attributed to the buoyancy forces caused by the density gradients which happen because of temperature disparity. The mentioned recirculation improves the heat and mixing transfer in the molten PCM that is justified by the fact that the points close to the upper sector get to the melting temperature faster than the lower ones. It should be mentioned that the molten PCM density is less than the density in solid phase. The molten PCM region develops in order to cover the bigger regions of PCM tanks at higher operating times.

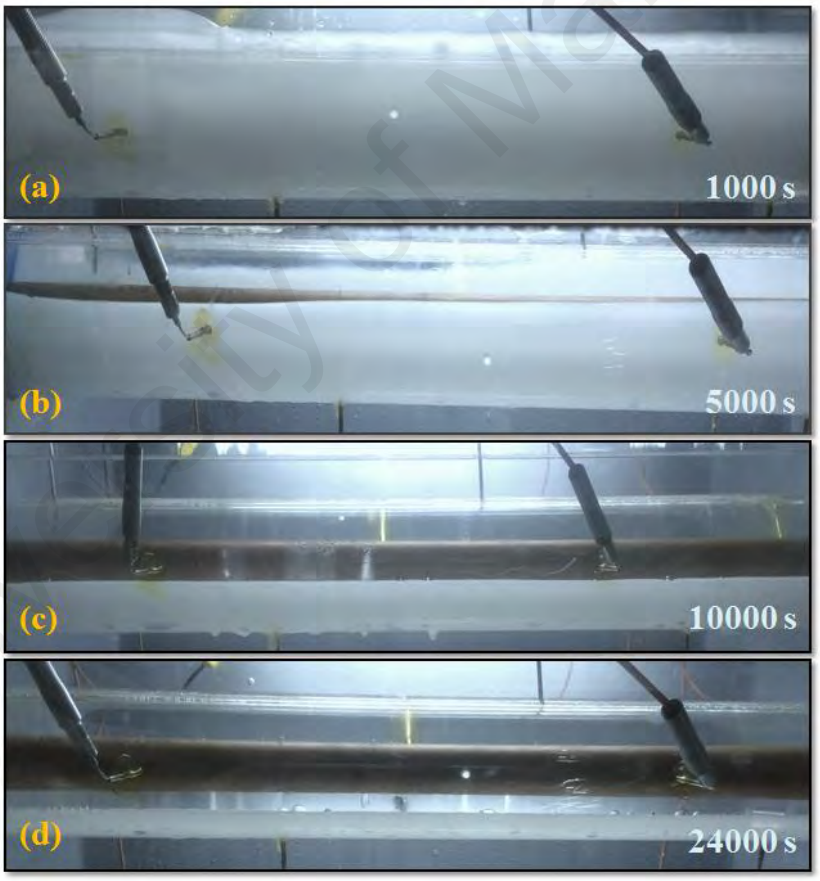

Figure 4.16: Melting Process for distill water at Re=1000 and T_i= 70°C in tube #1 at (a) 1000s, (b) 5000s, (c) 10000s and (d) 24000s.

As it has been discussed in the design of thermocouples B section, thermocouples are mutually comparable in terms of the position and distance from copper tube which this

effect can clearly be seen in the Figures 4.12, 4.13, 4.14 and 4.15. The figures also suggest that the variations and trends of thermal curves are also mutually comparable which are shown by an upper or lower step shift. This phenomenon is due to the temperature differences between HTF at the input and output of the copper tube. The figures also depict the PCM variation in the melting situation for different HTFs used in this experiment including distilled water, TiO_2 (0.05% and 0.1%), CNT (0.05% and 0.1%) and GNP (0.05% and 0.1%) for the input temperatures of T_i=70 °C and T_i=80°C with different flow rates. Based on the Figures 4.12, 4.13, 4.14 and 4.15 the variations can be categorized into three groups according to their located positions from copper tube and the PCM container which have similar trends as: T_1 & T_5 (zone A), T_3 & T_7 (zone B) and T_2 & T_4 &T_6 &T_8 (zone C). The zone A and C are for upper side and down side of the container respectively and the zone B is the edge of copper tube as shown in Figure 4.17. For instance, the PCM located in the first group reaches to the temperature higher than the melting temperature of paraffin in less than 1000s as shown in the Figure 4.14b while for the second group, even after 9000s, it did not reach at the melting point. This phenomenon is due to the changing of paraffin density during the melting process since the density of solid paraffin is higher than liquid paraffin which induces the solid paraffin to be deposited at the bottom of the container.

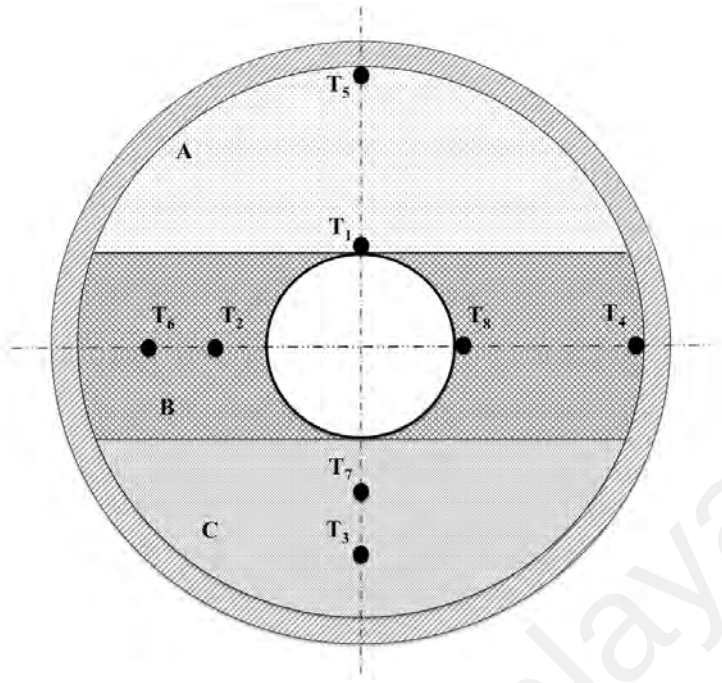

Figure 4.17: Position of thermocouples in cross section of PCM's container.

As it can be seen in Figure 4.14b, T2, T4, T6 and T8 which are placed at the edge of the copper tube with different radial and axial positions, show comparable trends with similar fluctuations caused by replacing solid PCM to molten PCM at the edge of copper tube. From Figure 4.12a, it can be observed that T2 ,T4 , T6 and T8 reach to the stable state (completely melted) after 8000s while for zone A (T1 and T5) this process takes 4000s which is more than two times faster compared to the zone B. For (T2 ,T4 , T6 & T8) and (T1 & T5) the processes of melting takes 6000s and 2000s respectively to complete where zone A needs a third timing comparative to zone B. This phenomenon is due to the increase of Reynolds number from 1500 to 2000 and depicted in Figure 12b. When the inlet temperature went up, it improves the melting inside as anticipated.

Moreover, the increase in T_i resulted in getting the points inside phase change material to the melted state in shorter periods as displayed in Figures 4.12, 4.13, 4.14 and 4.15. Due to the increase of T_i from 70°C to 80°C, the final temperature of the curves become different and it can be observed that the melting process also becomes faster due to the increase of Re and T_i which shortens the melting process time from 20000s to 17000s

(Figure 4.12 (a and b)). On the other hand, for (T_3 & T_7), no considerable changes can be observed regarding the increase of the inlet temperature and Reynolds number. That is to say, that the adequate heat energy did not reach this side of the container and finally the paraffin had not been melted. Different nanofluids with different weight percentages have been used in this experiment to increase the heat transfer performance leading to increase the thermal conductivity. Table 4.8 demonstrates the melting times for different nanofluids with different temperatures and Reynolds numbers.

4.3.1.1 Effect of Flow Rate, Nanofluids and Inlet Temperature on Melting Process

By comparing the melting process times which are listed in Table 4.8, it can be concluded that changing HTF from distilled water to TiO_2 (0.05%) can reduce 10% of the melting process time and by increasing the density of TiO_2, this improvement could be about 18%. In case of CNT with weight percentage of 0.1%, the melting process time decreased 37% compared to water while CNT (0.05%) improves this process by 23%. It is notable that GNP has the highest performance in comparison to TiO_2 and CNT in decreasing the melting process time from 39% to 62% in 0.05 and 0.1 weight percentages, respectively. According to the results listed in Table 4.8, it can be observed that the variation of inlet temperature of HTF from 70°C to 80°C can reduce 8-15% of the melting process time. For distilled water with Re=1000 and temperature of 70°C and 80°C, the melting process time decreases from 24000s to 21720s which has 9.5 % reduction. From the aspect of inlet temperatures, the variation of melting time was between 8-10%. As can be seen in Table 4.8, with the increasing of inlet temperature by 10 degree for GNP (0.05) at Reynolds 1500, the melting time was reduced to 9.5% from 12780s to 11560s. For TiO_2 (0.1%), the melting time has been reduced from 16800s to 15360s at temperature 70°C and 80°C with Re= 1500 which has the improvement of almost 9%. About the similar improvement (10 %) can be obtained for the CNT (0.05%) with Re=2000 at 70°C with 14700s and at 80°C with 13140s.

Table 4.8 listed the experimental results in which the melting process times were measured based on the equal inlet temperatures and HTF with different Reynolds numbers. In addition, variation of flow rate can affect and reduce the melting time by 11% to 25%. For distilled water with 70°C inlet temperature, the melting time decreases from 24000s to 20520s when Reynolds number increases from 1000 to 1500 which is 14.5 % of reduction in the melting time.

Table 4.8: Melting time for different inlet temperatures, different nonofluids and HTF flow rates.

Flow rate (Re)	Melting Temperature (°C)	Type of HTF		Melting Time (s)
1000	70	Water		24000
		TiO_2	0.05	21780
			0.1	19080
		CNT	0.05	17880
			0.1	14580
		GNP	0.05	14260
			0.1	9430
	80	Water		21720
		TiO_2	0.05	19740
			0.1	17160
		CNT	0.05	16440
			0.1	13560
		GNP	0.05	13000
			0.1	8470
1500	70	Water		20520
		TiO_2	0.05	18000
			0.1	16800
		CNT	0.05	16080
			0.1	13140
		GNP	0.05	12780
			0.1	7920
	80	Water		18900
		TiO_2	0.05	16380
			0.1	15360
		CNT	0.05	14400
			0.1	12000
		GNP	0.05	11560
			0.1	7480
2000	70	Water		19140
		TiO_2	0.05	17220
			0.1	15480
		CNT	0.05	14700
			0.1	11700
		GNP	0.05	11210
			0.1	7230
	80	Water		17100
		TiO_2	0.05	14820
			0.1	14040
		CNT	0.05	13140
			0.1	10740
		GNP	0.05	10650
			0.1	6640

For TiO_2 (0.05%) at 80°C inlet temperature, increasing of the Reynolds number from 1000 to 2000 causes diminishing of the melting time from 19740s to 14820s that is 25% of reduction. For CNT (0.05%) at 70°C inlet temperature, changing of the Reynolds number from 1500 to 2000 can reduce 11% of the melting time from 17880s to 16080s. In the same condition for GNP (0.05), the melting time also reduced 12.3% from 12780s to 11210s.

4.3.2 Solidification Process

By the help of flowing cold water through the system, solidification and discharging process tests disapprove the charging experiment. As can be seen in Figure 4.18, at first, the phase change material is the liquid-phase. System conduction for discharging aims to indicate sudden temperature alterations because of a higher temperature disparity between HTF and PCM which is followed by a relatively slow alteration. A sensible-type heat transfer happens inside the PCM at every point where the phase change material gets the solidification temperature. Solidification takes place faster at the points close to the HTF wall as predicted. Temporal difference of radial temperature distribution at the radial points which is placed radially at the same interval from the HTF tube wall is displayed in Figure 4.18 to explore the physics of the process comprehensively. By passing the time, the radial temperature of phase change material constantly diminishes at the specified radial position. After some time, the temporal variation was found to be radially homogenous which is due to the impact of natural convection on the heat transfer. Next, the conduction acts as the dominant heat transfer mechanism with less convection effects as compared to the melting or charging which can be justified by the point that the natural convection of melted PCM — affected the circulation and –decreased the time. It corresponds the solidification growth at the outward of the HTF tube.

Figure 4.18: Solidification Process for distill water at Re=1000 and T_i= 30°C in tube #1 at (a) 1000s, (b) 3000s, (c) 5000s and (d) 7000s.

PCM temperature variations for different HTF of GNP (0.1% and 0.05%) ,CNT (0.1% and 0.05%), TiO_2 (0.1% and 0.05%) and distilled water with different Reynolds numbers of1000, 1500 and 2000 as well as different inlet temperatures (T_i= 20°C and 30°C) at different radial points are given in Figures 4.19, 4.20, 4.21 and 4.22.

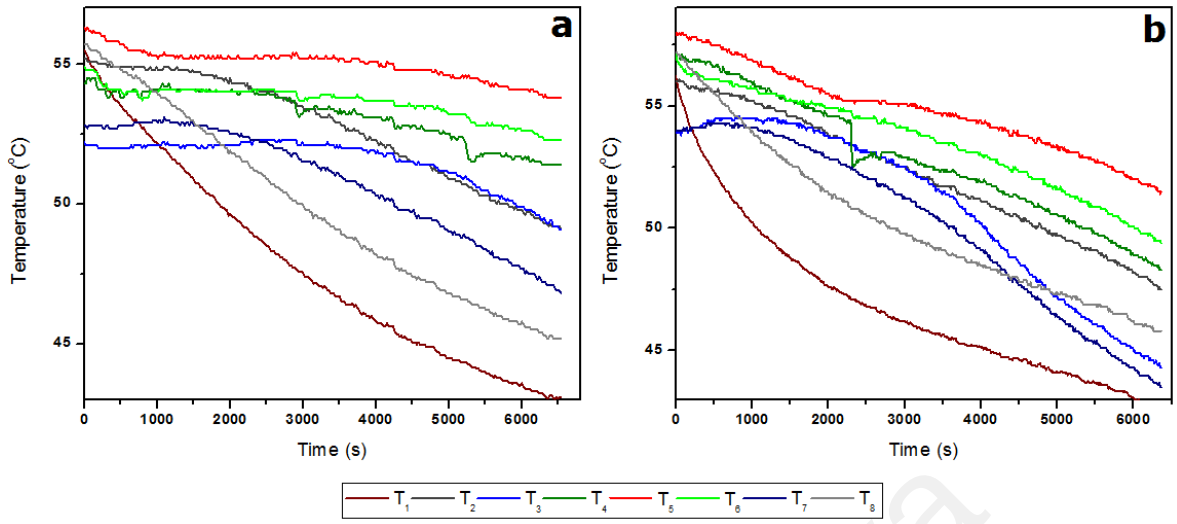

Figure 4.19: Temperature measurement records in the solidification process for tube #1 with Distilled Water as HTF at a) Re=1500 (Temp=30), b) Re=2000 (Temp=20).

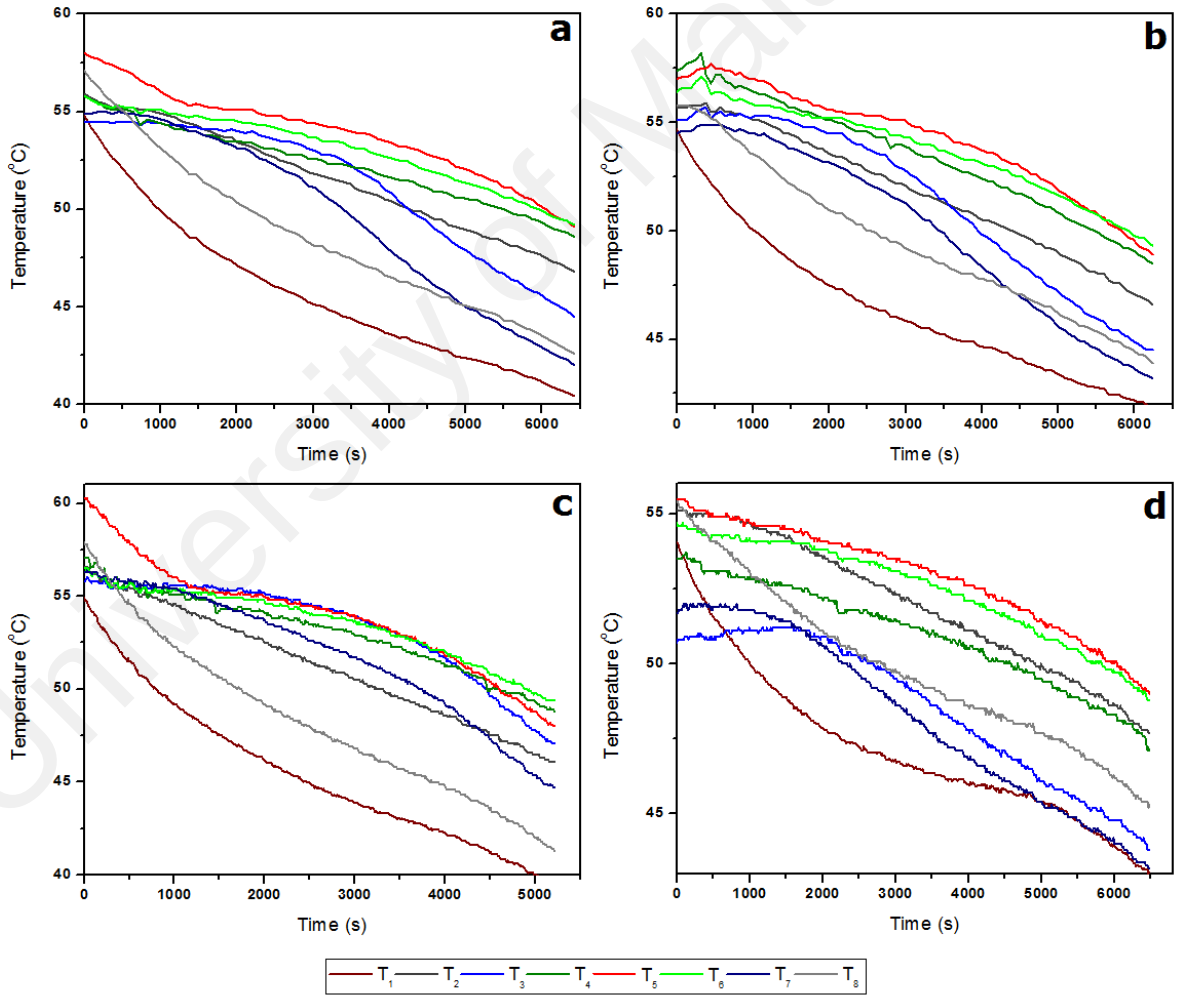

Figure 4.20: Temperature measurement records in the solidification process for tube #1 with TiO_2 (0.05 %wt) as HTF at a) Re=1000 (Temp=30), b) Re=1500 (Temp=20) with TiO_2 (0.1 %wt) as HTF at c) Re=1000 (Temp=20), d) Re=2000 (Temp=30).

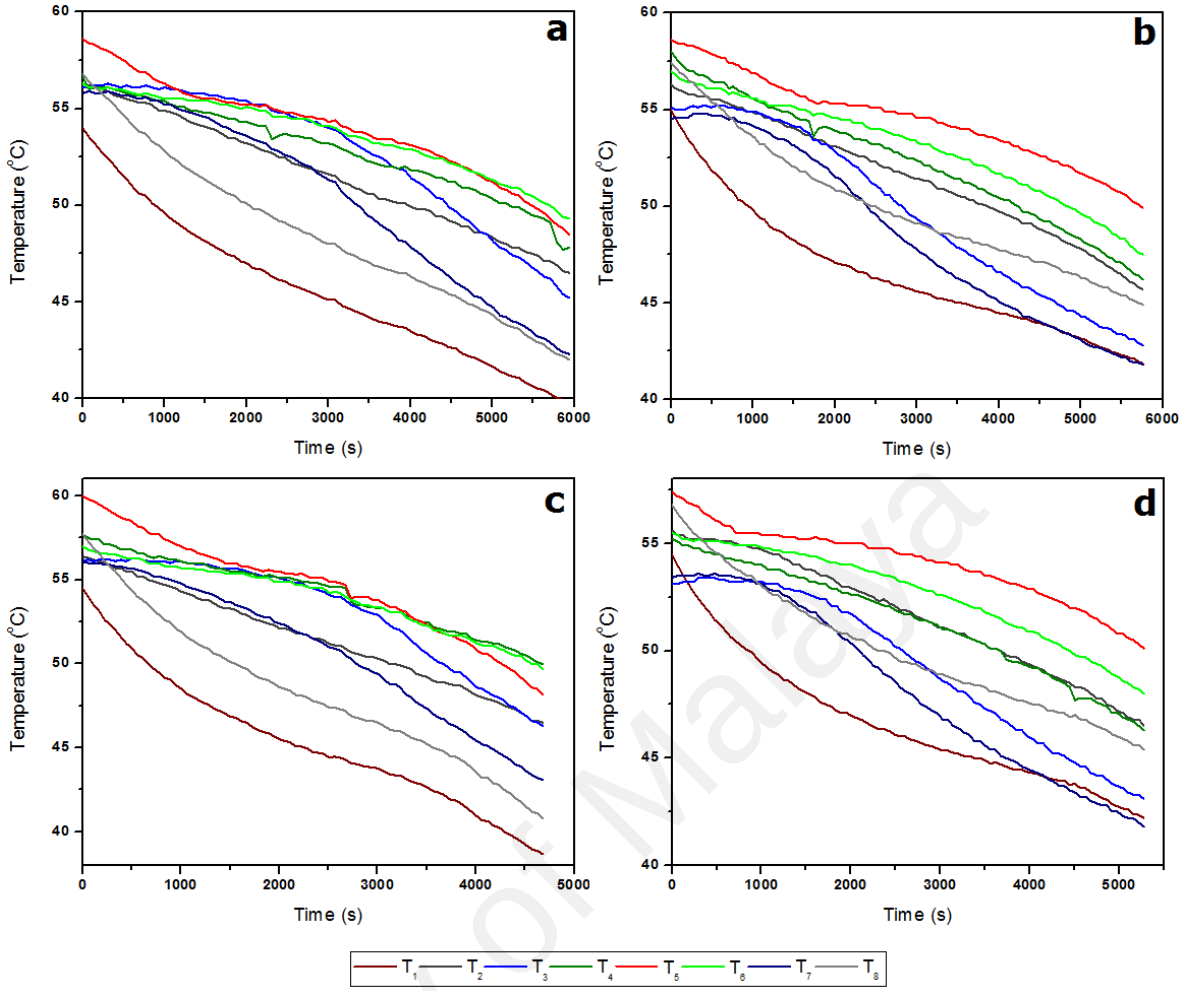

Figure 4.21: Temperature measurement records in the solidification process for tube #1 with CNT (0.05 %wt) as a HTF at a) Re=1000(Temp=30), b) Re=1500 (Temp=20) andwith CNT (0.1 %wt) as HTF at c) Re=1000(Temp=20), d) Re=2000 (Temp=30).

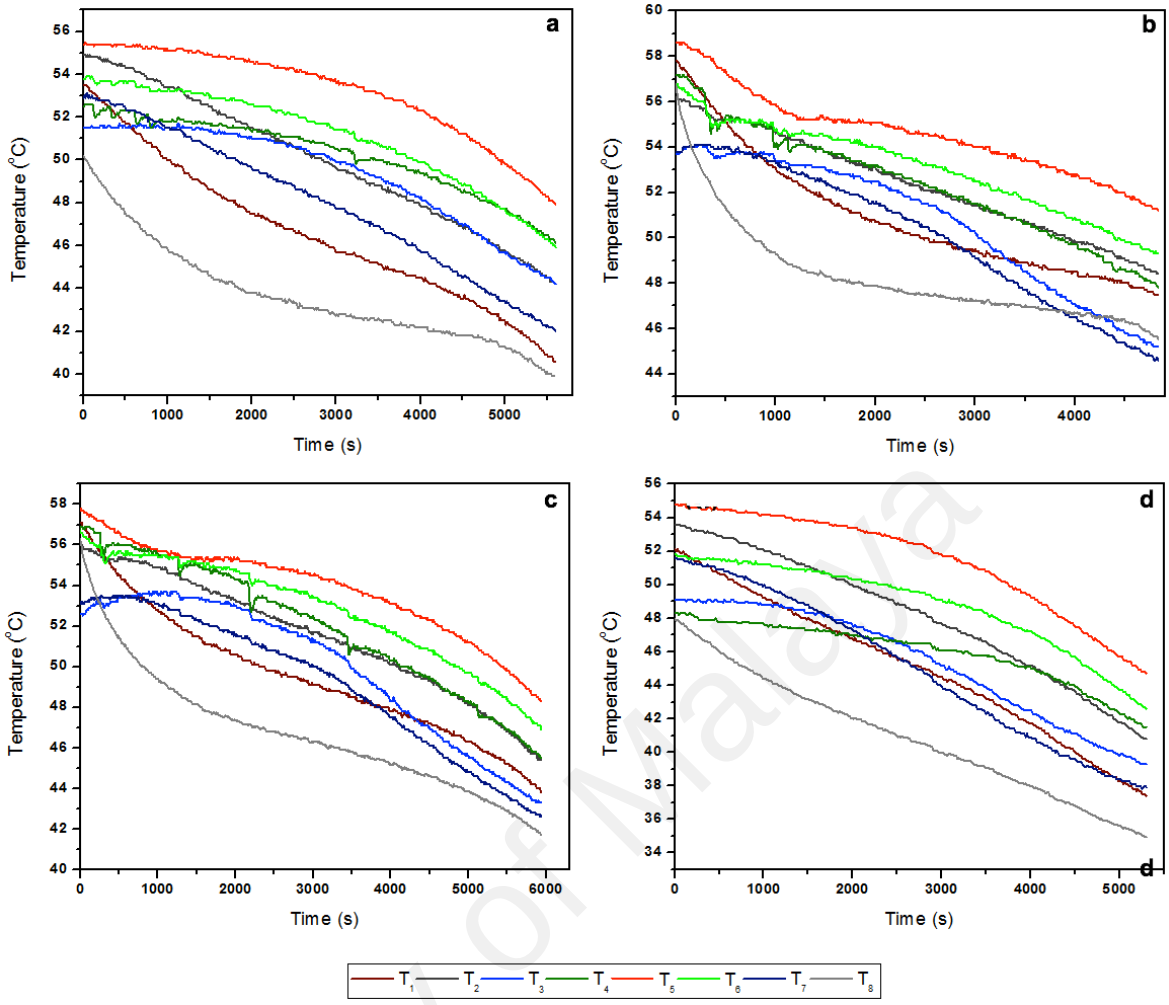

Figure 4.22: Temperature measurement records in the solidification process for tube #1 with GNP (0.05 %wt) as a HTF at a) Re=1000(Temp=30), b) Re=1500 (Temp=20) and with GNP (0.1 %wt) as HTF at c) Re=1000(Temp=20), d) Re=2000 (Temp=30).

As it is seen the charts have the similar trend but with the different slopes. This is also obvious in the Figure 4.18 that the solidification growth is radially and around the copper tube. This method causes that PCM is solidified symmetrically around the copper tube and the diameter of PCM increases over the time. As a result, the areas that have been stuck to the copper tube surface become solidified sooner. Another important point in this part of the experiment is expressible due to the higher temperature difference between PCM and HTF at the inlet compared to the outlet. The solidification growth is faster near the inlet compared to the outlet and the PCM form spindly which is more like a cylindrical. All the charts in Figures 4.19, 4.20, 4.21 and 4.22 are shown to express the behavior of decline trend of PCM temperatures for the different conditions. From the

practical consideration, the total solidification time is important. The primary goal is to remove the stored thermal energy, i.e. to supply it to the desired location, in a time as short as possible. In order to have a much clearer insight onto the effect the eccentricity, its effect on the total solidification time is depicted in Figures 4.19, 4.20, 4.21 and 4.22. Likewise, when the inlet temperatures drops down (for the discharging process), the solidification speeds up.

4.3.2.1 Effect of Flow Rate, Nanofluids and Inlet Temperature on Solidification Process

Flow rate is one of the foundations of heat transfer, increase of which generally makes the enhancement in heat transfer. In this part, the impact of this factor is considered on the solidification process with the presence of nanofluids. Table 4.9 demonstrates the solidification times for different nanofluids with different temperatures and Reynolds numbers. According to the table, time reduction of solidification for distilled water with the inlet temperature of 20°C and for Re=1000, and 1500 was dropped from 6900s to 6360s and it was equal to 8%. Moreover, the most time reduction is related to increasing the Reynolds number from 1000 to 2000 which is 15%. For CNT (0.1%) and inlet temperature 30°C, this Reynolds number change causes solidification time reduction by 6120s to 5220s. So, it is noteworthy that 8% time reduction by increasing the Reynolds number of 1500 to 2000 is almost similar to the Reynolds number increment from 1000 to 1500. This increasing of Reynolds number has caused solidification time reduction by 6780s to 6240s for TiO_2 (0.05%) when the inlet temperature was 20°C. As can be seen in Table 4.8, with doubling the Reynolds number from 1000 to 2000 for GNP (0.1) at 20°C, the solidification time was reduced to 15.3% from 5480s to 4640s.

Basically, nanoparticles cause thermal conductivity enhancement and increases the heat transfer which leads the solidification time reduction. In this section, the effect of

nanofluids on solidification process is considered. Table 4.9 shows the solidification times for different nanofluids with variuos weight percentages so that Reynolds numbers and inlet temperatures are equal to represent the impact of nanofluids on solidification process. As it is seen in the table, the most reduction is related to GNP (0.1%), about 20% and the least reduction is for TiO_2(0.05%), about 1.9%. However, GNP(0.05%), TiO_2(0.1%) and CNT(0.05%) cause solidification time reduction around 16.%, 4.6% and 9.2%, repectively. For instance, this time has reduced from 6900s to 6600s for TiO_2(0.1%) in inlet temperature 20°C and Re=1000. Similarly, the amount of time reduction is of 6900s to 5760s for CNT(0.1%) in the same conditions that it is equal to 14.3%. The last factor, which must be considered in this experiment, is the impact of inlet temperature reduction on solidification process. In precise study, this factor is sorted based on the same nanofluids as well as same Reynolds numbers in Table 4.9.

Table 4.9: Solidification times for different inlet temperature, different nonofluids and HTF flow rates values.

Flow rate (Re)	Solidification Temperature (°C)	Type of HTF		Solidification Time (s)
1000	30	Water		7140
		TiO_2	0.05	7020
			0.1	6840
		CNT	0.05	6540
			0.1	6120
		GNP	0.05	5940
			0.1	5710
	20	Water		6900
		TiO_2	0.05	6780
			0.1	6600
		CNT	0.05	6240
			0.1	5880
		GNP	0.05	5650
			0.1	5480
1500	30	Water		6660
		TiO_2	0.05	6480
			0.1	6360
		CNT	0.05	6000
			0.1	5640
		GNP	0.05	5550
			0.1	5260
	20	Water		6360
		TiO_2	0.05	6240
			0.1	6060
		CNT	0.05	5760
			0.1	5400
		GNP	0.05	5320
			0.1	5030
2000	30	Water		6120
		TiO_2	0.05	6060
			0.1	5820
		CNT	0.05	5520
			0.1	5220
		GNP	0.05	5110
			0.1	4840
	20	Water		5880
		TiO_2	0.05	5760
			0.1	5580
		CNT	0.05	5280
			0.1	4980
		GNP	0.05	4860
			0.1	4640

According to the presented times in this table, it is observed that reducing the inlet temperature about 10°C, decreases the solidification time between 4.5% to 5%. It can be indicated that solidification time reduces from 6120s to 5880s for distilled water at Re=2000 by reduction of inlet temperature from 30°C to 20°C. Also, for TiO_2 (0.1%) at Re=1500, reducing of the inlet temperature from 30°C to 20°C makes decrement of solidification time by 6360s to 6060s. In addition, variation of inlet temperature can affect and reduce the solidification time by 4.02% for GNP (0.1) at Re=1000, the solidification time there decreases from 5710s to 5480s.

CHAPTER 5: CONCLUSIONS AND RECOMMENDATIONS

5.1 Conclusions

In this study, the effects of various nanofluids at different constructions, fin density, inlet and flow rate of HTF on storing latent thermal energy were investigated experimentally. These effects were observed for both charging and discharging of the latent heat energy. For this purpose, a series of experiments were performed and the results were recorded. The inlet temperature would primarily affect the energy storage, especially on the speed of melting and solidification. As described in the previous chapters, the different shaped tubes were used in the tests in order to figure out the effects of the fin spacing on the energy storage.

The experiments brought out some interesting results about the effect of the fin density on the energy storage. As expected, increasing of the fin density resulted in more energy storage during melting process. It has been noted that the increasing of fin density causes more energy storage than the increasing of the Reynolds number. For the solidification process, the results are more complicated than those of the melting. The effect of the natural convection on these results cannot be certainly ignored at this point. It has been observed that the amount of the discharged thermal energy is increased by the increment of the fin density. The impact of the fin area enhancement in melting is 20% more than its effect on the solidification. According to the study, the effects of flow rate on melting and solidification, provide similar results for design A and B where the effect of growth of flow rate on melting is approximately 1.5 times more than that for the solidification. It is seen that impact of the 10°C change of inlet temperature in melting process causes the processing time reduction around 50% more than observed in the case of solidification process at the same temperature variation. Thus the nanofluids have the minimum impact on the solidification compared to the melting process. Thus the melting time 3 to 5 times diminishes more compared to the reduction on solidification time. The reason of this

happening is due to the radial growth of the solidification process from the conduction heat transfer after establishment of the first layer of solid PCM around the copper tube. This plays a vital role in the decrement of nanofluids effect on the solidification process.

The ideology of this experiment is the decreasing of the melting time and increasing of the solidification time. Nanofluids are the best to enhance the performance which predicts that it can achieve the significant performance for this experiment by using nanofluids with higher thermal conductivity as well as the internal fins. Likewise, if we design a system in which the Reynolds number can be adjusted in higher values but less than 2300 for charging at the lower values for discharging the highest amount of stored energy which can be resulted in shorter time.

5.2 Recommendations

Many studies, experiments and efforts have been incorporated in the present thesis, there are still some blurry points which must be solved by much improved designs and also by using new materials as well as accurate optimization.

It has also been shown that PCM wax stores a large amount of thermal energy from latent heat. Furthermore, increasing of the stored energy brings additional benefit to these systems which effect the other parameters which needs further investigation. To sum up, the concerns which ought to be considered in the future works are listed as below:

- Apply Coating on the tubes of the PCMs with various Nano particles
- Changing the design of tube:
    - Example: Diameter, fin design, type of tubes and the material of the tubes
- Using of the various PCMs:
    - Example: Fatty Acid, palmitic acid, salt hydrate and myristic acid
- Study on the high HTF flow rates (Re>2300)

REFERENCES

Abbasian Arani, A. A., & Amani, J. (2012). Experimental study on the effect of TiO2–water nanofluid on heat transfer and pressure drop. *Experimental Thermal and Fluid Science, 42*(0), 107-115.

Abhat, A. (1983). Low temperature latent heat thermal energy storage: heat storage materials. *Solar energy, 30*(4), 313-332.

Abouali, Omid, & Ahmadi, Goodarz. (2012). Computer simulations of natural convection of single phase nanofluids in simple enclosures: A critical review. *Applied Thermal Engineering, 36*, 1-13.

Afshar, Hossein, Shams, Mehrzad, Nainian, Seyed Mojtba Mousavi, & Ahmadi, Goodarz. (2012). Two-phase study of fluid flow and heat transfer in gas-solid flows (nanofluids). *Applied Mechanics and Materials, 110*, 3878-3882.

Agyenim, F., Eames, P., & Smyth, M. (2009). A comparison of heat transfer enhancement in a medium temperature thermal energy storage heat exchanger using fins. *solar energy, 83*(9), 1509-1520.

Agyenim, F., Eames, P., & Smyth, M. (2010). Heat transfer enhancement in medium temperature thermal energy storage system using a multitube heat transfer array. *Renewable Energy, 35*(1), 198-207.

Agyenim, F., & Hewitt, N. (2010). The development of a finned phase change material (PCM) storage system to take advantage of off-peak electricity tariff for improvement in cost of heat pump operation. *Energy and Buildings, 42*(9), 1552-1560.

Akgün, M., Aydın, O., & Kaygusuz, K. (2007). Experimental study on melting/solidification characteristics of a paraffin as PCM. *Energy conversion and management, 48*(2), 669-678.

Akhtari, M, Haghshenasfard, M, & Talaie, MR. (2013). Numerical and Experimental Investigation of Heat Transfer of α-Al_2O_3/Water Nanofluid in Double Pipe and Shell and Tube Heat Exchangers. *Numerical Heat Transfer, Part A: Applications, 63*(12), 941-958.

Al-Abidi, Abduljalil A, Mat, Sohif, Sopian, K, Sulaiman, MY, & Mohammad, Abdulrahman Th. (2013). Numerical study of PCM solidification in a triplex tube heat exchanger with internal and external fins. *International Journal of Heat and Mass Transfer, 61*, 684-695.

Al-Hinti, I., Al-Ghandoor, A., Maaly, A., Abu Naqeera, I., Al-Khateeb, Z., & Al-Sheikh, O. (2010). Experimental investigation on the use of water-phase change material storage in conventional solar water heating systems. *Energy Conversion and Management, 51*(8), 1735-1740.

ALVA S, LH, Gonzalez, JE, & Dukhan, N. (2006). Initial analysis of PCM integrated solar collectors. *Journal of solar energy engineering, 128*(2), 173-177.

Anoop, Kanjirakat, Cox, Jonathan, & Sadr, Reza. (2013). Thermal evaluation of nanofluids in heat exchangers. *International Communications in Heat and Mass Transfer, 49*, 5-9.

Arkar, C, & Medved, S. (2007). Free cooling of a building using PCM heat storage integrated into the ventilation system. *Solar Energy, 81*(9), 1078-1087.

Aydın, Ahmet Alper, & Okutan, Hasancan. (2011). High-chain fatty acid esters of myristyl alcohol with even carbon number: Novel organic phase change materials for thermal energy storage—1. *Solar Energy Materials and Solar Cells, 95*(10), 2752-2762.

Aydın, Orhan, Akgün, Mithat, & Kaygusuz, Kamil. (2007). An experimental optimization study on a tube-in-shell latent heat storage. *International journal of energy research, 31*(3), 274-287.

Azmi, WH, Sharma, KV, Sarma, PK, Mamat, Rizalman, Anuar, Shahrani, & Sundar, L Syam. (2014). Numerical validation of experimental heat transfer coefficient with SiO_2 nanofluid flowing in a tube with twisted tape inserts. *Applied Thermal Engineering, 73*(29), 294-304.

B len, K, Takgil, F, & Kaygusuz, K. (2008). Thermal energy storage behavior of CaCl2. 6H2O during melting and solidification. *Energy Sources, Part A, 30*(9), 775-787.

Bajnoczy, G., Gagyi Palffy, E., & Prépostffy, E. (1999). Heat storage by two-grade phase change material. *PERIODICA POLYTECHNICA CHEMICAL ENGINEERING, 43*(2), 137-147.

Balikowski, JR, & Mollendorf, JC. (2007). Performance of phase change materials in a horizontal annulus of a double-pipe heat exchanger in a water-circulating loop. *Journal of heat transfer, 129*(3), 265-272.

Bathelt, AG, Viskanta, R, & Leidenfrost, W. (1979). An experimental investigation of natural convection in the melted region around a heated horizontal cylinder. *Journal of Fluid Mechanics, 90*(02), 227-239.

Bellecci, C., & Conti, M. (1993). Phase change thermal storage: transient behaviour analysis of a solar receiver/storage module using the enthalpy method. *International journal of heat and mass transfer, 36*(8), 2157-2163.

Cabeza, L.F., Ibanez, M., Sole, C., Roca, J., & Nogués, M. (2006). Experimentation with a water tank including a PCM module. *Solar Energy Materials and Solar Cells, 90*(9), 1273-1282.

Cabeza, LF, Mehling, H., Hiebler, S., & Ziegler, F. (2002). Heat transfer enhancement in water when used as PCM in thermal energy storage. *Applied thermal engineering, 22*(10), 1141-1151.

Çakmak, Gülşah, & Yıldız, Cengiz. (2011). The drying kinetics of seeded grape in solar dryer with PCM-based solar integrated collector. *Food and Bioproducts Processing, 89*(2), 103-108.

Canbazoğlu, S., Şahinaslan, A., Ekmekyapar, A., Aksoy, Ý.G., & Akarsu, F. (2005). Enhancement of solar thermal energy storage performance using sodium

thiosulfate pentahydrate of a conventional solar water-heating system. *Energy and buildings, 37*(3), 235-242.

Cao, Y., Faghri, A., & Juhasz, A. (1991). A PCM/forced convection conjugate transient analysis of energy storage systems with annular and countercurrent flows. *ASME Transactions Journal of Heat Transfer, 113*, 37-42.

Cao, Yiding, & Faghri, Amir. (1990). Thermal protection from intense localized moving heat fluxes using phase-change materials. *International journal of heat and mass transfer, 33*(1), 127-138.

Cao, Yrn, & Faghri, A. (1991). Performance characteristics of a thermal energy storage module: a transient PCM/forced convection conjugate analysis. *International journal of heat and mass transfer, 34*(1), 93-101.

Castell, A., Solé, C., Medrano, M., Roca, J., Cabeza, L.F., & García, D. (2008). Natural convection heat transfer coefficients in phase change material (PCM) modules with external vertical fins. *Applied Thermal Engineering, 28*(13), 1676-1686.

Chandra Sekhara Reddy, M., & Vasudeva Rao, Veeredhi. (2014). Experimental investigation of heat transfer coefficient and friction factor of ethylene glycol water based TiO_2 nanofluid in double pipe heat exchanger with and without helical coil inserts. *International Communications in Heat and Mass Transfer, 50*(0), 68-76.

Cheralathan, M, Velraj, R, & Renganarayanan, S. (2007). Performance analysis on industrial refrigeration system integrated with encapsulated PCM-based cool thermal energy storage system. *International Journal of Energy Research, 31*(14), 1398-1413.

Choi, S.U.S, & Eastman, J.A. (1995). Enhancing thermal conductivity of fluids with nanoparticles: Argonne National Lab., IL (United States).

Choudhury, C, Chauhan, PM, & Garg, HP. (1995). Economic design of a rock bed storage device for storing solar thermal energy. *Solar Energy, 55*(1), 29-37.

Chun, Byung-Hee, Kang, Hyun Uk, & Kim, Sung Hyun. (2008). Effect of alumina nanoparticles in the fluid on heat transfer in double-pipe heat exchanger system. *Korean Journal of Chemical Engineering, 25*(5), 966-971.

Cossi, Maurizio, Rega, Nadia, Scalmani, Giovanni, & Barone, Vincenzo. (2003). Energies, structures, and electronic properties of molecules in solution with the C-PCM solvation model. *Journal of computational chemistry, 24*(6), 669-681.

Dincer, Ibrahim, & Rosen, Marc. (2002). *Thermal energy storage: systems and applications*: John Wiley & Sons.

Ding, Yulong, Alias, Hajar, Wen, Dongsheng, & Williams, Richard A. (2006). Heat transfer of aqueous suspensions of carbon nanotubes (CNT nanofluids). *International Journal of Heat and Mass Transfer, 49*(1), 240-250.

Duangthongsuk, Weerapun, & Wongwises, Somchai. (2009). Heat transfer enhancement and pressure drop characteristics of TiO_2-water nanofluid in a double-tube counter

flow heat exchanger. *International Journal of Heat and Mass Transfer, 52*(7-8), 2059-2067.

Dutil, Y., Rousse, D.R., Salah, N.B., Lassue, S., & Zalewski, L. (2011). A review on phase-change materials: Mathematical modeling and simulations. *Renewable and Sustainable Energy Reviews, 15*(1), 112-130.

Dutta, Ritabrata, Atta, Arnab, & Dutta, Tapas Kumar. (2008). Experimental and numerical study of heat transfer in horizontal concentric annulus containing phase change material. *The Canadian Journal of Chemical Engineering, 86*(4), 700-710.

Dwivedi, Anil Kumar, & Das, Sarit Kumar. (2007). Dynamics of plate heat exchangers subject to flow variations. *International journal of heat and mass transfer, 50*(13), 2733-2743.

El Qarnia, H. (2009). Numerical analysis of a coupled solar collector latent heat storage unit using various phase change materials for heating the water. *Energy Conversion and Management, 50*(2), 247-254.

Elias, MM, Saidur, R, Rahim, NA, Sohel, MR, & Mahbubul, IM. (2014). Performance Investigation of a Plate Heat Exchanger Using Nanofluid with Different Chevron Angle. *Advanced Materials Research, 832*, 254-259.

Erek, A., Ilken, Z., & Acar, M.A. (2005). Experimental and numerical investigation of thermal energy storage with a finned tube. *International journal of energy research, 29*(4), 283-301.

Ettouney, H., El-Dessouky, H., & Al-Kandari, E. (2004). Heat transfer characteristics during melting and solidification of phase change energy storage process. *Industrial & engineering chemistry research, 43*(17), 5350-5357.

Ezan, Mehmet Akif, Ozdogan, Muhammet, & Erek, Aytunç. (2011). Experimental study on charging and discharging periods of water in a latent heat storage unit. *International Journal of Thermal Sciences, 50*(11), 2205-2219.

Farid, M.M., Khudhair, A.M., Razack, S.A.K., & Al-Hallaj, S. (2004). A review on phase change energy storage: materials and applications. *Energy conversion and management, 45*(9), 1597-1615.

Fernandez, AI, Martínez, M., Segarra, M., Martorell, I., & Cabeza, LF. (2010). Selection of materials with potential in sensible thermal energy storage. *Solar Energy Materials and Solar Cells, 94*(10), 1723-1729.

Fotukian, SM, & Nasr Esfahany, M. (2010). Experimental investigation of turbulent convective heat transfer of dilute γ-Al_2O_3/water nanofluid inside a circular tube. *International Journal of Heat and Fluid Flow, 31*(4), 606-612.

Fung, Chin-Ping. (2003). Manufacturing process optimization for wear property of fiber-reinforced polybutylene terephthalate composites with grey relational analysis. *Wear, 254*(3), 298-306.

Gaitonde, V. N., Karnik, S. R., Achyutha, B. T., & Siddeswarappa, B. (2008). Taguchi optimization in drilling of AISI 316L stainless steel to minimize burr size using

multi-performance objective based on membership function. *Journal of Materials Processing Technology, 202*(1–3), 374-379.

Gong, Z.X., & Mujumdar, A.S. (1997). Finite-element analysis of cyclic heat transfer in a shell-and-tube latent heat energy storage exchanger. *Applied thermal engineering, 17*(6), 583-591.

Goodarzi, M, Safaei, MR, Vafai, K, Ahmadi, G, Dahari, M, Kazi, SN, & Jomhari, N. (2014). Investigation of nanofluid mixed convection in a shallow cavity using a two-phase mixture model. *International Journal of Thermal Sciences, 75*, 204-220.

Hamada, Y., Ohtsu, W., & Fukai, J. (2003). Thermal response in thermal energy storage material around heat transfer tubes: effect of additives on heat transfer rates. *Solar energy, 75*(4), 317-328.

Haq, A. Noorul, Marimuthu, P., & Jeyapaul, R. (2008). Multi response optimization of machining parameters of drilling Al/SiC metal matrix composite using grey relational analysis in the Taguchi method. *The International Journal of Advanced Manufacturing Technology, 37*(3-4), 250-255. doi: 10.1007/s00170-007-0981-4

Hasnain, SM. (1998). Review on sustainable thermal energy storage technologies, Part I: heat storage materials and techniques. *Energy Conversion and Management, 39*(11), 1127-1138.

Hassan, Mohammadreza, Sadri, Rad, Ahmadi, Goodarz, Dahari, Mahidzal B, Kazi, Salim N, Safaei, Mohammad R, & Sadeghinezhad, Emad. (2013). Numerical Study of Entropy Generation in a Flowing Nanofluid Used in Micro-and Minichannels. *Entropy, 15*(1), 144-155.

Hawlader, MNA, Uddin, MS, & Khin, Mya Mya. (2003). Microencapsulated PCM thermal-energy storage system. *Applied energy, 74*(1), 195-202.

Hedayati, F, Malvandi, A, Kaffash, MH, & Ganji, DD. (2015). Fully developed forced convection of alumina/water nanofluid inside microchannels with asymmetric heating. *Powder Technology, 269*, 520-531.

Hosseini, MJ, Ranjbar, AA, Sedighi, K, & Rahimi, M. (2012). A combined experimental and computational study on the melting behavior of a medium temperature phase change storage material inside shell and tube heat exchanger. *International Communications in Heat and Mass Transfer, 39*(9), 1416-1424.

Huminic, Gabriela, & Huminic, Angel. (2011). Heat transfer characteristics in double tube helical heat exchangers using nanofluids. *International Journal of Heat and Mass Transfer, 54*(19–20), 4280-4287.

I, Douglas C. Montgomery. (2009). *Introduction to Statistical Quality Control* (6th ed.). Printed in the United States of America.: John Wiley & Sons, Inc.

Ismail, KAR, & Lino, FAM. (2011). Fins and turbulence promoters for heat transfer enhancement in latent heat storage systems. *Experimental thermal and fluid science, 35*(6), 1010-1018.

Jegadheeswaran, S., & Pohekar, S.D. (2009). Performance enhancement in latent heat thermal storage system: a review. *Renewable and Sustainable Energy Reviews, 13*(9), 2225-2244.

Jesumathy, Stella P, Udayakumar, M, & Suresh, S. (2012). Heat transfer characteristics in latent heat storage system using paraffin wax. *Journal of mechanical science and technology, 26*(3), 959-965.

Jian-you, L. (2008). Numerical and experimental investigation for heat transfer in triplex concentric tube with phase change material for thermal energy storage. *Solar Energy, 82*(11), 977-985.

Kabeel, AE, El Maaty, T Abou, & El Samadony, Y. (2013). The effect of using nano-particles on corrugated plate heat exchanger performance. *Applied Thermal Engineering, 52*(1), 221-229.

Kabelac, S, & Kuhnke, JF. (2006). *Heat transfer mechanisms in nanofluids—Experiments and theory.* Paper presented at the Annals of the assembly for international heat transfer conference.

Kapur, Kailash C., & Chen, Guangming. (1988). Signal-to-noise ratio development for quality engineering. *Quality and Reliability Engineering International, 4*(2), 133-141. doi: 10.1002/qre.4680040208

Karakilcik, Mehmet, Dincer, Ibrahim, & Rosen, Marc A. (2006). Performance investigation of a solar pond. *Applied Thermal Engineering, 26*(7), 727-735.

Karimipour, Arash, Esfe, Mohammad Hemmat, Safaei, Mohammad Reza, Semiromi, Davood Toghraie, Jafari, Saeed, & Kazi, SN. (2014). Mixed convection of copper–water nanofluid in a shallow inclined lid driven cavity using the lattice Boltzmann method. *Physica A: Statistical Mechanics and its Applications, 402*, 150-168.

Karmo, Diala, Ajib, Salman, & Khateeb, Ayman Al. (2013). New method for designing an effective finned heat exchanger. *Applied Thermal Engineering, 51*(1–2), 539-550.

Kaygusuz, K. (1995). Experimental and theoretical investigation of latent heat storage for water based solar heating systems. *Energy conversion and management, 36*(5), 315-323.

Kaygusuz, K., & Sari, A. (2005). Thermal energy storage system using a technical grade paraffin wax as latent heat energy storage material. *Energy sources, 27*(16), 1535-1546.

Kays, WM. Convective heat and mass transfer 1966: McGraw-Hill, New York.

Kenisarin, M., & Mahkamov, K. (2007). Solar energy storage using phase change materials. *Renewable and Sustainable Energy Reviews, 11*(9), 1913-1965.

Khairul, MA, Alim, MA, Mahbubul, IM, Saidur, R, Hepbasli, A, & Hossain, A. (2014). Heat transfer performance and exergy analyses of a corrugated plate heat exchanger using metal oxide nanofluids. *International Communications in Heat and Mass Transfer, 50*, 8-14.

Khoshvaght-Aliabadi, M, Zamzamian, A, & Hormozi, F. (2014). Wavy channel and different nanofluids effects on performance of plate-fin heat exchangers. *Journal of Thermophysics and Heat Transfer, 28*(3), 474-484.

Koca, A., Oztop, H.F., Koyun, T., & Varol, Y. (2008). Energy and exergy analysis of a latent heat storage system with phase change material for a solar collector. *Renewable Energy, 33*(4), 567-574.

Kurt, Mustafa, Bagci, Eyup, & Kaynak, Yusuf. (2009). Application of Taguchi methods in the optimization of cutting parameters for surface finish and hole diameter accuracy in dry drilling processes. *The International Journal of Advanced Manufacturing Technology, 40*(5-6), 458-469.

Kwon, YH, Kim, D, Li, CG, Lee, JK, Hong, DS, Lee, JG, . . . Kim, SH. (2011). Heat transfer and pressure drop characteristics of nanofluids in a plate heat exchanger. *Journal of nanoscience and nanotechnology, 11*(7), 5769-5774.

Lacroix, M. (1993). Study of the heat transfer behavior of a latent heat thermal energy storage unit with a finned tube. *International journal of heat and mass transfer, 36*(8), 2083-2092.

Lafdi, K, Mesalhy, O, & Elgafy, A. (2008). Graphite foams infiltrated with phase change materials as alternative materials for space and terrestrial thermal energy storage applications. *Carbon, 46*(1), 159-168.

Lamberg, P. (2004). Approximate analytical model for two-phase solidification problem in a finned phase-change material storage. *Applied Energy, 77*(2), 131-152.

Layton, Astrid, Reap, John, Bras, Bert, & Weissburg, Marc. (2012). Correlation between thermodynamic efficiency and ecological cyclicity for thermodynamic power cycles. *PloS one, 7*(12), e51841.

Lee, Alex HW, & Jones, Jerold W. (1996). Modeling of an ice-on-coil thermal energy storage system. *Energy conversion and management, 37*(10), 1493-1507.

Li, Qiang, Xuan, Y, & Wang, J. (2003). Investigation on convective heat transfer and flow features of nanofluids. *Journal of Heat transfer, 125*, 151-155.

Liang, Weidong, Chen, Pinsong, Sun, Hanxue, Zhu, Zhaoqi, & Li, An. (2014). Innovative spongy attapulgite loaded with n-carboxylic acids as composite phase change materials for thermal energy storage. *RSC Advances, 4*(73), 38535-38541.

Liao, Y. S., Huang, J. T., & Su, H. C. (1997). A study on the machining-parameters optimization of wire electrical discharge machining. *Journal of Materials Processing Technology, 71*(3), 487-493.

Liu, MinSheng, Lin, Mark ChingCheng, & Wang, ChiChuan. (2011). Enhancements of thermal conductivities with Cu, CuO, and carbon nanotube nanofluids and application of MWNT/water nanofluid on a water chiller system. *Nanoscale research letters, 6*(1), 1-13.

Liu, Z., Wang, Z., & Ma, C. (2006). An experimental study on the heat transfer characteristics of a heat pipe heat exchanger with latent heat storage. Part II:

Simultaneous charging/discharging modes. *Energy conversion and management, 47*(7), 967-991.

Maddah, Heydar, Aghayari, Reza, Farokhi, Morshed, Jahanizadeh, Shabnam, & Ashtary, Khatere. (2014). Effect of Twisted-Tape Turbulators and Nanofluid on Heat Transfer in a Double Pipe Heat Exchanger. *Journal of Engineering, 2014*.

Maddah, Heydar, Alizadeh, Mostafa, Ghasemi, Nahid, & Alwi, Sharifah Rafidah Wan. (2014). Experimental study of Al 2 O 3/water nanofluid turbulent heat transfer enhancement in the horizontal double pipes fitted with modified twisted tapes. *International Journal of Heat and Mass Transfer, 78*, 1042-1054.

Malvandi, A, & Ganji, DD. (2014). Effects of nanoparticle migration on force convection of alumina/water nanofluid in a cooled parallel-plate channel. *Advanced Powder Technology, 25*(4), 1369-1375.

Maruoka, Nobuhiro, & Akiyama, Tomohiro. (2003). Thermal stress analysis of PCM encapsulation for heat recovery of high temperature waste heat. *Journal of chemical engineering of Japan, 36*(7), 794-798.

Maruoka, Nobuhiro, Sato, Kazushi, Yagi, Jun-ichiro, & Akiyama, Tomohiro. (2002). Development of PCM for recovering high temperature waste heat and utilization for producing hydrogen by reforming reaction of methane. *ISIJ international, 42*(2), 215-219.

Mat, Sohif, Al-Abidi, Abduljalil A, Sopian, K, Sulaiman, MY, & Mohammad, Abdulrahman Th. (2013). Enhance heat transfer for PCM melting in triplex tube with internal–external fins. *Energy Conversion and Management, 74*, 223-236.

Mehling, H., & Cabeza, L.F. (2008). *Heat and cold storage with PCM: an up to date introduction into basics and applications*: Springer.

Mehling, H., Cabeza, LF, Hippeli, S., & Hiebler, S. (2003). PCM-module to improve hot water heat stores with stratification. *Renewable Energy, 28*(5), 699-711.

Mettawee, E.B.S., & Assassa, G.M.R. (2006). Experimental study of a compact PCM solar collector. *Energy, 31*(14), 2958-2968.

Mettawee, E.B.S., & Assassa, G.M.R. (2007). Thermal conductivity enhancement in a latent heat storage system. *Solar Energy, 81*(7), 839-845.

Mettawee, Eman-Bellah S, & Assassa, Ghazy MR. (2006). Experimental study of a compact PCM solar collector. *Energy, 31*(14), 2958-2968.

Mohamed, Mousa M. (2005). Solidification of phase change material on vertical cylindrical surface in holdup air bubbles. *International journal of refrigeration, 28*(3), 403-411.

Mohammed, H. A., Hasan, Husam A., & Wahid, M. A. (2013). Heat transfer enhancement of nanofluids in a double pipe heat exchanger with louvered strip inserts. *International Communications in Heat and Mass Transfer, 40*, 36-46. doi: 10.1016/j.icheatmasstransfer.2012.10.023

Murray, R., Desgrosseilliers, L., Stewart, J., Osbourne, N., Marin, G., Safatli, A., . . . White, M.A. (2011). *Design of a Latent Heat Energy Storage System Coupled with a Domestic Hot Water Solar Thermal System.* Paper presented at the Proceedings of the World Renewable Energy Congress-WREC.

Murray, R.E., & Groulx, D. (2011). *Modeling Convection during Melting of a Phase Change Material.* Paper presented at the Proceedings of the COMSOL Conference Boston 2011.

Nagano, K. (2004). Experiments on fin-effects for increasing heat transfer coefficients during charging heat and heat release between PCMs and thermal medium. *IEA annex, 17*.

Nallusamy, N, Sampath, S, & Velraj, R. (2007). Experimental investigation on a combined sensible and latent heat storage system integrated with constant/varying (solar) heat sources. *Renewable Energy, 32*(7), 1206-1227.

Nasiri, M, Etemad, S Gh, & Bagheri, R. (2011). Experimental heat transfer of nanofluid through an annular duct. *International Communications in Heat and Mass Transfer, 38*(7), 958-963.

Nemykin, Victor N, Makarova, Elena A, Grosland, Jeffrey O, Hadt, Ryan G, & Koposov, Alexey Y. (2007). Preparation, characterization, molecular and electronic structures, TDDFT, and TDDFT/PCM study of the solvatochromism in cyanovinylferrocenes. *Inorganic chemistry, 46*(23), 9591-9601.

Nsofor, Emmanuel C. (2005). Investigations on the packed bed for high-temperature thermal energy storage. *International journal of green energy, 2*(4), 337-351.

Ogoh, W., & Groulx, D. (2012). Effects of the heat transfer fluid velocity on the storage characteristics of a cylindrical latent heat energy storage system: a numerical study. *Heat and Mass Transfer, 48*(3), 439-449.

Oon, CS, Al-Shamma'a, A, Kazi, SN, Chew, BT, Badarudin, A, & Sadeghinezhad, E. (2014). Simulation of heat transfer to separation air flow in a concentric pipe. *International Communications in Heat and Mass Transfer, 57*, 48-52.

Pak, Bock Choon, & Cho, Young I. (1998). Hydrodynamic and heat transfer study of dispersed fluids with submicron metallic oxide particles. *Experimental heat transfer: an international journal, 11*(2), 151-170.

Pandey, Shive Dayal, & Nema, VK. (2012). Experimental analysis of heat transfer and friction factor of nanofluid as a coolant in a corrugated plate heat exchanger. *Experimental Thermal and Fluid Science, 38*, 248-256.

Pantzali, MN, Kanaris, AG, Antoniadis, KD, Mouza, AA, & Paras, SV. (2009). Effect of nanofluids on the performance of a miniature plate heat exchanger with modulated surface. *International Journal of Heat and Fluid Flow, 30*(4), 691-699.

PJ., Ross, & ((1996)). *Taguchi techniques for quality engineering*. International Editions, Singapore: McGraw-Hill.

Rabin, Y., Bar-Niv, I., Korin, E., & Mikic, B. (1995). Integrated solar collector storage system based on a salt-hydrate phase-change material. *Solar Energy, 55*(6), 435-444.

Regin, A.F., Solanki, SC, & Saini, JS. (2006). Latent heat thermal energy storage using cylindrical capsule: Numerical and experimental investigations. *Renewable energy, 31*(13), 2025-2041.

Regin, A.F., Solanki, SC, & Saini, JS. (2008). Heat transfer characteristics of thermal energy storage system using PCM capsules: A review. *Renewable and Sustainable Energy Reviews, 12*(9), 2438-2458.

Roy, Indranil, Rana, Dipak, Sarkar, Gunjan, Bhattacharyya, Amartya, Saha, Nayan Ranjan, Mondal, Soumya, . . . Chattopadhyay, Dipankar. (2015). Physical and electrochemical characterization of reduced graphene oxide/silver nanocomposites synthesized by adopting a green approach. *RSC Advances, 5*(32), 25357-25364.

Safaei, Mohammad, Goodarzi, Marjan, & Mohammadi, Mohammadali. (2011). Numerical modeling of turbulence mixed convection heat transfer in air filled enclosures by finite volume method. *The International Journal of Multiphysics, 5*(4), 307-324.

Safaei, Mohammad Reza, Goshayeshi, Hamid Reza, Razavi, B Saeedi, & Goodarzi, Marjan. (2011). Numerical investigation of laminar and turbulent mixed convection in a shallow water-filled enclosure by various turbulence methods. *Scientific Research and Essays, 6*(22), 4826-4838.

Sarı, A., & Kaygusuz, K. (2002). Thermal and heat transfer characteristics in a latent heat storage system using lauric acid. *Energy Conversion and Management, 43*(18), 2493-2507.

Sasaguchi, K., Kusano, K., & Viskanta, R. (1997). A numerical analysis of solid-liquid phase change heat transfer around a single and two horizontal, vertically spaced cylinders in a rectangular cavity. *International journal of heat and mass transfer, 40*(6), 1343-1354.

Sasaguchi, K., Yoshida, M., & Nakashima, S. (1990). Heat transfer characteristics of a latent heat thermal energy storage unit with a finned tube (effects of fin configuration). *Heat transfer. Japanese research, 19*(1), 11-27.

Sato, Hirofumi, & Sakaki, Shigeyoshi. (2004). Comparison of electronic structure theories for solvated molecules: RISM-SCF versus PCM. *The Journal of Physical Chemistry A, 108*(9), 1629-1634.

Seeniraj, RV, & Lakshmi Narasimhan, N. (2008). Performance enhancement of a solar dynamic LHTS module having both fins and multiple PCMs. *Solar energy, 82*(6), 535-542.

Seeniraj, RV, & Narasimhan, N Lakshmi. (2008). Performance enhancement of a solar dynamic LHTS module having both fins and multiple PCMs. *Solar Energy, 82*(6), 535-542.

Sharma, A., Tyagi, VV, Chen, CR, & Buddhi, D. (2009). Review on thermal energy storage with phase change materials and applications. *Renewable and Sustainable Energy Reviews, 13*(2), 318-345.

Sharma, S Dutt, & Sagara, Kazunobu. (2005). Latent heat storage materials and systems: a review. *International Journal of Green Energy, 2*(1), 1-56.

Sharma, SD, Iwata, Takeshi, Kitano, Hiroaki, & Sagara, Kazunobu. (2005). Thermal performance of a solar cooker based on an evacuated tube solar collector with a PCM storage unit. *Solar Energy, 78*(3), 416-426.

Shatikian, V., Ziskind, G., & Letan, R. (2008). Numerical investigation of a PCM-based heat sink with internal fins: Constant heat flux. *International Journal of Heat and Mass Transfer, 51*(5), 1488-1493.

Shmueli, H, Ziskind, G, & Letan, R. (2010). Melting in a vertical cylindrical tube: numerical investigation and comparison with experiments. *International Journal of Heat and Mass Transfer, 53*(19), 4082-4091.

Shukla, A., Buddhi, D., & Sawhney, RL. (2009). Solar water heaters with phase change material thermal energy storage medium: A review. *Renewable and Sustainable Energy Reviews, 13*(8), 2119-2125.

Stritih, U. (2004). An experimental study of enhanced heat transfer in rectangular PCM thermal storage. *International journal of heat and mass transfer, 47*(12), 2841-2847.

Stritih, Uroš, & Butala, Vincenc. (2010). Experimental investigation of energy saving in buildings with PCM cold storage. *International journal of refrigeration, 33*(8), 1676-1683.

Sundar, L Syam, & Sharma, KV. (2010). Heat transfer enhancements of low volume concentration Al_2O_3 nanofluid and with longitudinal strip inserts in a circular tube. *International Journal of Heat and Mass Transfer, 53*(19), 4280-4286.

Sundarraj, Pradeepkumar, Maity, Dipak, Roy, Susanta Sinha, & Taylor, Robert A. (2014). Recent advances in thermoelectric materials and solar thermoelectric generators–a critical review. *RSC Advances, 4*(87), 46860-46874.

Taguchi, Genchi, Chowdhury, Subir, & Taguchi, Shin. (2000). *Robust engineering*: McGraw-Hill.

Taguchi, Genichi, Chowdhury, Subir, & Wu, Yuin. (2005). *Taguchi's Quality Engineering Handbook*: John Wiley & Sons, Inc., Hoboken, New Jersey.

Tang, Qianqiu, Sun, Jun, Yu, Shuangmin, & Wang, Gengchao. (2014). Improving thermal conductivity and decreasing supercooling of paraffin phase change materials by n-octadecylamine-functionalized multi-walled carbon nanotubes. *RSC Advances, 4*(69), 36584-36590.

Taws, Matthew, Nguyen, Cong Tam, Galanis, Nicolas, & Gherasim, Iulian. (2012). *Experimental Investigation of Nanofluid Heat Transfer in a Plate Heat Exchanger*. Paper presented at the ASME 2012 Heat Transfer Summer Conference collocated with the ASME 2012 Fluids Engineering Division Summer Meeting and the

ASME 2012 10th International Conference on Nanochannels, Microchannels, and Minichannels.

Tiwari, Arun Kumar, Ghosh, Pradyumna, & Sarkar, Jahar. (2013). Heat transfer and pressure drop characteristics of CeO 2/water nanofluid in plate heat exchanger. *Applied Thermal Engineering, 57*(1), 24-32.

Tosun, Nihat. (2006). Determination of optimum parameters for multi-performance characteristics in drilling by using grey relational analysis. *The International Journal of Advanced Manufacturing Technology, 28*(5-6), 450-455.

Trp, A., Lenic, K., & Frankovic, B. (2006). Analysis of the influence of operating conditions and geometric parameters on heat transfer in water-paraffin shell-and-tube latent thermal energy storage unit. *Applied Thermal Engineering, 26*(16), 1830-1839.

Vajjha, Ravikanth S, Das, Debendra K, & Kulkarni, Devdatta P. (2010). Development of new correlations for convective heat transfer and friction factor in turbulent regime for nanofluids. *International Journal of Heat and Mass Transfer, 53*(21), 4607-4618.

Velraj, R., Seeniraj, RV, Hafner, B., Faber, C., & Schwarzer, K. (1999). Heat transfer enhancement in a latent heat storage system. *Solar energy, 65*(3), 171-180.

Wang, Yunming, Tang, Bingtao, & Zhang, Shufen. (2012). Light–thermal conversion organic shape-stabilized phase-change materials with broadband harvesting for visible light of solar radiation. *RSC Advances, 2*(30), 11372-11378.

Wen, Dongsheng, & Ding, Yulong. (2004). Experimental investigation into convective heat transfer of nanofluids at the entrance region under laminar flow conditions. *International Journal of Heat and Mass Transfer, 47*(24), 5181-5188.

Wu, Zan, Wang, Lei, & Sunden, Bengt. (2013). Pressure drop and convective heat transfer of water and nanofluids in a double-pipe helical heat exchanger. *Applied Thermal Engineering, 60*(1-2), 266-274. doi: 10.1016/j.applthermaleng.2013.06.051

Yang, Ying, Zhang, Z George, Grulke, Eric A, Anderson, William B, & Wu, Gefei. (2005). Heat transfer properties of nanoparticle-in-fluid dispersions (nanofluids) in laminar flow. *International Journal of Heat and Mass Transfer, 48*(6), 1107-1116.

Yarmand, Hooman, Gharehkhani, Samira, Kazi, Salim Newaz, Sadeghinezhad, Emad, & Safaei, Mohammad Reza. (2014). Numerical investigation of heat transfer enhancement in a rectangular heated pipe for turbulent nanofluid. *The Scientific World Journal, 2014*.

Zalba, B., Sanchez-valverde, B., & Marín, J.M. (2005). An experimental study of thermal energy storage with phase change materials by design of experiments. *Journal of Applied Statistics, 32*(4), 321-332.

Zamzamian, Amirhossein, Oskouie, Shahin Nasseri, Doosthoseini, Ahmad, Joneidi, Aliakbar, & Pazouki, Mohammad. (2011). Experimental investigation of forced convective heat transfer coefficient in nanofluids of Al_2O_3/EG and CuO/EG in a

double pipe and plate heat exchangers under turbulent flow. *Experimental Thermal and Fluid Science, 35*(3), 495-502. doi: 10.1016/j.expthermflusci.2010.11.013

Zeinali Heris, Saeed, Etemad, S Gh, & Nasr Esfahany, M. (2006). Experimental investigation of oxide nanofluids laminar flow convective heat transfer. *International Communications in Heat and Mass Transfer, 33*(4), 529-535.

Zhang, Tianyu, Tang, Qing, Lu, Huilin, Wang, Shuai, & Sun, Liyan. (2015). Numerical study of melted PCM inside a horizontal annulus with threads in a three-dimensional model. *RSC Advances, 5*(16), 12178-12185.

Zhang, Y., & Faghri, A. (1996a). Heat transfer enhancement in latent heat thermal energy storage system by using the internally finned tube. *International journal of heat and mass transfer, 39*(15), 3165-3173.

Zhang, Y., & Faghri, A. (1996b). Semi-analytical solution of thermal energy storage system with conjugate laminar forced convection. *International journal of heat and mass transfer, 39*(4), 717-724.

Zhou, Dan, Zhao, Chang-Ying, & Tian, Yuan. (2012). Review on thermal energy storage with phase change materials (PCMs) in building applications. *Applied Energy, 92*, 593-605.

Zivkovic, B., & Fujii, I. (2001). An analysis of isothermal phase change of phase change material within rectangular and cylindrical containers. *Solar energy, 70*(1), 51-61.

LIST OF PUBLICATIONS AND PAPERS PRESENTED

- ***ISI Journals:***

1. ***Paria, S****., Sarhan, A. A. D., Goodarzi, M. S., Baradaran, S., Rahmanian, B., Yarmand, H., ... & Metselaar, H. S. C. (2015). Indoor Solar Thermal Energy Saving Time with Phase Change Material in a Horizontal Shell and Finned-Tube Heat Exchanger. The Scientific World Journal, 2015.*

2. ***Paria, S.,*** *Baradaran, S., Amiri, A., Sarhan, A. A. D., & Kazi, S. N. Performance evaluation of latent heat energy storage in horizontal shell-and-finned tube for solar application. Journal of Thermal Analysis and Calorimetry, 1-11.*

- ***Conference:***

1. ***S. Paria****,*, A. Jarrahi , S. Baradaran, A.A.D. Sarhan, S. N .Kazi, Effect of finned tube surface area on saving energy performance using unique horizontal shell unit for solar application, International Conference on Chemical and Biochemical Engineering Paris (France), 20-22 July 2015,ISBN: 978-84-*944311-1-1,

- ***Patents:***

1. *MOHAMMED, S.A.A., CORNELIS, M.H.S****., PARIA, S.****, BARADARAN, S., NEWAZ, K.S., & ZALNEHZAD, E. (2015). Horizontal heat exchanger for thermal energy storage: Google Patents. (PCT/MY2015/050005)*

2. *MOHAMMED, S.A.A., CORNELIS, M.H.S.,* ***PARIA, S.****, BARADARAN, S., NEWAZ, K.S., & ZALNEHZAD, E. (2014). Horizontal heat exchanger for thermal energy storage: (PI2014700388)*

❖ ***Awards:***

1. Gold medal: *Malaysia Technology EXPO 2013 (MTE 2013), Ministry of Science, Technology & Innovation, Malaysia, 21st 23rd February 2013, Putra World Trade Centre, Kuala Lumpur., 2013, (INTERNATIONAL)*

2. Gold medal: *The 24th International Invention, Innovation & Technology Exhibition (ITEX 2013) Ministry of Science, Technology & Innovation, Malaysia, 9 - 11 May 2013, Kuala Lumpur Convention Centre, 2013, (INTERNATIONAL)*

APPENDIX A: 2-D DRAWING OF ENERGY STORAGE UNIT

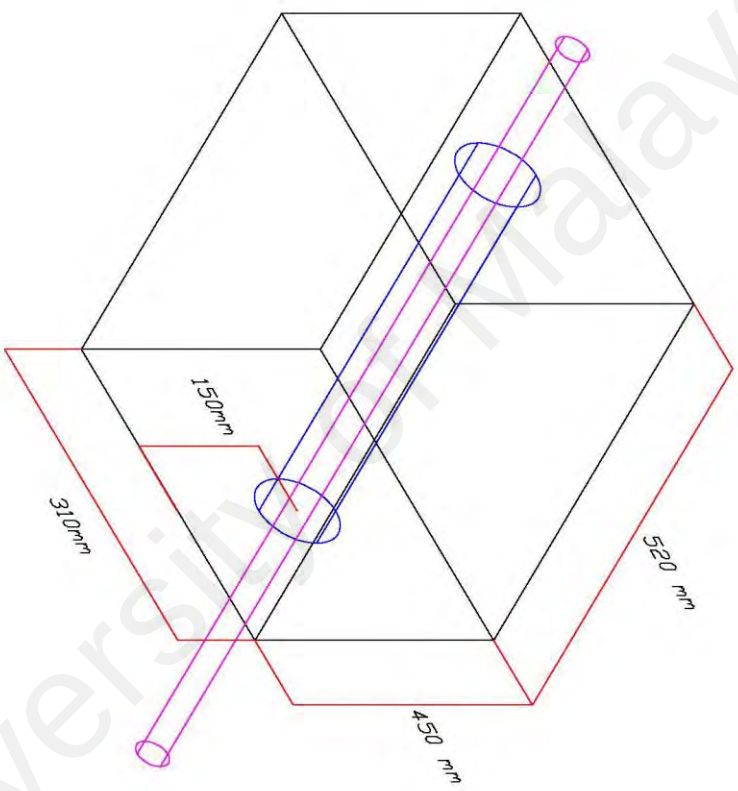

APPENDIX B: 2-D DRAWING OF FLUID TANK

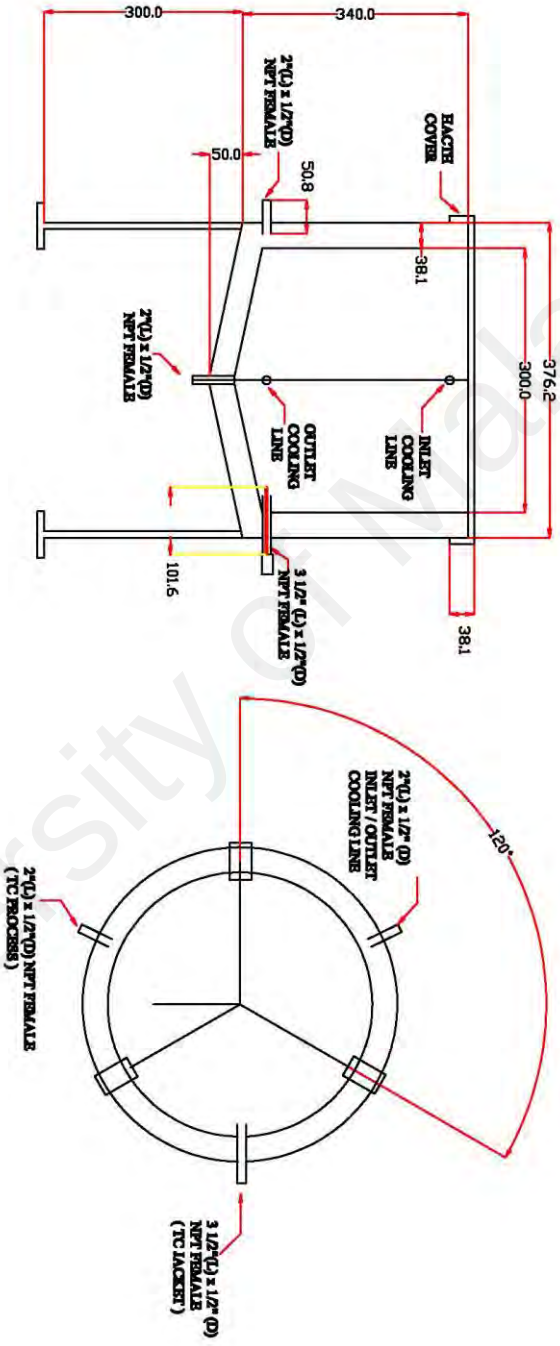

APPENDIX C: PUMP SPECIFICATIONS

----------ARAKI----------EX-SERIES----------

PERFORMANCE CURVE (EX-SERIES) 50Hz

EX-55R TO EX-100R

EX-55R
Max. Capacity:60LPM
Max. Head:5.8M

EX-70R
Max. Capacity:85LPM
Max. Head:6.8M

EX-100R
Max. Capacity:120LPM
Max. Head:9M

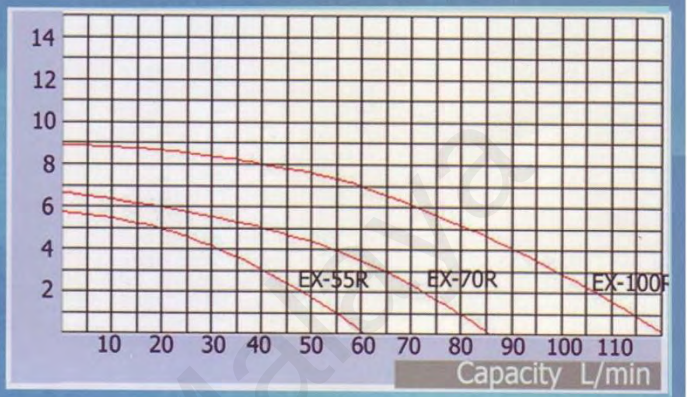

PUMP SPECIFICATION

Type	Hose connected		Threaded connected		Max Capacity	Max head	Standard duty point	Temp.	S.G.	Motor		
	Inlet	Outlet	In/Out	Union						Output	Input	Phase
	mm	mm	Inch	mm	L/min	m	m-L/min	°C		W	W	
EX-30R(M)-N	20	20	G 3/4	16	32	3.8	2.5-16	0-80	1.3	45	60	1
EX-40R(M)-N	20	20	G 3/4	16	45	4.6	4-22	0-80	1.1	65	90	1
EX-55R(M)	26	26	G 1	20	60	5.6	4-30	0-80	1.2	90	130	1
EX-70R(M)	26	26	G 1	20	86	6.7	4-50	0-80	1.0	150	265	1OR3
EX-100R(M)	26	26	G 1	20	120	8.6	6.5-60	0-80	1.2	260	245	1OR3

DIMENSIONS (EX-SERIES)

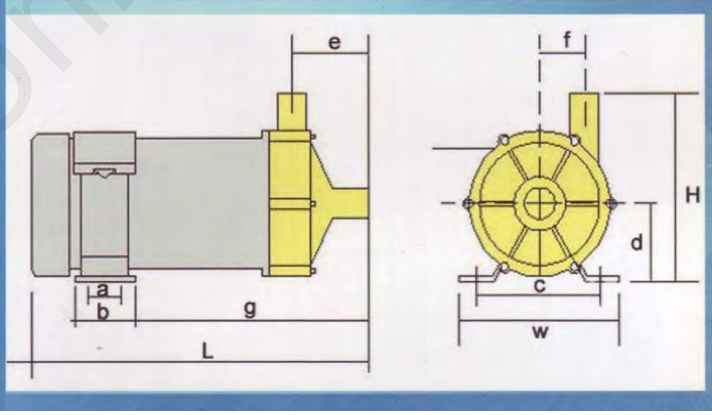

Model	EX-55R(M)	EX-70R(M)	Unit
a	40	40	mm
b	64	60	mm
c	100	110	mm
d	65	65	mm
e	61.5(60.8)	53	mm
f	40	43	mm
g	166.7(165.8)	149	mm
W	120	130	mm
H	155	155	mm
L	273.5	258	mm

TB2WE Two-wire System
Turbine Flow Meter Wiring Scheme

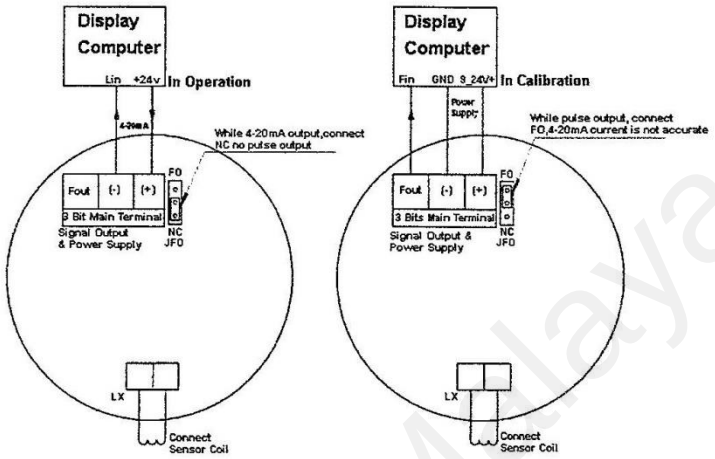

TB3WE Three-wire System
Turbine Flow Meter Wiring Scheme